

Department of Precision and Microsystems Engineering

Design of compliant variable stiffness ball joint

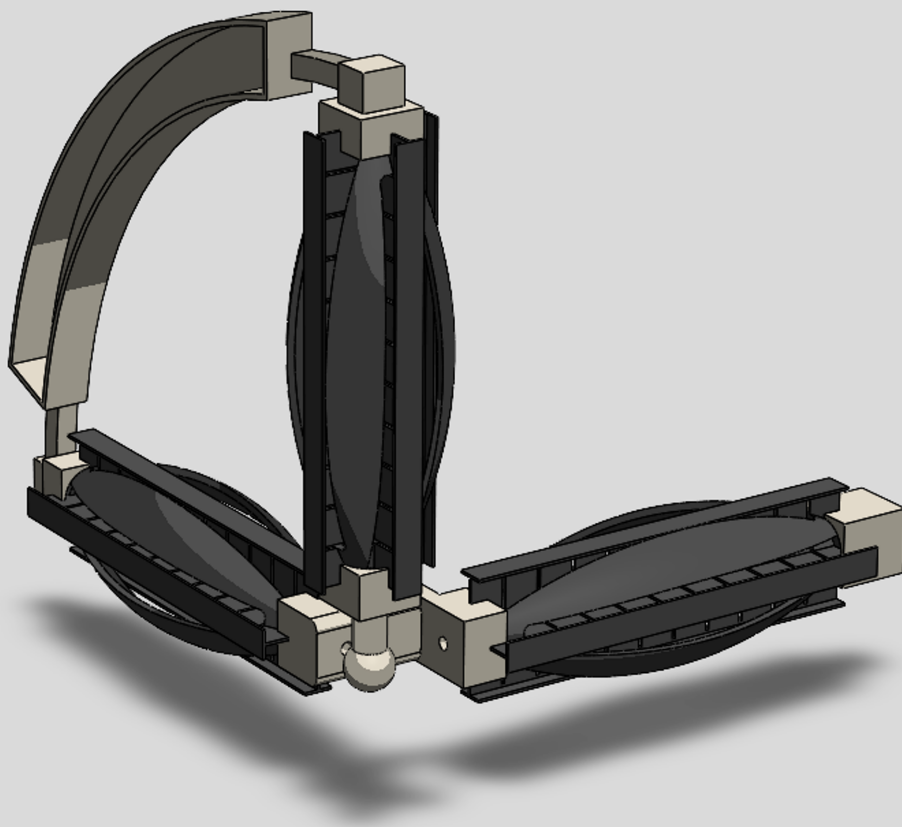
Tzu Lee

Report no :2023.082
Coach :Dr. ir. A.A. Nobaveh, Dr. ir. G. Radaelli
Professor :Prof. dr. ir. J.L. Herder
Specialisation :MSD
Type of report :Master thesis
Date :29th September 2023

Design of compliant variable stiffness ball joint

MSC Thesis

Tzu Lee



Abstract

This report begins with an exploration of existing variable torsional stiffness (VTS) mechanisms. The evaluation reveals a research gap in developing compliant mechanisms with continuous tunability in torsional stiffness. Consequently, two research objectives are formulated: (1) Designing a monolithic, compliant element with continuous variable torsional stiffness. (2) Designing a variable stiffness ball joint based on this element.

To accomplish the first objective, three compliant VTS concepts are devised. With the aim of attaining continuous stiffness adaptability, the concept exhibiting the utmost performance is chosen to undergo parametric analysis with FEM simulation. This analysis investigates the sensitivity between various parameters and their corresponding responses, ultimately optimizing the shape of the VTS element. Once the optimal shape is determined, three of these elements are interconnected in series, each oriented perpendicularly to the others. This configuration gives rise to the compliant variable stiffness ball joint, thereby achieving the second objective.

Successively, the behavior of the compliant VS ball joint is studied. Since the reaction force of the ball joint is dependent on its stiffness and input displacement, the analytical model of the ball joint describing the relation between these two variables and the reaction force is developed. This quantitative analysis empowers us to achieve meticulous control over the motion of the ball joint.

Experimentally, both the compliant VTS element and the compliant VS ball joint are fabricated using 3D printing technology. An experiment is carried out to measure the stiffness of the VTS element, thereby validating the FEM simulation result and proving by applying prestress to the VTS element, its torsional stiffness can be tuned from positive to zero value. Hence, the stiffness of the ball joint can also be modulated by adjusting the prestress along the three perpendicular axes.

Acknowledgement

I would like to express my gratitude to the individuals whose contributions have made this project possible. First and foremost, I am thankful to my daily supervisors, Dr. Ali Amoozandeh Nobaveh and Dr. Giuseppe Radaelli for providing me with this fascinating research opportunity. Your insightful discussions and constructive feedback have been instrumental in shaping this project. It has been a fun and meaningful journey working with them, for their incredible passion in the field of compliant mechanisms has also spiked my enthusiasm.

I appreciate Professor Just Herder for granting me the opportunity to conduct my thesis research under the shell-skeletons research group. Your guidance and suggestions have been invaluable for the project's improvement.

Additionally, I am thankful to Spiridon van Veldhoven, IWM, and Patrick van Holst for providing Lab resources to conduct my experiments. Their efficiency and kindness have amazed me. Without them, my thesis project could have been delayed for weeks.

Special thanks to my sister because she said so. I am deeply grateful for the substantial emotional and financial backing provided by my parents and aunt Ming Lee, Hui-chu Chen, Hui-Zhao Chen. Their unwavering support has enabled me to pursue my master's degree at TU Delft. In loving memory of my grandmother, I would like to express my heartfelt gratitude to her and my grandfather, who have always believed in me and got me through tough times.

Finally, I gave my deepest gratitude to my friends who provided me with invaluable mental support by unexpectedly showing up at my door with a generous supply of alcohol. Without them, I would not have been able to spend more time at this marvelous Delft University of Technology.

Tzu Lee

Delft, September 2023

Contents

Abstract	i
Acknowledgement	ii
1 Introduction	1
1.1 Motivation and background	1
1.2 Thesis objectives	1
1.3 Thesis outline	2
2 Literature Overview	3
3 Main Paper	17
4 Conclusion	38
References	39
A Concept generation- compliant VTS mechanism	40
A.1 Chapter Introduction	40
A.2 Concept overview	41
A.2.1 Concept I	41
A.2.2 Concept 2	42
A.2.3 Concept 3	43
A.3 Performance Comparison	45
A.4 Summary	46
B Sensitivity Analysis	48
B.1 APDL code	48
B.2 Sensitivity analysis results	79
C RSM	84
C.1 Factorial point	84
C.2 Predictive model of responses	85
C.3 Response surfaces	88
C.4 Predictive model vs FEM data	93
D GUI	94
D.1 GUI layout	94
D.2 GUI matlab code	94

1

Introduction

1.1. Motivation and background

Compliant mechanisms (CM) are elastic mechanical structures that achieve motion transmission and energy storage through the deformation of their flexible components, replacing traditional rigid linkages, hinges, or joints. CMs offer numerous advantages over rigid-body mechanisms. For example, their monolithic structure reduces overall part numbers thereby eliminating the need for lubrication, complex assemblies, and cumbersome manufacturing. This also helps improve precision, enhance reliability, and reduce wear due to the absence of friction and backlash. The simplicity of CMs makes scaling much easier, which is beneficial in many applications such as robotics, aerospace, automotive, medical devices, and micro/nano-scale systems that require lightweight and miniature structures.

Unlike traditional mechanisms that utilize rigid components with infinite stiffness, CMs exploit the inherent flexibility and elasticity of the material to achieve desired movements. The relation between motions and loads depends on the component stiffness. Therefore, the study of stiffness becomes the most crucial task when designing CMs. To be able to adjust the motion under specified loads, traditional mechanisms usually rely on gears, belts, or sliders, while CMs require variable stiffness characteristics to achieve the same adjustability without such intermediate components.

Various ways to tune the stiffness of compliant elements can be found in the literature, including changing the material properties and applying prestress. For instance, the phase of shape memory alloy/polymer(SMA/SMP) changes according to the temperature [4]. The stiffness of a beam drops drastically when it is buckled[2]. However, the majority of research focuses on variable bending stiffness. There is scarce literature on variable torsional stiffness(VTS) and the achievable stiffness is either discrete or highly nonlinear. Finite torsional stiffness allows for mechanisms to have rotational DoFs. Common examples are revolute joints, universal joints, and ball joints. These joints are widely used in prostheses, medical devices, biomimicry, and haptic feedback for joysticks. Therefore, designing a compliant variable stiffness joint has great potential since it could achieve multifunctionality as well as substantially improve the strength-to-weight ratio of the aforementioned applications.

1.2. Thesis objectives

Research on compliant variable stiffness joints is scarce and in early stages.[2] presents a binary stiffness revolute joint by buckling and unbuckling thin plates. [3] proposes a binary stiffness universal joint using the same technique, however, instead of thin plates that ensure planar motion, wire beams are

used to allow for 2 rotational DoFs. While several compliant variable stiffness joints are developed, most of them only provide binary or discrete stiffness states but not continuous stiffness variability. Moreover, the variable stiffness feature has not yet been integrated to a ball joint. These research gaps shaped up the objectives of this thesis:

- To propose a design of a compliant ball joint with continuous variable stiffness.
- To maximize the stiffness variation range and range of motion of the ball joint within a limited space.
- To minimize the actuation force for tuning stiffness.
- To investigate the effect of support stiffness on the behavior of the ball joint.

In this work, the compliant variable stiffness (VS) ball joint is realized by connecting three variable torsional stiffness (VTS) elements in series, with each element perpendicular to the others. Therefore, the proposed VTS element is expected to have relatively low torsional but high bending and axial stiffness in order to provide rotational DoFs and translational constraints.

However, compliant components always have finite stiffness that contributes to error. This is especially critical for mechanisms with compliant elements connected in series since the error accumulates. As a result, developing an analytical model of the ball joint that accounts for its support stiffness and errors enables a more precise behavior prediction.

Additional work to improve the performance of the ball joint includes parametric studies of numerous design parameters. The goal is to optimize the stiffness variation range, range of motion (RoM), and required actuation force. These parametric studies are carried out utilizing software Ansys APDL, Ansys Workbench, and Design Expert.

1.3. Thesis outline

This thesis comprises an introduction chapter and two papers. In Paper I, the study addresses the research gap between traditional rigid and compliant joints in VTS designs. It reviews existing VTS methods using specific criteria to identify limitations.

In Paper II, a compliant VTS element and a compliant variable stiffness ball joint are proposed. The VTS element consists of two fundamental structures: T beam and diagonal beam. To assess how the design parameters influence the stiffness, RoM, maximum stress, and actuation force, sensitivity analyses are performed for each fundamental structure. Afterwards, the optimal VTS element shape is determined according to the thesis objectives. Moreover, FEM simulation results of the VTS element are validated through experiments. Next, the VTS element is used to create the compliant variable stiffness ball joint, along with an analytical model developed to predict its reaction under external input displacement. In a nutshell, Paper II highlights the contribution of this research for developing adaptable ball joints.

Additionally, to provide a profound understanding of the concept generation process, Appendix A demonstrates three initial concepts of compliant VTS elements, including the one introduced in Paper II. Their working principle and performances are elucidated, illustrating the rationale for the final concept selection.

2

Literature Overview

This literature review presents an overview of the methods of variable torsional stiffness(VTS). The aim of this study is to gather prior designs of VTS mechanisms, and analyze their performance quantitatively in order to provide a design guideline for future researchers. The obtained data not only reveals the methods that best align with the design objective but also highlights the substantial advantages of compliant VTS mechanisms over traditional rigid VTS mechanisms, thus emphasizing the immense potential of this thesis project. Furthermore, it is evident that compliant VTS concepts are still in the early stages of development, underscoring the need for a comprehensive review to gain deeper insights into the limitations of compliant VTS mechanisms.

Review on methods of variable torsional stiffness

Tzu Lee

Abstract—This literature study presents an overview of the designs of variable torsional stiffness mechanisms. The working principles employed in the designs are classified into four categories: material property, geometric structure, prestress, and boundary condition. Adjusting one or more of these factors allows the torsional stiffness to be varied as desired. A comprehensive comparison of the designs is done based on selected criteria in the aspect of stiffness, deflection, energy efficiency etc., and real-life application constraints such as compactness and light-weightiness. Due to the huge qualitative difference between fully compliant mechanisms and rigid-body mechanisms incorporating elastic elements, two evaluation tables are formed separately to compare the designs in a more accurate manner. It is found that while recent designs show great improvement in compactness, they usually have a trade-off between performance and complexity, illustrating the importance of optimization for practical application.

Index Terms - Variable torsional stiffness, material property, geometric structure, prestress, boundary condition, compliant and rigid body mechanism

I. INTRODUCTION

In the field of mechatronic design, stiffness plays a vital role in determining the level of precision and safety. High stiffness allows for precise position control and enhances the robustness of the structure while low stiffness allows for precise force control and provides a safer working environment. In order to achieve both features, and be able to tune stiffness on demand, variable stiffness design has become a promising topic that is of interest in various fields.

In aerospace engineering, variable stiffness contributes to the shape-morphing ability of the wings. In biomechanical engineering, changing the stiffness allows reproducing physiological structures in animals to mimic their advantageous behavior [1]. Medical devices featuring variable stiffness ensure an intrinsically safer yet still precise interaction between the patient and the instruments [2]. Other applications include using variable stiffness to output different haptic feedback, and enlarging the bandwidth of sensible force [3] [4]. In addition, variable stiffness facilitates the controllability of natural frequencies, therefore can also be used in the following frequency-dependent applications: actuators and sensors

with customized sensitivity and resolution [5], energy harvesters that can tune the stiffness to collect energy from ambient vibrations of a wide range of frequencies [6], vibration dampers that adjust their resonant frequencies to filter out targeted vibrations [7], resonant tip-tilt mirrors with changeable passive scanning speed [8], mechanical transistors that allow or prevent stress waves to pass through. Among all types of stiffness, the tunability of the torsional stiffness is especially beneficial for designing robot joints, variable stiffness actuators (VSA), and human joint rehabilitation devices.

This review aims to gather the existing variable torsional stiffness designs. First, sort them into two groups based on component characteristics. Second, classify them into four categories based on working principles, and finally by analyzing the data obtained from the literature, compare their advantages and shortcomings for future researchers reference.

The rest of this review is structured as follows: Section II starts with the search method for variable torsional stiffness designs. The reason for separating the gathered designs into two groups: rigid-body mechanisms and fully compliant mechanisms is stated afterward. Moreover, four types of working principles for varying stiffness are explained. In section III the designs found in the literature are examined and further classified based on their working principles. In section IV quantitative comparisons of the designs are performed under a list of criteria, giving readers an insight into the gap between existing solutions and future objectives. Section V concludes this review.

II. METHOD

A. Search method

The literature introduced in this review are found using Google Scholar as the search engine. The following keywords as shown in Table I are cross-coupled with OR/AND operators to systematically search for variable torsional stiffness designs.

B. Rigid-body-based VS fully compliant mechanism

It is found in the literature that in the past, variable stiffness designs are mostly accomplished by assembling

elastic elements (e.g., springs, belts, beams) and rigid parts (e.g., lead screws, pulleys, rollers). In some cases, the mechanisms can achieve zero to infinite stiffness and infinite stroke by adjusting the transmission ratio between components. However, these conventional rigid-body-based mechanisms suffer from low power-to-weight ratio, low efficiency due to friction, low precision due to backlash, complex assembly, higher cost, and low compactness. In order to eliminate these problems, recent designs indicate a trend of using fully compliant mechanisms to replace rigid parts, as fully compliant mechanisms can be fabricated monolithically and thereby solving all the problems resulting from assembling. Moreover, since multiple states are integrated into a simple monolithic configuration, devices can be miniaturized for metamaterial applications. On the other hand, due to intrinsic compliance, fully compliant mechanisms are impossible to reach infinite stiffness, and their range of motion is usually limited by material property. As a result of the incomparable and distinct nature between rigid-body-based mechanisms and fully compliant mechanisms, the designs are categorized into the two aforementioned groups and the comparisons are done separately to ensure fidelity.

C. Classification - working principles for changing stiffness

The working principles presented in the literature can be classified into four categories based on the factors that influence the stiffness of the mechanism.

1) *Material property*: Smart materials are materials whose properties can be controlled by external stimuli. For example, shape memory alloys/polymers (SMA,SMP) change phases under different temperatures. Magnetorheological fluids (MRF) changes viscosity when subjected to different magnetic field intensity. These smart materials are commonly used in variable stiffness designs since the stiffness can be varied dramatically due to phase change.

2) *Geometric structure*: Unlike the other three working principles, which change the stiffness by employing external stimuli or external constraints, this category describes the concepts whose stiffness is inherently changed. This means that different stages of stiffness are built within the structure. When the shape of the structure is changed, the second moment of area along with the stiffness changes correspondingly. Therefore, the major disadvantage of this working principle is that the stiffness is constantly changing when deforming. On the other

hand, variable stiffness can be achieved without extra excitation or additional counterparts.

3) *Prestress*: Elastic elements such as springs and beams can store energy when subjected to stress. This energy is sometimes converted into stiffness. Normally, the stiffness increases proportionally with stress until the material buckles or the yield stress is reached. At this stage, the stiffness experiences a drastic drop, enabling the structure to exhibit negative stiffness.

4) *Boundary condition*: In this category, stiffness is tuned by changing the constraint conditions such as varying the effective length of elastic elements and implementing contact-aided mechanisms (e.g., guideways). Designs operating on this working principle usually require additional restraint components, resulting in larger and heavier configurations. Moreover, the interaction between components induces problems of friction and inaccuracy.

AND			
variable	torsional	stiffness	actuator
changeable	rotational	impedance	joints
adjustable		compliance	designs
controllable			metamaterials
tunable			mechanism
adaptive			exoskeleton

TABLE I: Search terms

III. RESULTS

In sections III-A and III-B, variable torsional stiffness designs found in the literature are displayed in an organized way according to the categories addressed in Section II. Section III-C comprehensively compares the performance of the designs based on a list of criteria.

A. Rigid-body-based mechanism

1) *Material properties:* In [9] proposed a design of changeable stiffness magnetorheological fluids (MRF) leg. The variation of torsional stiffness is accomplished by the design of the MRF damper shown in Fig. III. Within the damper, MRF is stored in the reservoir formed by the outer cylinder, piston, side cover, and electromagnetic coil. When MRF is subjected to different magnetic fields caused by current, the viscosity alters correspondingly and thereby changing the torsional stiffness of the damper. Although the control of torsional stiffness is instantaneous, MRF dampers suffer from hysteresis which leads to nonlinear characteristics. [10] proposes a self-adapting model to accurately describe this nonlinear hysteretic characteristic under varying conditions.

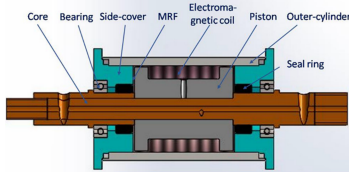


Fig. 1: Structure of the rotary MRF damper.

In [11], a shape memory alloy-based torsional elastic component (SMA-TE) is presented Fig. 2. Two pairs of SMA springs connected by an output shaft are arranged confrontationally. When the SMA springs are heated or cooled respectively, temperature-induced phase transformation occurs and causes the output shaft to experience torsional stiffness changes due to the special configuration of SMA-TE. Other similar but more compact concepts are proposed in [12] and [13]. Two antagonistically arranged SMA or shape memory polymer (SMP) springs allow for continuous adjustment of torsional stiffness Fig. 3 and Fig. 4 by controlling the temperature. SMA/SMP-based variable torsional stiffness concepts are found in many papers, yet they all operate on the same principle as mentioned above. The range of torsional stiffness can be easily determined by the spring parameters and arrangement. Despite the advantage of an extremely high power-to-weight ratio, SMA/SMP springs suffer from slow response, hysteresis,

and nonlinearity, which reduces the overall performance and limits their application. Therefore, research regarding the optimization of the properties of SMA/SMP is of crucial importance [14] [15].

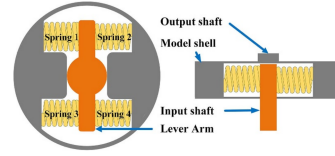


Fig. 2: Simplified SMA-TE structure model.

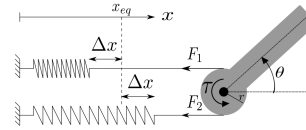


Fig. 3: Schematics of variable stiffness joint with two antagonistic SMP springs

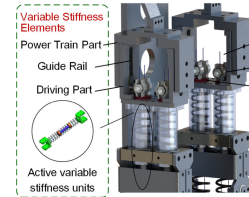


Fig. 4: Structure of variable stiffness elements used in knee exoskeleton.

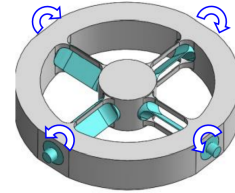


Fig. 5: Structure of rotary flexure hinge.

2) *Geometric structure:* In [16], a structure-controlled variable stiffness actuator (VSA) based on rotary flexure hinges is designed. It is known that the second moment of area is a geometric factor that influences the stiffness of structures. In this design, the authors make use of this property to realize variable torsional stiffness by circularly stacking four rotary flexure shafts (RFS) (light blue) in a stationary housing (grey) Fig. 5. When the RFSs rotate around their geometry centerline, the second moment of area with respect to the frame alters, thereby changing the torsional stiffness of the output shaft. Noted

that as addressed in Section II, a disadvantage of the category of geometric structure is the constantly varying stiffness under an applied torque. This design is a special case that contradicts the statement in Section II. It solves the problem by using additional actuation to separate the input shaft and output frame, making it possible to control stiffness and position separately. An issue of parasitic deflection of RFSs is observed when torque is applied at the output frame (Fig.6). In order to minimize this deflection, a follow-up work [17] studies and compares the performance of six configurations with different numbers of RFSs and different rotation directions.

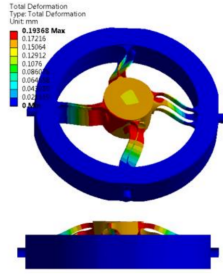


Fig. 6: Parasitic deflection of RFSs.

3) *Prestress*: In [18], a wearable joint support with variable stiffness is shown. Based on granular jamming technique, the stiffness of this device can be tuned by confining the space in which the granular particles are placed Fig.7. As the air in the tubes is vacuumed out, the distance between granular particles decreases, leading to higher internal friction, which further increases the stiffness of the device in all directions. The disadvantages of this technique are that uni-directional stiffness control is not possible. Also since the movement of the granular particles is less predictable than layer jamming technique [19], the precision performance of this design is rather unsatisfactory.

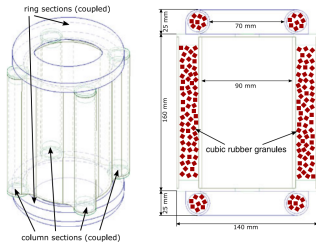


Fig. 7: Structure and cross-section of the granular jamming sleeve.

In [20], 8 antagonistic variable stiffness joints based on equivalent quadratic torsion spring (EQTS) are demon-

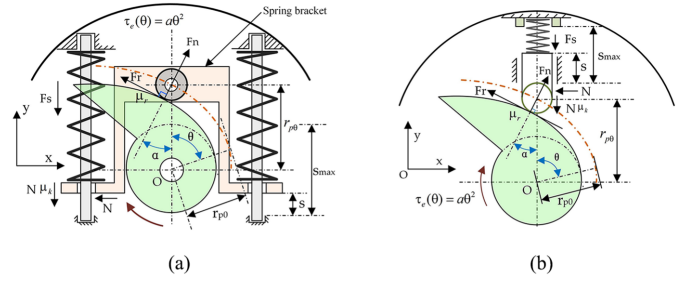


Fig. 8: (a) The conceptual layout of the EQTS and (b) the schematic of the EQTS

strated. These concepts arrange nonlinear springs antagonistically against a cam with a designed profile Fig.8. When the cam rotates, its profile changes the prestress in the springs, allowing for stiffness variation of EQTS. Other designs that utilize the prestress in compression springs to adjust torsional stiffness are presented as follows: In [21], a Mechanically Adjustable Compliance and Controllable Equilibrium Position Actuator (MACCEPA) is used for controlling passive walking. Below depicts the 3 essential parts of MACCEPA: a left body (upper leg), a smaller lever arm, and a right body (lower leg), which all pivot around a common rotation axis Fig.9. There are two ways to adjust the torque on the right body. One is angle-dependent whereas the other is pretension-dependent. When the right body moves away from its equilibrium position ($=0$), the force due to the elongation of the spring will generate a torque, trying to restore the right body to its equilibrium position. Therefore, the torque increases with α . For a fixed angle α , the torque can be varied by pulling the cable connected to the spring to generate pretension in the spring, forming an equivalent variable stiffness torsional spring at the pivot point. The MACCEPA concept is later used in many applications [22] [23] [24] [25]. (Fig.10 Fig.11 Fig.12 Fig.13) Noted that in [25], the right body and lever arm are replaced by a disk and a cam respectively so as to perform infinite number of turns.

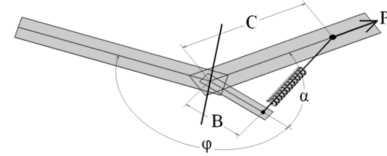


Fig. 9: Fundamental structure of MACCEPA

4) *Boundary condition* : In [26], a magnetic variable stiffness spring-clutch (MAVERIC) is presented Fig.14. The device is composed of an inner rotor and an

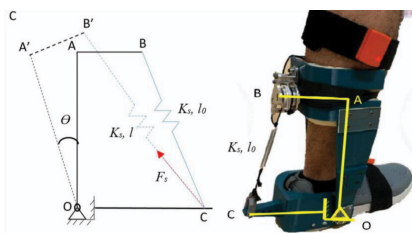


Fig. 10: Schematic and realization of an augmentation ankle skeleton

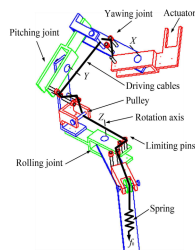


Fig. 11: Structure of a wrist joint

outer rotor, which are both magnetized radially with even numbers of poles. By adjusting the axial offset of the inner magnet, the overlapping area of two magnetic fields is changed accordingly. As a result of the combined magnetic attraction and repulsion force, the torsional stiffness between two rotors can be tuned. One of the advantages of these magnetic springs is that the maximum stroke can be easily increased by stacking more magnetic springs along the rotational axis. However, the torsional stiffness variation of this design is nonlinear which in some cases is undesirable. Two solutions are found in [27] and [28]. In [27], the inner rotor (green component shown in Fig. 15a) is magnetized axially rather than radially to achieve linearity. While in [28], the air gap between two rotors is specially designed with respect to the relative angle in order to compensate for the non-linearity Fig. 15b.

It is noticed that a great number of designs found in the literature achieve variable torsional stiffness by changing the effective length of elastic elements. The shorter the effective length, the stiffer the elastic element. For example, [29] demonstrates a variable torsional stiffness (VTS) mechanism using a relocatable counter bearing to adjust the effective length of an elastic torsion element (Fig. 16). two follow-up works are presented in [30] and [31], which respectively discuss the dimensioning of the elastic element and power analysis for optimization purposes. In

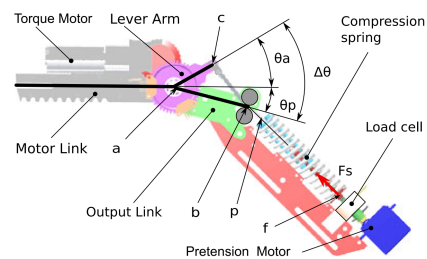


Fig. 12: Structure of a modular smart variable stiffness actuators

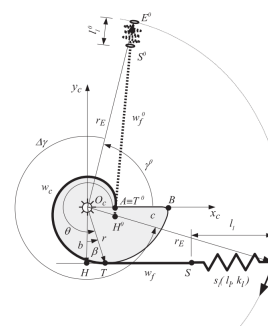


Fig. 13: Schematic of Rotational cam-based VSA

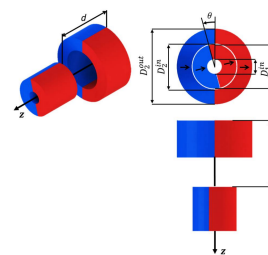
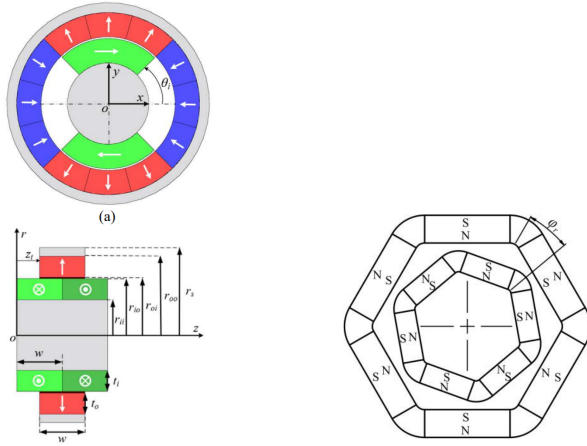


Fig. 14: Permanent magnet set up of MAVERIC

[32], [33] and [34], relocatable flanges (Fig. 17), rollers (Fig. 18) and sliders (Fig. 19) are used to clamp the beams at desired locations and thereby changing the effective length of the beams. These designs have the advantage of being relatively compact and simple compared to those using conventional springs. However, the maximum allowable deflection decreases when the effective length is shortened. A solution to this problem is to stack more elastic elements circularly [35]. This way the higher stiffness state can be achieved without compromising the deflection range.

In [36], a VSTA transverse plane adapter (Fig. 20) works on the same principle to vary its torsional stiffness. Noted that there is a functional difference between the lever arm C in [36] and the elastic element used in [29] and [32]. Although variable stiffness is still realized by changing the effective length of the lever arm, the main



(a) Front view and side view of a variable stiffness torsional magnetic spring

(b) A variable stiffness torsional spring based on flat magnets FMS

Fig. 15: Two solutions to eliminate nonlinearity in MAVERIC

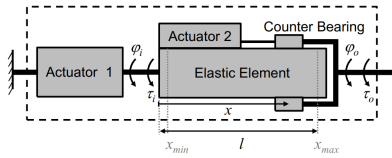


Fig. 16: Schematic of VTS mechanism

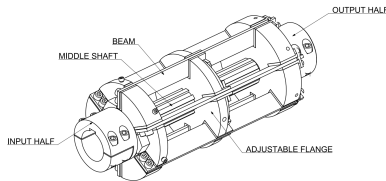


Fig. 17: VTS mechanism with relocatable flanges

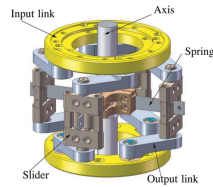


Fig. 18: VTS mechanism with relocatable rollers

elastic element in [B6] is the torsional spring. The lever arm simply acts as the media between the input torque and the torsional spring with a variable transmission ratio. This setup allows for infinite stiffness (locked) when the pivot coincides the carriage D, yet on the other hand, the misalignment of the pivot and the torsional spring center will lead to the lengthening of the lever arm when VSTA

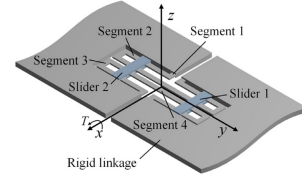


Fig. 19: structure of Inside-Deployed Lamina Emergent Joint (ID-LEJ).

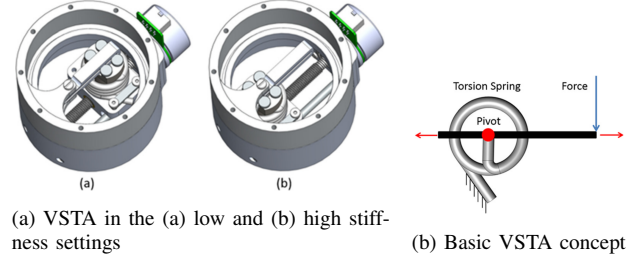


Fig. 20: Design detail of VSTA.

is rotated. To eliminate this problem, the same research team proposed another VSTA-ii [B7](Fig.21). Instead of using a lever arm to change the transmission ratio, VSTA-ii uses five torsion springs in parallel to provide five discrete stiffness together with an additional locked state. The variation of stiffness is achieved by switching on/off the torsional springs.

[B8] proposes another VSA that can change the transmission ratio between the input torque and output angular deflection (Fig.22). The mechanism as shown in fig consists of an input link, a rigid lever that is pinned to a compliant flexure at one end, and a movable pivot point for changing the transmission ratio. Since the input link and lever have non-concentric centers, the angular deflection of the rigid lever θ depends not only on the deflection of the input link, ϕ , but also on the pivot point position, 12. Compared to the effective length-dependent concepts, the advantage of changing the transmission ratio is that the maximum deflection will not diminish when increasing the stiffness, since the length of the compliant flexure is fixed.

B. Fully compliant mechanism

1) *Material properties*: None of the designs found in the literature fits in this category.

2) *Geometric structure*: [B9] presents a variable stiffness filleted leaf hinge as shown in Fig.23. The planer hinge consists of a flexible segment and 12 rigid supports. When the segment deforms, the rigid support contacts

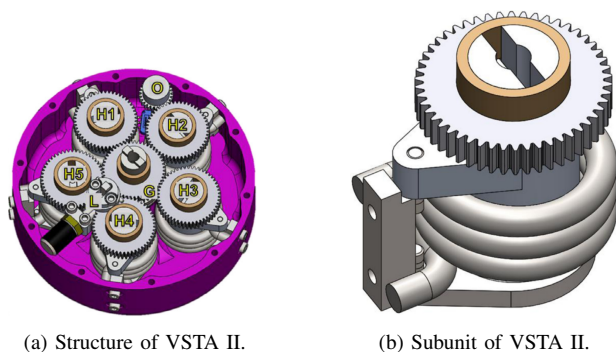


Fig. 21: Design detail of VSTA II.

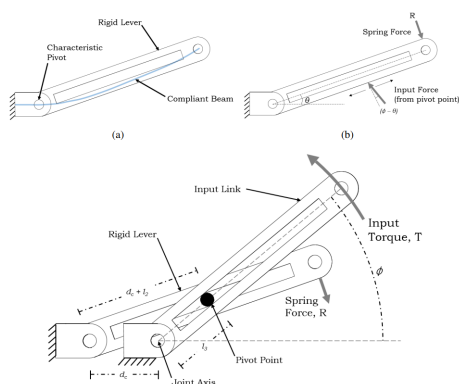


Fig. 22: Functional diagram of the transmission compliant VSA

the segments and changes its effective length, thereby changing the hinge stiffness (Fig. 24).

In [40], a variable stiffness joint (VSJ) uses two compliant transmission elements (CTE) shown in Fig. 25 as nonlinear torsional springs. This nonlinearity allows for the variation of joint stiffness, which is dependent on the angular deflection of the CTEs. Due to the asymmetric geometry of the CTE, two CTEs should be mounted antagonistically to achieve symmetric behavior. With two motors connected to the two nonlinear springs, this kind of antagonistic joints has the advantage to control its position and stiffness separately as shown in fig.

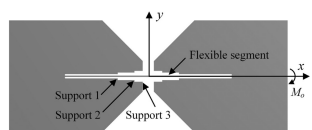


Fig. 23: Variable stiffness filleted leaf hinge.

3) *Prestress*: In [41] presents a compliant mechanism that uses bistable switches to buckle and unbuckle the wire beams to achieve binary stiffness (i.e., high and

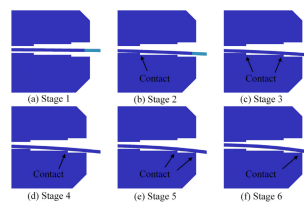


Fig. 24: Six deformation stages of leaf hinge.

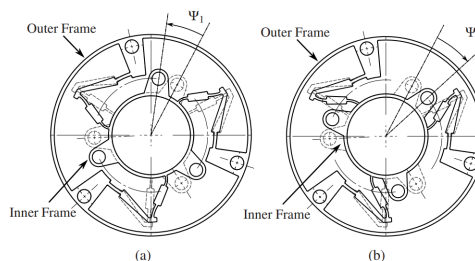


Fig. 25: Different deformation of the CTE leading to different torsional stiffness.

low stiffness) along two degrees of freedom Fig. 26. The fundamental principle of this mechanism is stiffness cancellation. When flexible elements with positive stiffness are placed in parallel with those with negative stiffness, the stiffness cancels out and the mechanism exhibits zero stiffness. In this case, the wire beams shown in fig exhibit negative stiffness when theyre buckled by the bistable switch. This negative stiffness cancels out the positive stiffness from the leaf springs and allows for the low-stiffness state of the mechanism. When the beams are unbuckled, they exhibit positive stiffness and constraint the 2 degrees of rotational freedom, leading to the higher-stiffness state. Another design with the same working principle is presented in [42](Fig. 27). However, instead of using wire beams as elastic elements, plate springs are employed to ensure a planer motion, providing extremely high stiffness in other directions.

4) *Boundary condition*: In [43], a tunable variable-torque compliant hinge using open-section shells is proposed as demonstrated in Fig. 28. The design employs a pair of symmetrically arranged open-section shells (building blocks) as the elastic element. They are connected by a rigid segment to which a follower is attached. Around this rigid segment, a contact-aided guideway is used to guide the follower. As the follower slides through the guideway, the varying contact force bends and twists the open-section shells, therefore providing target torque at particular angles. By changing the profile of the guideway, the torsional stiffness about the rotational axis can be designed. To achieve large range deflection, the

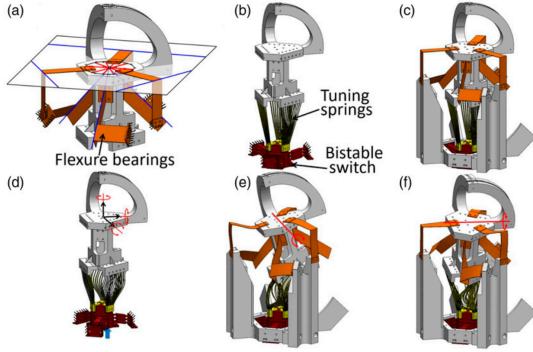


Fig. 26: Binary-stiffness compliant mechanism design that achieves two rotational DOFs.

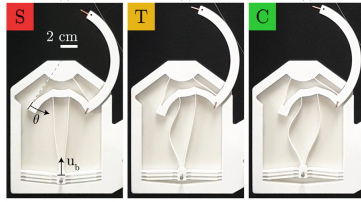


Fig. 27: A chronological photo sequence of the rotary device from stiff to compliant.

elastic elements are arranged in series. This configuration however leads to a trade-off between compactness and rotational axis drift. Moreover, since the contact force simultaneously influences the geometry and stress of the open shells, it is hard to derive an analytical model for torsional stiffness. FE simulation is also computationally expensive since torque is a function of θ , s , and $ds/d\theta$. As a result, the authors proposed a strain energy-based design method for guideway profile synthesis, in which the strain energy only depends on θ and s .

[11] proposed a variable stiffness flapping (VaSF) mechanism inspired by dolphins (Fig. 29). The main concept is to compress and extend the mechanism as shown in fig in order to change the shape (second moment of area) of the compliant segments and thereby tune the bending and torsional stiffness of the mechanism.

IV. DISCUSSION

A. Evaluation

Table I and Table II compare the performance of rigid-body-based and fully compliant mechanisms. Noted that not all the designs mentioned in Section III are listed in the tables since some of them operate on the same principle, and the difference only lies in the dimensions and irrelevant components. The fact that slight changes in dimensions could lead to large variations in stiffness

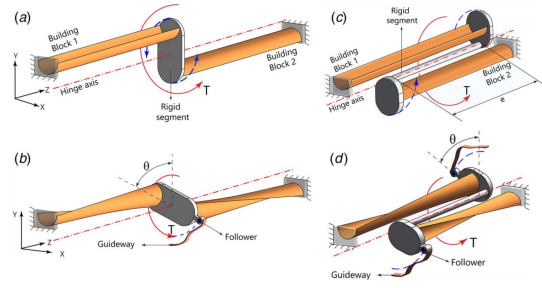


Fig. 28: Compliant-hinge mechanism with tunable-torque-angle characteristics: (a) compliant hinge with no offset, (b) tunable-torque mechanism with no offset, (c) compliant hinge with finite offset, and (d) tunable-torque mechanism with a finite offset.

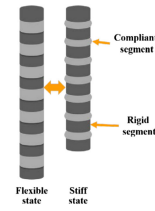


Fig. 29: Schematic of VaSF mechanism.

obscures the intended focus of working principle-related differences. As a result, only one design is chosen from similar concepts for comparison.

The criteria are chosen based on the accessibility of data in the literature. In other words, criteria such as compactness, stiffness and deflection range are usually specified in the literature. Hence, they are included in the comparison tables. Whereas criteria such as manufacturability, modularity, and recyclability are rarely mentioned in the literature and can only be inferred from the authors (the author of this review) point of view. Hence, they are excluded and are later discussed in a more general way. This being said, not all literature provides sufficient data for the criteria in the tables, therefore, the " \emptyset " sign is used to represent the unspecified data. In addition, the "-" sign under the light-weight column means the devices are relatively heavy, even though the value is not presented, the weight level can be easily deduced from size and material.

The column linearity describes the relation between actuation and torsional stiffness, while actuation is the stimuli that influence the stiffness. For example, in the case of MRF-damper, the stiffness is adjusted by controlling current, and the relation between current and torsional stiffness is linear. The torsional stiffness of angle-actuated designs only depends on the input an-

	stiffness(Nm/rad)			deflection(deg)			compactness	light-weight(kg)	actuation	precision	energy efficiency	reaction time(s)
	range	linearity	continuity	range	direction	DoF						
MRF damper [9]	0	lin	con	infinite	bi	1	d=36mm l=60mm	-	current	high	low	0
SMA-TE [10]	2.6 - 6.8	quasi-lin	con	12	bi	1	68x26mm	0.3	temperature angle	low (temp)	low	2.52
antagonistic SMA [13]	0	quasi-lin	con	40	bi	1	l=140mm	0.0685	temperature angle	low (temp)	low	1.4
rotary flexure [16]	323.7-1444.5	non-lin	con	6	bi	1	d=150mm l=120mm	2.83	motor	low (parasitic)	high	0.83
granular jamming [18]	0.37-0.5	non-lin	con	55	bi	4	l=210mm	0.7	pressure	very low (high fric)	fair	20
EQTS-i [20]	4.5-8.78	lin	con	126	uni	1	0	0	angle	high	very high	0
smart MACCEPA [24]	5-110	lin	con	60	bi	1	0	2.4	servo motor	high	high	10
RotWWC-SEA [25]	Max/min ratio=10	non-lin	con	114.6	bi	1	r >1m	-	motor	high	high	0
MAVERIC [26]	-/+ 0.11	lin for small deg	con	90/Npp	bi	1	d=115mm l=55.3mm	-	0	high	high	0
linear magnet [27]	-/+ 47.6	lin	con	45	bi	1	d=47mm	1.8	motor	high	high	0
FMS [28]	0	lin	con	31.5	bi	1	0	-	motor	high	high	0
relocatable flange [32]	8k-26k	non-lin	con	0	bi	1	d=157mm	0	manual/motor	fair (friction)	high	0
relocatable roller [33]	252-3648	non-lin	con	0	bi	1	d=146mm l=144mm	4.95	motor	fair (friction)	high	0
ID-LEJ [34]	0.1-0.28	quasi-lin	con	0	bi	1	40x38mm	0	manual	low (axis shift)	high	0
VSTA [36]	6.9-52.1	lin	con	30	bi	1	d=111mm l=90mm	1.56	motor	low (axis shift)	high	0
VSTA II [37]	17.8-73.9	non-lin	discon	30	bi	1	d=104mm l=75mm	0.88	current	fair (friction)	fair	0.03
transmission VSA [38]	0-5.16	lin	con	0	bi	1	~60x60mm	0	servo motor	fair (friction)	high	0

Note: compactness is the volume of the mechanism and working space altogether.

TABLE II: Comparison of Rigid-body-based mechanisms

	stiffness(Nm/rad)			deflection(deg)			compactness	light-weight(kg)	actuation	precision	energy efficiency	reaction time(s)
	range	linearity	continuity	range	direction	DoF						
filleted leaf [39]	0.2-0.74	non-lin	discon	0	bi	1	100x40x10mm	0	angle	high	very high	0
CTE [40]	0.3-120	non-lin	con	60	uni	1	d=46mm l=4.7mm	0	angle	high	very high	0
binary 2DoF [41]	1.7-17.2	non-lin	binary	0	bi	2	~d=16cm ~l=24cm	-	manual	high	high	0
binary 1DoF [42]	0.01-10.2	non-lin	binary	23	bi	1	10x12x0.7cm	0	manual	high	high	0
open shell [2]	max=24	non-lin	con	50	bi	1	d=94mm l=400mm	0	angle	low (axis drift)	very high	0
VaSF [11]	0	non-lin	con	0	bi	3	0	0	servo motor	high	high	0

Note: compactness is the volume of the mechanism and working space altogether.

TABLE III: Comparison of fully compliant mechanisms

Grade	Description
very high	Energy is not required for changing stiffness and maintaining stiffness.
high	Energy is only required when changing stiffness.
fair	Energy is only required when changing stiffness, but the changing duration is long or multiple actuation is needed.
low	Energy is required for changing stiffness and maintaining stiffness.

TABLE IV: Four grades of energy efficiency.

gular deflection and is not stimulated by any external actuation. The column deflection range is the maximum relative deflection between the equilibrium position and deform position. However, infinite number of turns can be achieved regardless of the deflection range as long as the equilibrium position can vary 360 deg. The column precision specifies the cause of performance degradation, including ambient temperature-sensitive characteristics, parasitic deformation, friction-induced energy loss, and output axis drift. As the power-to-performance ratio of the designs is difficult to evaluate in absence of energy consumption data, the column energy efficiency is graded based on the standards displayed in Table IV.

B. Performance comparison

Numerous variable torsional stiffness designs are listed in Section III. Since they operate on a wide variety of principles and thus exhibit vastly distinct properties, it is hard to tell which designs excel the others at first glance. In order to qualitatively compare the designs for future applications, the performance of the design from the tables is discussed below.

1) *Rigid-body-based mechanism:* To begin with, one of the most essential criteria is stiffness range. As can be seen in Table III, designs that tune stiffness by varying the effective length or second moment of area of compliant elements have the largest maximum stiffness ([33][32][16]). However, the high intrinsic stiffness of the material leads to a larger minimum stiffness, which not only results in lower max-to-min stiffness ratios but also limits the maximum deflection since the internal stress increases sharply with stiffness. Although magnetic springs ([26][27][28]) have adequate stiffness ranges and can exhibit negative stiffness, the major drawback lies in the cost and the maximum deflection, which the latter is always less than 90 degrees. This is because the magnetic spring should contain at least one pole pair (180 deg/pole), when the outer rotor rotates more than 90 degrees, the torsional stiffness starts to repeat its value with an opposite sign. For SMA-TE and transmission VSA, both the stiffness range and maximum stiffness are small. A possible explanation could be that the size of these two designs are roughly two times smaller than the others. Even though it is reasonable to assume their stiffness will increase with the dimensions, the analytical relation between dimensions and stiffness is not stated in the literature, making their stiffness performance incomparable to the other designs. Among all, designs that tune stiffness by prestressing springs ([20][24][25]) have the highest max-to-min stiffness ratio

and the largest maximum deflection. For the deflection direction, cam-based structures or asymmetric geometry only provide unidirectional stiffness change. This issue is however trivial since bi-directional stiffness can be easily achieved by an antagonistic arrangement.

The weight of the devices is of crucial importance when it comes to exoskeletons or aerospace applications. SMA and granular jamming designs have extraordinary weight performance compared to the others. This is mainly a result of their actuation type and simpler configuration. Without the heavy motors and additional moving parts, the weight can be significantly reduced. However, the downside of using temperature as the actuation is that the precision is easily affected by ambient temperature and the reaction time is long, especially during the cooling process. As for pressure-actuated designs, the reaction time is even longer than temperature-actuated ones. Noted that the reaction time of smart MACCEPA is also long, yet this is not a consequence of actuation, the main cause is the processing time of its closed-loop feedback system. Apart from temperature, friction is another critical factor that reduces the precision of the designs. The moving flanges, rollers, or sliders used to change the effective length of compliant elements usually generate friction. Moreover, the clearance between contacting parts also deteriorates the precision performance. Energy efficiency is an important indicator of cost. Unlike the other categories which can employ non-back-drivable actuation to hold the deflected components, the designs from the material property category require constant energy input for devices to maintain their stiffness, hence the lower energy efficiency.

In addition to the above criteria, there are some qualities that also help in the decision-making process. For example, fail-safe is important for human interaction. Magnetic springs have a higher safety level since overloading will not lead to any damage to the springs due to lack of contact. Materials with hysteresis issues such as SMA and magnets have lower repeatability which introduces errors in stiffness. The recyclability of MRF is low because of material degradation. Depending on the components used, the modularity and testability can also be evaluated.

In conclusion, the prestress category has the best overall performance. This includes wide ranges of stiffness, large maximum deflection, high precision, and high energy efficiency. However, to prestress the springs, motors are still the most commonly used actuator, which compro-

mises the light-weightness of the designs. Besides, conventional springs lead to high complexity of assembling, making it difficult to implement the prestress designs in small-scale devices. One way to improve the light-weightness and compactness is to replace conventional springs with simple compliant elements such as beams, leaf springs, or shell-like structures. With a lighter and smaller structure, the prestress can then be done by piezoelectric or thermal actuators, eliminating the need for bulky motors. This has shown the promising future of fully compliant mechanisms.

2) *fully compliant mechanism*: At this moment, fully compliant VTS designs are still in their early stages. Only very few concepts are found in the literature, and their working principle often fits into multiple categories. In compliant designs, the boundary condition acts more like an actuation for changing the geometric structure (second moment of area) or changing the prestress in elastic elements. As a result, the working principle of the existing fully compliant VTS can be simplified into two categories: geometric structure and prestress. The former has specially designed geometry that allows torsional stiffness to vary with input angular deflection. This stiffness variation is intrinsic and though it doesn't require additional actuation, these designs aren't able to remain at the same stiffness stage for a large range of deflection. On the other hand, the latter often uses bi-stable switches or other position-confining components to introduce stress into compliant elements. This stress-dependent stiffness change can be further divided into two stages: before buckling and after buckling. Usually the stiffness increases with preload, however, when the stress is large enough to buckle the elastic element, the stiffness drops drastically to a negative value. This characteristic provides large ranges of stiffness over large ranges of deflection.

For other criteria, it is shown that all fully compliant mechanisms have rather high precision and high energy efficiency, except for the open-shell design that suffers from a trade-off between deflection range and axis drift. Although to improve precision, the deflection range might be compromised, open-section shells can still undergo larger rotational deformation with significant bending and axial stiffnesses compared to compliant beams. The compactness is less relevant for performance comparison of planer designs since the dimensions can be easily scaled down. To conclude, when constant stiffness over a large range of deflection is not required, the geometric structure category is preferred in terms of simplicity. When large stiffness and deflection range or negative

stiffness are favored, the prestress category would be a more suitable choice.

V. CONCLUSION

Variable torsional stiffness (VTS) has become a promising field of research for multi-task integration and environmental adaption. This review gathers, examines, and compares the VTS designs through two aspects of classification. The first classification is component-based: (i)rigid-body-based and (ii)fully compliant mechanism. The second classification is working principle-based: (a)material property, (b)geometric structure, (c)prestress, and (d)boundary condition. These classification methods help analyze the advantages and disadvantages of VTS designs. When design purposes or parameters are chosen, referring to these results and insights provides a more efficient way to fulfill the expectation. The working principles of the rigid-body-based VTS designs mainly fall into the boundary condition category, more specifically changing the effective length of elastic elements. This principle simplifies the stiffness calculation and design process as compared to other categories. Prestressing is also popular for it has the best overall performance. In comparison, only two smart materials were found for VTS application. Since they are relatively new concepts, the material property category is mainly in its experimental stage and both its technology and business readiness are low. The geometry structure category gets rid of the need for additional actuation, therefore allowing for instant stiffness change. However, the stiffness calculation is complicated and often can only be done by FEM or experiments.

Although the existing fully compliant VTS designs are mostly conceptual, optimization is not accounted for and their real-life applications are undetermined, the monolithic characteristic still shows their prospects in the microscopic world. If stiffness can be altered within a miniature module, stacking the modules could form significant changes in the properties.

Future work for VTS researchers includes performance optimization, enhancing the technology/business readiness, and identifying the bottleneck of fully compliant VTS design. Another potential research field is the multi-DoF VTS mechanism. So far the works mainly focus on 1 DoF, which in the compliant scope can also be considered as planer motion. The development of spatial VTS could be beneficial for designing artificial ball joints and contribute greatly to the field of soft robotics.

REFERENCES

- [1] Y. J. Park, T. M. Huh, D. Park, and K.-J. Cho, "Design of a variable-stiffness flapping mechanism for maximizing the thrust of a bio-inspired underwater robot," *Bioinspiration biomimetics*, vol. 9, p. 036002, 03 2014.
- [2] S. Hampali, A. Pai, and G. Ananthasuresh, "A tunable variable-torque compliant hinge using open-section shells," *Journal of Mechanisms and Robotics*, vol. 12, pp. 1–25, 06 2020.
- [3] O. C. Kara and V. Patoglu, "Vnstylus: A haptic stylus with variable tip compliance," *IEEE Transactions on Haptics*, vol. 13, no. 4, pp. 777–790, 2020.
- [4] M. Smreczak, L. Rubbert, and C. Baur, "Design of a compliant load cell with adjustable stiffness," *Precision Engineering*, vol. 72, pp. 259–271, 2021.
- [5] K. Takashima, K. Ota, and H. Cho, "Variable-sensitivity force sensor based on structural modification," *Sensors*, vol. 23, no. 4, 2023.
- [6] P. Ibrahim, O. Nassar, M. Arafa, and Y. Anis, "On adjusting the rotary inertia of a cantilever-type energy harvester for wideband operation," *Procedia Engineering*, vol. 199, pp. 3422–3427, 12 2017.
- [7] Q. Wang, G. Senatore, K. Jansen, and P. Habraken, Arjanand Teuffel, "Vibration suppression through variable stiffness and damping structural joints," *Frontiers in Built Environment*, vol. 6, 2020.
- [8] G. Aigouy, A. Guignabert, E. Betsch, C. Cote, J. Rebufa, X. Lepine, M. Fournier, S. Duc, O. Sosnicki, P. Personnat, and F. Claeysen, "Large stroke fast steering mirror for free-space optical communication," p. 203, 06 2021.
- [9] J. Zijun, S. Shuaishuai, O. Yiming, Z. Shiwu, L. Weihua, and Z. Jinjin, "Design and modeling analysis of a changeable stiffness robotic leg working with magnetorheological technology.," *Intelligent Material Systems and Structures*, pp. 3725–3736, 2018.
- [10] X. Lian, H. Deng, G. Han, M. Ma, X. Zhong, Y. Gao, and R. Hu, "Self-adapting model for variable stiffness magnetorheological dampers," *Smart Materials and Structures*, vol. 31, p. 025006, dec 2021.
- [11] J. Xiong, Y. Sun, J. Zheng, D. Dong, and L. Bai, "Design and experiment of a sma-based continuous-stiffness-adjustment torsional elastic component for variable stiffness actuators," *Smart Materials and Structures*, vol. 30, p. 105021, sep 2021.
- [12] M. Folgheraiter, B. Aubakir, and H. A. Varol, "Thermally-controlled coiled polymeric wire as a novel variable elastic element," in *2017 IEEE International Conference on Advanced Intelligent Mechatronics (AIM)*, pp. 466–471, 2017.
- [13] J. Zhang, M. Cong, D. Liu, Y. Du, and H. Ma, "A lightweight variable stiffness knee exoskeleton driven by shape memory alloy," *Industrial Robot: the international journal of robotics research and application*, vol. ahead-of-print, 02 2022.
- [14] A. Li, A. Challapalli, and G. Li, "4d printing of recyclable lightweight architectures using high recovery stress shape memory polymer," *Scientific Reports*, vol. 9, p. 7621, 05 2019.
- [15] S. Poorasadion, J. Arghavani, R. Naghdabadi, and s. Sohrabpour, "An improvement on the brinson model for shape memory alloys with application to two-dimensional beam element," *Journal of Intelligent Material Systems and Structures*, vol. 25, pp. 1905–1920, 11 2013.
- [16] X. Li, W. Chen, and W. Lin, "Design of a structure-controlled variable stiffness actuator based on rotary flexure hinges," pp. 45–50, 05 2017.
- [17] X. Li, H. Zhu, W. Lin, W. Chen, and K. H. Low, "Structure-controlled variable stiffness robotic joint based on multiple rotary flexure hinges," *IEEE Transactions on Industrial Electronics*, vol. 68, no. 12, pp. 12452–12461, 2021.
- [18] S. Hauser, M. Robertson, A. Ijspeert, and J. Paik, "Jammjoint: A variable stiffness device based on granular jamming for wearable joint support," *IEEE Robotics and Automation Letters*, vol. 2, no. 2, pp. 849–855, 2017.
- [19] T. Wang, J. Zhang, Y. Li, J. Hong, and M. Y. Wang, "Electrostatic layer jamming variable stiffness for soft robotics," *IEEE/ASME Transactions on Mechatronics*, vol. 24, no. 2, pp. 424–433, 2019.
- [20] J. Guo, "Conceptual mechanical design of antagonistic variable stiffness joint based on equivalent quadratic torsion spring," *Science Progress*, vol. 103, p. 003685042094129, 07 2020.
- [21] R. Van Ham, B. Vanderborght, M. Damme, B. Verrelst, and D. Lefeber, "Maccepa: The mechanically adjustable compliance and controllable equilibrium position actuator for 'controlled passive walking'," vol. 2006, pp. 2195 – 2200, 06 2006.
- [22] K. Li, P. Xing, X.-K. Zhang, and Q.-G. Xia, "Research on variable-stiffness mechanisms of

- robot wrists for compliant assembling-clamping,” 05 2021.
- [23] A. F. A.-K. S, M. Awad, D. Gan, and K. Kinda, “Modeling, simulation and proof-of-concept of an augmentation ankle exoskeleton with a manually-selected variable stiffness mechanism,” *Annals of Robotics and Automation*, pp. 013–017, 08 2020.
- [24] V. Grosu, C. Rodriguez-Guerrero, S. Grosu, B. Vanderborght, and D. Lefeber, “Design of smart modular variable stiffness actuators for robotic-assistive devices,” *IEEE/ASME Transactions on Mechatronics*, vol. 22, no. 4, pp. 1777–1785, 2017.
- [25] M. Malosio, G. Spagnuolo, A. Prini, L. Molinari Tosatti, and G. Legnani, “Principle of operation of rotwwc-vsa, a multi-turn rotational variable stiffness actuator,” *Mechanism and Machine Theory*, vol. 116, pp. 34–49, 2017.
- [26] A. Sudano, D. Accoto, L. Zollo, and E. Guglielmelli, “Design, development and scaling analysis of a variable stiffness magnetic torsion spring,” *International Journal of Advanced Robotic Systems*, vol. 10, pp. 1–11, 10 2013.
- [27] D. Che, J. Z. Bird, A. Hagnmüller, and M. E. Hossain, “An adjustable stiffness torsional magnetic spring with a linear stroke length,” in *2021 IEEE Energy Conversion Congress and Exposition (ECCE)*, pp. 5944–5948, 2021.
- [28] B. Kozakiewicz and T. Winiarski, “Spring based on flat permanent magnets: Design, analysis and use in variable stiffness actuator,” *Facta Universitatis, Series: Mechanical Engineering*, vol. 0, no. 0, 2021.
- [29] J. Schuy, P. Beckerle, J. Wojtus, S. Rinderknecht, and O. von Stryk, “Conception and evaluation of a novel variable torsion stiffness for biomechanical applications,” in *2012 4th IEEE RAS EMBS International Conference on Biomedical Robotics and Biomechanics (BioRob)*, pp. 713–718, 2012.
- [30] J. Schuy, P. Beckerle, J. Faber, J. Wojtus, S. Rinderknecht, and O. v. Stryk, “Dimensioning and evaluation of the elastic element in a variable torsion stiffness actuator,” in *2013 IEEE/ASME International Conference on Advanced Intelligent Mechatronics*, pp. 1786–1791, 2013.
- [31] P. Beckerle, J. Wojtus, J. Schuy, B. Strah, S. Rinderknecht, and O. Von Stryk, “Power-optimized stiffness and nonlinear position control of an actuator with variable torsion stiffness,” pp. 387–392, 07 2013.
- [32] K. Kinnunen, S. Laine, T. Tiainen, R. Viitala, A. Seppänen, T. Turrin, P. Kiviluoma, and R. Viitala, “Coupling with adjustable torsional stiffness,” *Proceedings of the Estonian Academy of Sciences*, vol. Volume 70, issue 4, p. 7, 2021.
- [33] J. Choi, S. Hong, W. Lee, S. Kang, and M. Kim, “A robot joint with variable stiffness using leaf springs,” *IEEE Transactions on Robotics*, vol. 27, no. 2, pp. 229–238, 2011.
- [34] Z. Xie, L. Qiu, and D. Yang, “Design and analysis of a variable stiffness inside-deployed lamina emergent joint,” *Mechanism and Machine Theory*, vol. 120, pp. 166–177, 2018.
- [35] F. Mei, S. Bi, L. Chen, and H. Gao, “A novel design of planar high-compliance joint in variable stiffness module with multiple uniform stress leaf branches on rigid-flexible integral linkage,” *Mechanism and Machine Theory*, vol. 174, p. 104889, 2022.
- [36] C. Pew and G. Klute, “Design of lower limb prosthesis transverse plane adaptor with variable stiffness,” *Journal of Medical Devices*, vol. 9, 04 2015.
- [37] C. Pew and G. Klute, “Second generation prototype of a variable stiffness transverse plane adapter for a lower limb prosthesis,” *Medical Engineering Physics*, vol. 49, 08 2017.
- [38] J. M. Robinson, “A compliant mechanism-based variable-stiffness joint,” 2015.
- [39] Z. Xie, L. Qiu, and D. Yang, “Analysis of a novel variable stiffness filleted leaf hinge,” *Mechanism and Machine Theory*, vol. 144, p. 103673, 2020.
- [40] G. Palli, C. Melchiorri, G. Berselli, and G. Vassura, “Design and modeling of variable stiffness joints based on compliant flexures,” vol. 2, 01 2010.
- [41] “Compliant mechanisms that achieve binary stiffness along multiple degrees of freedom. journal of composite materials,”
- [42] P. Kuppens, M. Bessa, J. Herder, and J. Hopkins, “Monolithic binary stiffness building blocks for mechanical digital machines,” *Extreme Mechanics Letters*, vol. 42, p. 101120, 2021.

3

Main Paper

Design of compliant variable stiffness ball joint

Tzu Lee

Abstract—This paper introduces a novel design of a compliant variable stiffness ball joint which can be advantageous in various applications such as exoskeleton and prostheses. The integration of compliant and variable stiffness features not only ensures scalability but also enhances the joint’s adaptability to perform multi-tasks. The objectives of this paper are: (1) Propose a compliant variable torsional stiffness (VTS) element, which is used for constructing a compliant variable stiffness (VS) ball joint. (2) Investigate the sensitivity of geometric parameters with respect to stiffness, range of motion (RoM), and stiffness tuning force, thereby obtaining the optimal shape of the design. (3) Quantitatively analyze the influence of support stiffness on the end effector of the proposed ball joint. The parametric sensitivity analysis and shape optimization are done using Finite Element Method (FEM) and Response Surface Methodology (RSM). Furthermore, an analytical model is formulated to describe the relation between stiffness, displacement, and reaction force of the ball joint. Finally, based on this analytical model, a graphical user interface (GUI) is developed to elucidate the interplay between design shape and performance. The simulation result shows that the optimized VTS element, using Nylon 12 as the material, can provide a 0.033 Nm/rad continuous range of adjustable torsional stiffness within a 0.2m x 0.04m x 0.04m space. This project holds great potential in achieving adaptable rotational movement for small-scale applications.

I. INTRODUCTION

Joints equipped with variable stiffness offer remarkable advantages in terms of adaptability and versatility. The term variable stiffness used in this paper refers to the stiffness adjustability of the mechanisms when they are stationary and not functioning, meaning the mechanism functions after the stiffness is tuned to the desired level. By modulating their stiffness, the movement of these joints can be adjusted, making them well-suited for performing a wide range of tasks and adapting to diverse conditions, thus enhancing their overall functionality and applicability. However, incorporating variable stiffness characteristics often leads to increased complexity within the mechanism. For example, traditional approaches [1][2] relied on rigid components such as gears and sliders to adjust the transmission ratio and achieve variable stiffness, which not only complicates the assembly process but also introduces undesirable issues stemming from friction and backlash.

To address these challenges, compliant components can be used as an alternative to rigid ones. By designing compliant mechanisms in a monolithic form, the need for assembling and the interaction between multiple parts are eliminated, thus reducing complexity and improving precision. Integrating the variable stiffness feature into compliant joints enables precise motion control under different loads, further enhancing their performance in various applications. This combination of variable stiffness and compliant structure opens up new possibilities for miniaturized systems to operate with enhanced precision and adaptability.

However, literature on compliant variable stiffness joints is very scarce. [3], [4], [5], and [6] proposed compliant mechanism-based variable stiffness joints. These joints utilize both compliant and rigid components to reduce part numbers while simultaneously achieving a large range of motion. Despite the more compact structures compared to fully rigid mechanisms, these hybrid mechanisms still utilize sliders, rollers, or cables to tune the transmission ratio between compliant and rigid components, meaning their stiffness variability relies on the engaging and disengaging of components. Therefore, intricate assembling is required and issues associated with abrasion and backlash are not fully resolved.

In regards to fully compliant variable stiffness joints, [7] presented a binary stiffness revolute joint that utilizes the buckling and unbuckling of thin plates. [8] proposed a binary stiffness universal joint that employs a similar technique but with wire beams instead of plates to enable two rotational degrees of freedom, allowing for tip-tilt motion. [9] proposed a variable stiffness ball joint using shape memory polymer (SMP) to generate different amounts of friction force, thereby controlling the stiffness of the ball joint. [10] presents a compliant twisting element that achieves continuous torsional stiffness variability, ranging from positive to negative stiffness. This element is further used as one of the fundamental mechanisms to form the compliant variable stiffness ball joint in this paper.

In conclusion, several compliant variable stiffness joints are developed. However, most of the designs only provide binary or discrete stiffness states. And while

[9] and [10] achieve continuous stiffness variability, the former requires a long heating time for stiffness tuning. The latter is not yet utilized for multi-DoF joint applications. Moreover, the relations between parameters and performances are not investigated. As a result, to fulfill this research gap, the goal of this paper is to present a novel compliant ball joint with continuous stiffness variability, optimize its performance, and develop an analytical model describing the ball joints behavior.

The configuration of the ball joint is realized by connecting three compliant variable torsional stiffness (VTS) elements (Fig. 1a) in series, each perpendicular to the others, as depicted in Fig. 1b. The proposed element exhibits relatively low torsional stiffness but high bending and axial stiffness, enabling rotational degrees of freedom while providing translational constraint. The optimization is achieved by conducting parametric analysis with Finite Element Method (FEM) and Response Surface Methodologies (RSM). After the optimal shape is acquired, an experiment is carried out to validate the parametric analysis result.

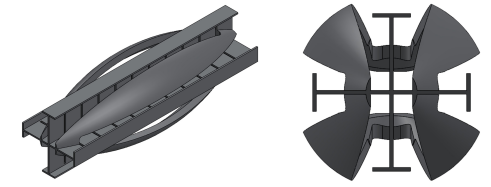
Despite the advantages of compliant mechanisms, one should be aware that compliant components inherently possess finite stiffness which contributes to error. This is especially critical for mechanisms with compliant elements in series as the error accumulates. As a result, an analytical model of the ball joint is derived and implemented in Matlab. It not only describes the relation between reaction moment and rotational displacement but also accounts for the translational displacement resulting from finite supporting stiffness. This comprehensive approach ensures a more accurate representation of the joint's behavior. Additionally, a GUI is developed to allow the users to check the reaction force/moment of the end effector under specified input displacement.

The remainder of this paper is structured as follows: Section II illustrates the working principle of the compliant VTS elements and introduces the method for parametric sensitivity analysis. In addition, the analytical relation between the reaction force/moment, stiffness, and displacement of the ball joint is established. Section III examines the results obtained from the FEM analysis and experiment. Next, Section IV evaluates the overall performances of the VTS element and ball joint. Finally, section V summarizes the contributions of this research.

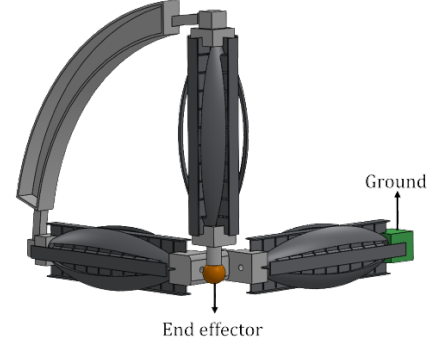
II. METHOD

A. Compliant VTS element design

This section presents the design details and working principle of the compliant variable torsional stiffness (VTS) element, which consists of two fundamental structures: T beam and diagonal beam, as depicted in Fig. 2a



(a) compliant variable torsional stiffness (VTS) element.



(b) compliant variable stiffness (VS) ball joint.

Fig. 1: The design of the compliant VTS element and compliant VS ball joint.

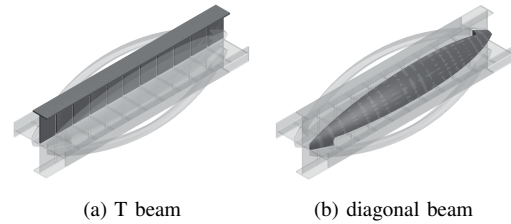


Fig. 2: Two fundamental structures of compliant VTS element

and 2b. T beam exhibits a unique behavior where its torsional stiffness can be continuously adjusted from positive to negative values by applying axial prestress. This behavior holds true for open-section beams with flanges such as I beam or cruciform beam (Fig. 3). Since these beams possess high warping constants, they tend to warp and carry torque when axially compressed, resulting in decreased torsional stiffness [10][11]. While this structure achieves a continuous variable torsional stiffness, a major drawback is encountered when used in a joint: negative stiffness implies bistability, causing the joint to rotate in one direction during the stiffness tuning process. This undesirable behavior conflicts with the objective of keeping the joint stationary while varying stiffness and allowing rotation only when subjected to an input moment.

To overcome this issue, a positive stiffness agent is integrated to counterbalance the negative stiffness of the T beam, thereby constraining rotation during the stiffness tuning process. The design criteria for the positive stiffness agent include a large RoM and low stiffness along the z-axis to minimize the prestress force, ensuring high energy efficiency in the overall design.

Among countless structures capable of providing positive stiffness, here, the diagonal beam structure is chosen as the stiffness compensator due to its elongated and slender shape, providing a relatively large range of motion and adequate torsional stiffness that matches the negative stiffness level of the T beam. To seamlessly combine the positive and negative stiffness, the diagonal beam is rigidly connected in parallel to the T beam. Moreover, the diagonal beam is designed in a curved shape for two reasons: Firstly, it reduces the z-axis stiffness. When compressed along the z-axis, the diagonal beam bends outward, and as the bending stiffness of beams is significantly lower than axial stiffness, the z-axis stiffness is greatly reduced. Secondly, the curved shape increases the range of motion. The diagonal connection results in an asymmetric behavior in clockwise (CW) and counterclockwise (CCW) directions (Fig. 20). Since the diagonal beam is pushed when a CCW moment is applied and pulled when a CW moment is applied, the range of motion in the CW direction is much smaller than in the CCW direction. Therefore, the curved diagonal beam mitigates this limitation and helps increase the range of motion in the CW direction. Overall, by adjusting the axial prestress on the VTS element, the torsional stiffness can be continuously tuned from positive to zero.



Fig. 3: The twisting deformation of open-section beam under axial compression.

B. Parametric analysis

To determine the optimal shape of the VTS element, parametric analyses using FEM are conducted. The goal is to maximize the stiffness variation range and RoM meanwhile minimizing the actuation force required for stiffness tuning.

The definition of RoM in this research is the motion range where within this range, the torsional stiffness change is less than 5 percent of the average value. In Fig. 4, the RoM of a compliant element under different prestress levels is shown. Take the orange moment-angle line for example, within the RoM -0.5 rad to 0.5 rad, the average torsional stiffness is $2.2E-02$ Nm/rad, and the maximum stiffness variation within this RoM is 5 percent of $2.2E-02$ Nm/rad, equating to $1.1E-03$ Nm/rad.

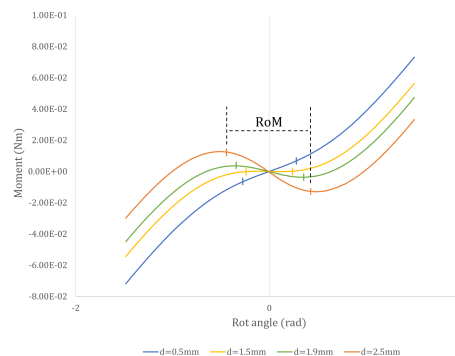


Fig. 4: Moment-Rot angle graph of T beam under different level of prestress. "d" is the displacement of actuated point.

The optimization focuses mainly on the T beam, as it plays an essential role in achieving the variable stiffness characteristic. By employing RSM in Design-Expert software, a thorough sensitivity analysis is performed to obtain the optimal shape of the T beam. On the other hand, the role of the diagonal beam is to complement the negative stiffness of the T-section beam, rather than being the main driver of variable stiffness characteristics. Therefore, the sensitivity analysis of the diagonal beam is not intended to obtain an optimal shape but to ensure the stiffness level and RoM correspond with the T beam. As a result, while the influence of the parameters is examined, RSM is considered redundant for acquiring a suitable geometry of the diagonal beam.

To summarize, this chapter utilizes FEM and RSM to conduct parametric studies, thereby developing an equation that describes the relation between parameters and the performance of the T beam. This equation serves as a tool for future designers to determine the optimal T beam shape that achieves the target torsional stiffness and RoM under specified stress and actuation force limitation. Moreover, the parametric study of the diagonal beam can be used as a reference for obtaining compatible positive stiffness with the negative stiffness of the T beam.

1) *T Beam*: The effect of the geometric parameters on torsional stiffness, RoM, maximum stress, and actuation

force is analyzed in order to identify the most influential factors and optimize the shape of the T beam accordingly. During the parametric analysis, the length of the T beam is treated as a control parameter and set to a fixed value of 180mm. This decision is based on the understanding that the length of a beam has a linear relation with its stiffness and range of motion. Eight variable parameters, as listed in Table I and depicted in Fig. 5 are chosen based on the following criteria:

- Changes in the parameter values will have little impact on the complexity of the manufacturing process.
- The geometry can be replicated along the torsional axis, allowing for easy scalability of the design's length.

Symbol	Parameter
t	thickness
w_w	web width
w_f	flange width
t_r	web thickness to flange thickness ratio
Δw_w	web width difference
w_g	gap width
l_g	gap length
N	section number

TABLE I: Parameter symbol - T beam

The parametric analysis is performed in two stages. The preliminary analysis focuses on the sensitivity of each parameter in order to exclude the irrelevant parameters from further investigation. After the influential parameters are identified, the advanced analysis studying the interaction between these parameters and performance is conducted by implementing RSM in the Design-Expert [12], a software package developed by Stat-Ease. The objective is to create a predictive model that approximates the performance of the T beam which allows for shape optimization without running exhaustive FEM simulations.

a) *Sensitivity analysis:* ANSYS Parametric Design Language (APDL) is used for modeling the T beam and simulating its behavior under prestress. The FEM simulation employs the same setup developed in [10] Section 3.2. Here, the prestress is realized by applying a -2.8mm displacement along the z-axis. The performance of interest includes torsional stiffness, RoM, maximum stress, and reaction force along the z-axis. The latter contains information regarding actuation force and axial

stiffness. The actuation force can be seen as an indicator of energy efficiency, while axial stiffness is a contributing factor in support stiffness of the ball joint. Without prestress, the axial stiffness of the T beam can be derived from the equation:

$$\text{Axial stiffness} = \frac{\text{Reaction force}}{\text{Displacement}}$$

When a prestress is applied, the axial stiffness becomes:

$$\text{Axial stiffness} = \frac{\text{Reaction force} + \text{Prestress force}}{\text{Displacement}}$$

Another contributing factor is bending stiffness. The FEM setup for obtaining bending stiffness differs from the previous one. Firstly, instead of modeling a T beam, an I beam formed by two opposing T beams (Fig. 6) is simulated. This choice is made since the centroid of the VTS element is the same as the I beam but not the T beam, ensuring a more accurate bending stiffness analysis. Secondly, the beam is not prestressed in this setup since the effect of prestress on bending stiffness is out of the scope for this parametric analysis.

In the simulation of x-axis bending stiffness, the I beam is constrained in all directions at two points at the fixed end. (indicated by orange triangles shown in Fig. 6). For the x-axis bending stiffness, a 5N force is applied at the center at the other end. While for the y-axis bending stiffness, a 1N force is applied. The reason for using different forces along two axes is that x-axis bending stiffness is much higher than y-axis. Applying different forces results in comparable deflection in two axes. This setup is beneficial as the bending deflection is an indicator of the translational motion of the ball joint. Comparable deflections in two axes provide a clear view of how much force is allowed to keep deflections under maximum acceptable value. The bending stiffness along two axes is then derived from the equation:

$$\text{Bending stiffness} = \frac{\text{External force}}{\text{Displacement}}$$

As a flanged cruciform beam is equivalent to combining two perpendicular I beams, the total bending stiffness of the flanged cruciform beam is the sum of x-axis and y-axis I Beam bending stiffness.

b) *RSM analysis:* After the relevant parameters are identified in the preliminary analysis, they undergo the advanced parametric analysis using RSM. Box-Behnken design is selected as the type of RSM to create the predictive models. A total of 55 factorial points (Appendix C.1) are generated from the four identified relevant

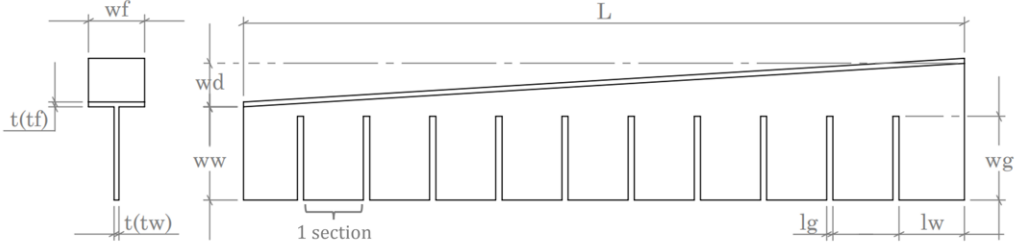


Fig. 5: Parameter - T beam

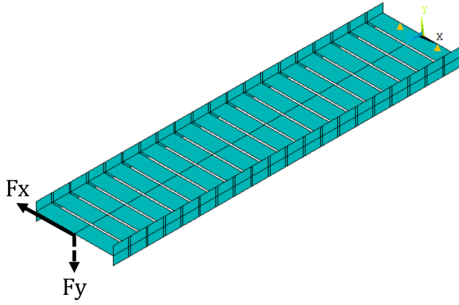


Fig. 6: Simulation setup for bending stiffness analysis

parameters, and the responses of interest are torsional stiffness, RoM, maximum stress, and actuation force.

Utilizing FEM data, predictive models are developed for these responses based on the selected factorial points. Through Analysis of variance(ANOVA), lack-of-fit tests, and residual analysis, the quadratic model is determined as the most suitable and accurate choice for predicting the responses.

2) *Diagonal beam*: In this section, the design detail of the diagonal beam and FEM setup are illustrated. This diagonal beam is used for providing positive stiffness that compensates for the negative stiffness of the T beam. The form of the diagonal beam originates from a section of an ellipsoid, as illustrated in Fig. 7 and Fig. 8, whose shape is determined by four parameters, as listed in Table II and depicted in Fig. 9.



Fig. 7: Shape of the diagonal beam.

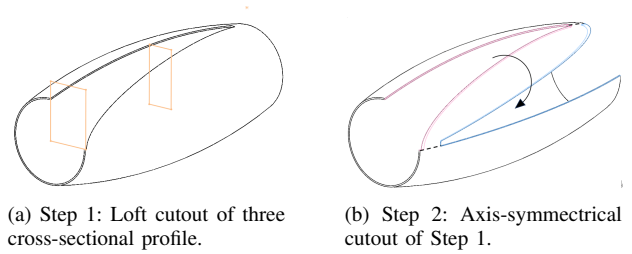


Fig. 8: Steps to obtain the shape of diagonal beam.

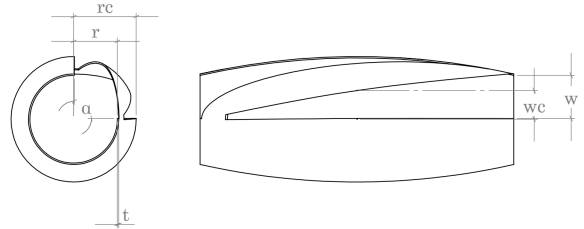


Fig. 9: Parameter - diagonal beam

Symbol	Parameter
Δr	radius difference
κ	curvature
α	connecting angle
t	thickness

TABLE II: Parameter symbol - diagonal beam

Δr refers to the difference between two radii: r , which is determined by the web width of the T beam, and r_c , which represents the central radius. Similarly, κ stands for the difference in width between two cross-sections, w and w_c . A loft cutout of the two rectangular cross-sectional profiles and a vertex (all marked in orange) generates the smooth and continuous curve of the diagonal beam. α represents the connecting angle between the two ends of the diagonal beam.

By adjusting these four parameters, the torsional stiffness, RoM, stress, and actuation force are investigated. The analysis is carried out through FEM simulation using ANSYS Workbench, selecting Nylon 12 as the material with Young's modulus of 1.7 GPa and Poissons ratio of 0.38. The element type chosen for the analysis is 3D shell.

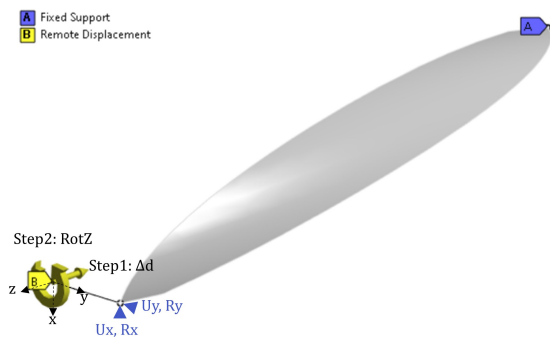


Fig. 10: FEM simulation setup of the diagonal beam.

The simulation setup is demonstrated in Fig. 10. The movement of point A (ground) is constrained in all directions, while the prestressed point is translationally and rotationally constrained in both the x and y directions. Next, two load steps are applied. First, a -2.8 mm displacement along the z-axis is applied to axis-point B at the prestressed side, which is rigidly connected to the prestressed point (remote displacement). Second, a α° or $-\alpha^\circ$ displacement is applied to point B. A large deflection nonlinear solver with 30 substeps is used for both load steps in order to record the force-displacement behavior of the first step and the moment-angle behavior of the second step.

C. compliant VTS element

1) *FEM simulation setup*: The FEM simulation of the VTS element is performed in Ansys Workbench using Nylon 12 as the material, with Tensile Modulus = 2331 MPa and Poisson ratio = 0.38. Note that the length (0.18m) used in the T beam and diagonal beam analysis is different from the length used in the VTS element design. The length of the VTS element is reduced to 0.112m due to the 3D printer limitations. As for the other T beam design parameters, the value used is the same as obtained from the RSM optimal shape.

Fig. 11 illustrates the simulation setup for retrieving the varying torsional stiffness of the VTS element. First, the axis point on one side is fixed hence the motion is constrained in all directions. Meanwhile, a displacement Δd is applied to the actuated point. Then, a 40° angular

displacement is applied to the actuated point in step 2. The z-axis reaction moment is recorded for torsional stiffness computation.

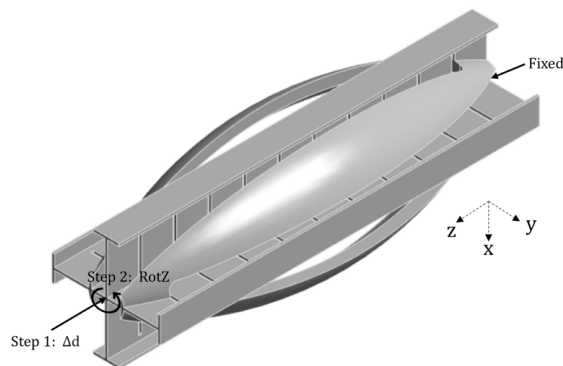


Fig. 11: FEM simulation setup of the VTS element.

2) *Experimental setup*: In this section, the experiment setup for measuring the torsional stiffness of the VTS element is explained. Firstly, the VTS element is fabricated using Ultimaker S5 and Fused deposition modeling (FDM) 3D printing technique, with Nylon 12 as the material. The Nylon 12 used has a Tensile Modulus = 2331 MPa, Tensile Strength = 63 MPa, and Poisson's ratio = 0.38.

To adjust the torsional stiffness, a threaded rod and nuts are used to prestress the axis point of the VTS element as shown in Fig. 12. Here, the magnitude of the prestress is expressed by the displacement of the axis point rather than the force applied. Fig. 13 shows that after attaining the target prestress, the VTS element is clamped to a test machine Zwick Z005. As Zwick Z005 rotates the VTS element on the actuated side, a torque-measuring transducer HBM T20WN is used to record the reaction moment. Finally, the torsional stiffness can be obtained with the applied rotation angle and the measured reaction moment data.



Fig. 12: Using a threaded rod and nuts to prestress VTS element.

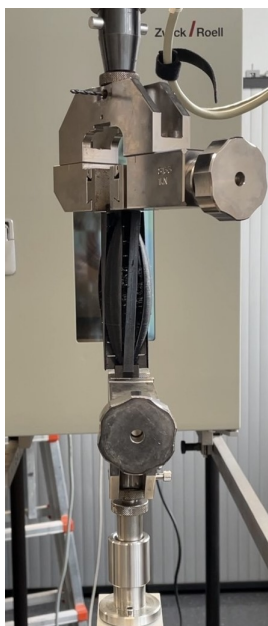


Fig. 13: Experimental setup

D. Compliant variable stiffness ball joint

In this section, the analytical model describing the behavior of the compliant VS ball joint is derived. Moreover, a GUI is developed by implementing this model in Matlab. This allows designers to calculate the reaction force/moment with specified input displacements of the ball joint.

1) *GUI*: Fig. 14 displays the GUI layout, including two segments from left to right: reaction force/moment calculation and ball joint visualization.

a) *Reaction force/moment calculation*: The top left section contains eighteen user-specified inputs, including beam length, axial stiffness, bending stiffness, and torsional stiffness values of VTS elements 1, 2, and 3, along with translational and rotational displacements of the ball joint in the x, y, and z directions. By clicking the calculate button, at the bottom left of the interface, users can obtain the reaction forces and moments provided by the ball joint.

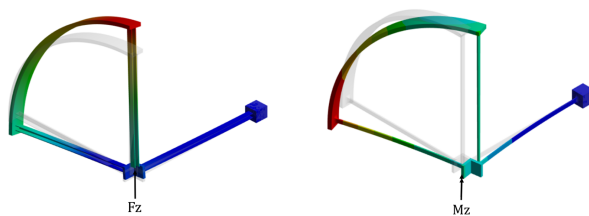
b) *Ball joint visualization*: The right section displays the schematic of the ball joint. The ball joint is composed of three VTS elements (black lines denoted as 1, 2, 3) connected in series and perpendicular to each other. The black cross linked to element 3 represents the ground, while the black dot connected to element 1 symbolizes the end effector of the ball joint. Two blue arcs, connecting element 1 to 2 and 2 to 3, signify rigid connections that do not allow deformation.

When a displacement is exerted on the end effector, the relatively high bending and axial stiffness of the

three VTS elements limits translational motion, while permitting rotational movement of the end effector in relation to the ground.

2) *Analytical model*: The ball joint comprises three VTS elements in series. One issue with structure connecting in series is the error accumulation. For compliant mechanisms, the farther away between the ground and the end effector, the more possible for deformations in unintended directions to enlarge.

As a result, the support stiffness becomes a pivotal factor in ball joint design. This support stiffness denotes the extent of rigidity within the structure responsible for holding or bolstering the compliant mechanism, preventing the end effector from straying into undesired paths. Theoretically, an infinitely high support stiffness would be the most ideal condition. Nevertheless, in reality, compliant elements always have finite stiffness. In the case of the compliant ball joint, the support stiffness comes from the bending stiffness and axial stiffness of the VTS elements. Hence when an external load is exerted, the overall displacement of the end effector is determined not only by torsional stiffness but also by bending and axial stiffness of the VTS elements.



(a) Total displacement of the end effector when a z-axis force is exerted.

(b) Total displacement of the end effector when a z-axis moment is exerted.

Fig. 15: Displacement of the ball joint's end effector under load.

The mathematical relation between the displacement, stiffness, and reaction force/moment is explained as follows with the aid of the ball joint schematic shown in Fig. 14.

The translational displacement of the end effector along each axis is contributed by five factors:

- Axial deformation of the beam aligned with the axis.
- Bending of the other two beams caused by forces.
- Bending of the other two beams caused by moments.

To provide a clearer understanding, the analytical model of the displacement along the z-axis will be explained first, while the models of the x-axis and y-axis can be derived in the same way.

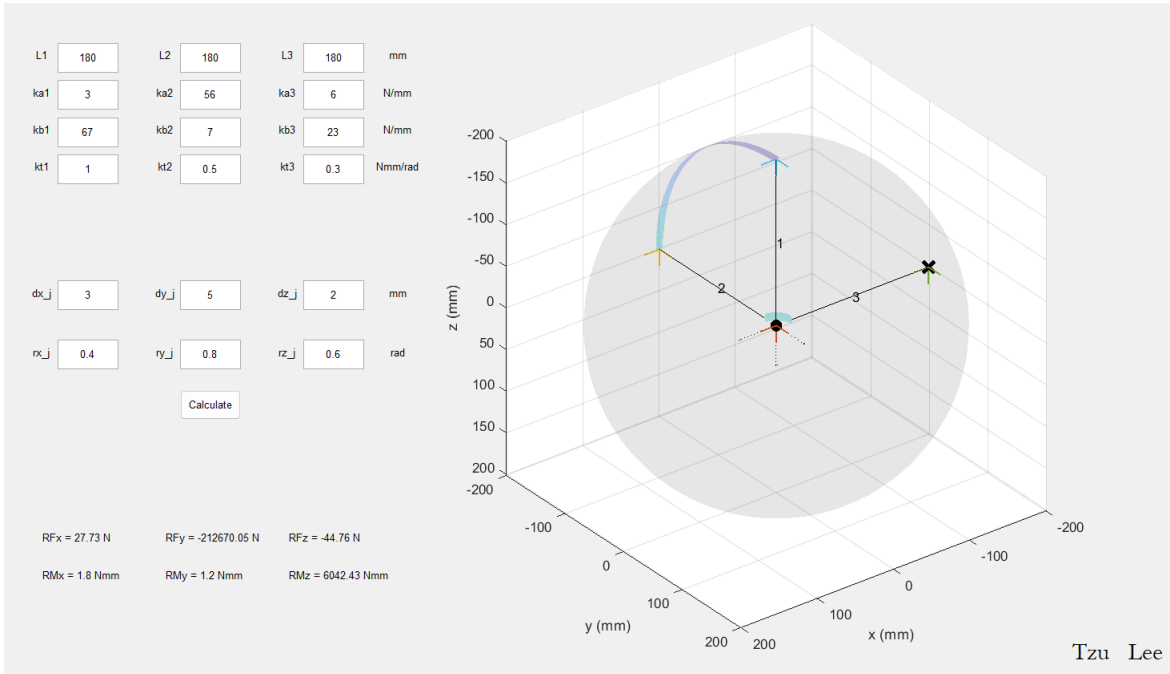


Fig. 14: GUI of the ball joint.

When a force along the z-axis is applied to the end effector, Beam 1 will deform axially, while Beam 2 and 3 will bend. When a moment is applied along the y-axis, not only Beam 2 rotates, but Beam 3 also bends. This bending of Beam 3 contributes to the z displacement. The same bending happens to Beam 2 when a moment is applied along the x-axis. Overall, the z displacement of the ball joint (Dz) along the z-axis can be expressed with the following equation:

$$Dz = dz_{1,a,f} + dz_{2,b,f} + dz_{3,b,f} + dz_{2,b,m} + dz_{3,b,m} \quad (1)$$

where the first subscript stands for the Beam number, the second subscript represents the deformation type, "a" is axial deformation, "b" is bending deformation, and "t" is torsional deformation. The third subscript indicates the stimulus type that causes the deformation, including force "f" and moment "m". The displacement along the x and y-axis can be derived in the same way, leading to eq. 2 and eq. 3.

$$Dy = dy_{2,a,f} + dy_{1,b,f} + dy_{3,b,f} + dy_{1,b,m} + dy_{3,b,m} \quad (2)$$

$$Dx = dx_{3,a,f} + dx_{1,b,f} + dx_{2,b,f} + dx_{1,b,m} + dx_{2,b,m} \quad (3)$$

On the other hand, the rotational displacements of the end effector along the y and z-axis are contributed

by one factor: The twisting of Beam 2 and Beam 1 caused by moment along the y and z-axis respectively. However, the rotational displacement along the x-axis is determined by two factors: The twisting of Beam 3 caused by the x-axis moment and the z-axis force. The z-axis force is transmitted to Beam 2 through the arc-shaped rigid link, creating a moment on Beam 1 with moment arm = the length of Beam 2. Therefore, the rotational displacement (denoted as R) along each axis can be expressed as follows:

$$Rz = rz_{1,t,m} \quad (4)$$

$$Ry = ry_{2,t,m} \quad (5)$$

$$Rx = rx_{3,t,m} + rx_{3,t,f} \quad (6)$$

To calculate the reaction force/moment results from an input displacement, the stiffness "k" of each beam must be specified. To differentiate types of stiffness, different subscripts are utilized. The first subscript represents the beam number and the second subscript represents the stiffness type. "a" stands for axial, "b" stands for bending, and "t" stands for torsional stiffness.

In a series configuration, the total force remains the same in every elastic element:

$$F_{total} = k_i d_i \quad (7)$$

According to eq. 7, employing Hook's law and Bernoulli-Euler Beam Theory (assume small deformation angles), the reaction forces and reaction moments can be expressed as follows:

$$Fz = k_{1,a}dz_{1,a,f} = k_{2,b}dz_{2,b,f} = k_{3,b}dz_{3,b,f} = \frac{k_{3,t}rx_{3,t,f}}{L_2} \quad (8)$$

$$Fy = k_{2,a}dy_{2,a,f} = k_{1,b}dy_{1,b,f} = k_{3,b}dy_{3,b,f} \quad (9)$$

$$Fx = k_{3,a}dx_{3,a,f} = k_{2,b}dx_{2,b,f} = k_{1,b}dy_{1,b,f} \quad (10)$$

$$Mz = k_{1,t}rz_{1,t,m} = k_{2,b}dx_{2,b,m}L_2 = k_{3,b}dy_{3,b,m}L_3 \quad (11)$$

$$My = k_{2,t}ry_{2,t,m} = k_{1,b}dx_{1,b,m}L_1 = k_{3,b}dz_{3,b,m}L_3 \quad (12)$$

$$Mx = k_{3,t}rx_{3,t,m} = k_{2,b}dz_{2,b,m}L_2 = k_{1,b}dy_{1,b,m}L_1 \quad (13)$$

Here, "L" stands for the beam length and the subscript indicates the beam number.

As derived in eq. 8-13, the total reaction force is equal to the three reaction forces generated by the deformation of three beams, including the axial deformation of the beam that aligns with the force direction and the bending of the other two beams. The extra term in eq. 8 comes from the twisting of Beam 3 caused by the z-axis force.

Similarly, the total reaction moment is equal to the three reaction moments generated by the deformation of three beams, including the twisting of the beam that aligns with the moment direction and the bending of the other two beams.

Although the relation between reaction force/moment and the deformations of beams is obtained, at this moment, the deformations are still unknown variables that depend on input displacement and beam stiffness. Therefore, the next step is to derive the relations between the input displacement and each deformation which is expressed with specified stiffness.

From eq. 8-13, the relation between the sub-displacements can be obtained as follows:

$$\begin{bmatrix} dz_{2,b,f} \\ dz_{3,b,f} \\ rx_{3,t,f} \end{bmatrix} = dz_{1,a,f}k_{1,a} \begin{bmatrix} \frac{1}{k_{2,b}} \\ \frac{1}{k_{3,b}} \\ \frac{L_2}{k_{3,t}} \end{bmatrix} \quad (14)$$

$$\begin{bmatrix} dy_{1,b,f} \\ dy_{3,b,f} \end{bmatrix} = dy_{2,a,f}k_{2,a} \begin{bmatrix} \frac{1}{k_{1,b}} \\ \frac{1}{k_{3,b}} \end{bmatrix} \quad (15)$$

$$\begin{bmatrix} dx_{2,b,f} \\ dx_{1,b,f} \end{bmatrix} = dx_{3,a,f}k_{3,a} \begin{bmatrix} \frac{1}{k_{2,b}} \\ \frac{1}{k_{1,b}} \end{bmatrix} \quad (16)$$

$$\begin{bmatrix} dx_{2,b,m} \\ dy_{3,b,m} \end{bmatrix} = rz_{1,t,m}k_{1,t} \begin{bmatrix} \frac{1}{k_{2,b}L_2^2} \\ \frac{1}{k_{3,b}L_3^2} \end{bmatrix} \quad (17)$$

$$\begin{bmatrix} dx_{1,b,m} \\ dz_{3,b,m} \end{bmatrix} = ry_{2,t,m}k_{2,t} \begin{bmatrix} \frac{1}{k_{1,b}L_1^2} \\ \frac{1}{k_{3,b}L_3^2} \end{bmatrix} \quad (18)$$

$$\begin{bmatrix} dz_{2,b,m} \\ dy_{1,b,m} \end{bmatrix} = rx_{3,t,m}k_{3,t} \begin{bmatrix} \frac{1}{k_{2,b}L_2^2} \\ \frac{1}{k_{1,b}L_1^2} \end{bmatrix} \quad (19)$$

By substituting the deformation terms in eq. 14-19 into eq. 8-6, eq. 20-23 can be obtained.

$$\begin{aligned} Dz &= \left(1 + \frac{k_{1,a}}{k_{2,b}} + \frac{k_{1,a}}{k_{3,b}}\right)dz_{1,a,f} \\ &+ \left(\frac{k_{2,t}}{k_{3,b}L_3}\right)ry_{2,t,m} \\ &+ \left(\frac{k_{3,t}}{k_{2,b}L_2}\right)rx_{3,t,m} \end{aligned} \quad (20)$$

$$\begin{aligned} Dy &= \left(1 + \frac{k_{2,a}}{k_{1,b}} + \frac{k_{2,a}}{k_{3,b}}\right)dy_{2,a,f} \\ &+ \left(\frac{k_{3,t}}{k_{1,b}L_1}\right)rx_{3,t,m} \\ &+ \left(\frac{k_{1,t}}{k_{3,b}L_3}\right)rz_{1,t,m} \end{aligned} \quad (21)$$

$$\begin{aligned} Dx &= \left(1 + \frac{k_{3,a}}{k_{2,b}} + \frac{k_{3,a}}{k_{1,b}}\right)dx_{3,a,f} \\ &+ \left(\frac{k_{2,t}}{k_{1,b}L_1}\right)ry_{2,t,m} \\ &+ \left(\frac{k_{1,t}}{k_{2,b}L_2}\right)rz_{1,t,m} \end{aligned} \quad (22)$$

$$Rz = rz_{1,t,m} \quad (23)$$

$$Ry = ry_{2,t,m} \quad (24)$$

$$Rx = rx_{3,t,m} + \left(\frac{k_{1,a}L_2}{k_{3,t}}\right)dz_{1,a,f} \quad (25)$$

To replace the unknown sub-displacement with known variables such as stiffness and input displacement, the equations are derived as follows. First, take D_z for example. By substituting eq. 24 and eq. 25 into eq. 20, eq. 20 becomes:

$$\begin{aligned}
Dz = & \left(1 + \frac{k_{1,a}}{k_{2,b}} + \frac{k_{1,a}}{k_{3,b}}\right) dz_{1,a,f} \\
& + \left(\frac{k_{2,t}}{k_{3,b}L_3}\right) R_y \\
& + \left(\frac{k_{3,t}}{k_{2,b}L_2}\right) \left(R_x - \left(\frac{k_{1,a}L_2}{k_{3,t}}\right) dz_{1,a,f}\right)
\end{aligned} \quad (26)$$

From eq. 26, $dz_{1,a,f}$ can be obtained:

$$dz_{1,a,f} = \frac{Dz - \left(\frac{k_{3,t}}{k_{2,b}L_2}\right) R_x - \left(\frac{k_{2,t}}{k_{3,b}L_3}\right) R_y}{\left(1 + \frac{k_{1,a}}{k_{2,b}} + \frac{k_{1,a}}{k_{3,b}} - \left(\frac{k_{3,t}}{k_{2,b}L_2}\right) \left(\frac{k_{1,a}L_2}{k_{3,t}}\right)\right)} \quad (27)$$

The same goes for the other sub-displacements:

$$dy_{2,a,f} = \frac{Dy - \left(\frac{k_{3,t}}{k_{1,b}L_1}\right) \left(R_x - \left(\frac{k_{1,a}L_2}{k_{3,t}}\right) dz_{1,a,f}\right) - \left(\frac{k_{1,t}}{k_{3,b}L_3}\right) R_z}{1 + \frac{k_{2,a}}{k_{1,b}} + \frac{k_{2,a}}{k_{3,b}}} \quad (28)$$

$$dx_{3,a,f} = \frac{Dx - \left(\frac{k_{2,t}}{k_{1,b}L_1}\right) R_y - \left(\frac{k_{1,t}}{k_{2,b}L_2}\right) R_z}{1 + \frac{k_{3,a}}{k_{2,b}} + \frac{k_{3,a}}{k_{1,b}}} \quad (29)$$

$$rz_{1,t,m} = R_z \quad (30)$$

$$ry_{2,t,m} = R_y \quad (31)$$

$$rx_{3,t,m} = R_x - \left(\frac{k_{1,a}L_2}{k_{3,t}}\right) dz_{1,a,f} \quad (32)$$

By obtaining $dz_{1,a,f}$, $dy_{2,a,f}$, $dx_{3,a,f}$, $rz_{1,t,m}$, $ry_{2,t,m}$, $rx_{3,t,m}$ in eq. 27- eq. 32, finally, the reaction force/moment can be expressed as a function of input displacement and stiffness.

$$F_z = dz_{1,a,f} k_{1,a} \quad (33)$$

$$F_y = dy_{2,a,f} k_{2,a} \quad (34)$$

$$F_x = dx_{3,a,f} k_{3,a} \quad (35)$$

$$M_z = rz_{1,t,m} k_{1,t} \quad (36)$$

$$M_y = ry_{2,t,m} k_{2,t} \quad (37)$$

$$M_x = rx_{3,t,m} k_{3,t} \quad (38)$$

eq. 33-38 are the reaction force and moment at the ground. The reaction force and moment provided by the

end effector to the user only encompasses the ones in the same direction as the input displacement. For example, when a D_z is applied, a reaction force F_z and a reaction moment M_x will appear at the ground, while the user will only receive the reaction force F_z .

eq. 33-38 are implemented in Matlab for the development of the GUI introduced in the previous section. Noted that the reaction force and moment displayed in the GUI are the ones received by the user.

III. RESULTS

A. FEM simulation

1) T beam:

a) *Sensitivity analysis*: Fig. 16 (a)-(e) illustrates the sensitivity of the five responses with regard to the eight parameters. In order to make the results comparable, the changes in the parameter value are normalized by distinct scales listed in Table. 11.

Results of Fig. 16a show that thickness-related parameters including t and t_r have a huge impact on torsional stiffness. Around $t=1.2$ mm, the T beam exhibits the most negative torsional stiffness. Then, as the thickness increases, torsional stiffness becomes less and less negative and will eventually become positive stiffness. At $t_r=1$, the torsional stiffness is the most negative, however, this could be a result of the thickness value itself rather than the thickness ratio since at $t_r=1$ (t_r =web thickness (t_w)/ flange thickness (t_f)), both t_w and t_f are equal to 1.2mm, which corresponds to the result: $t=1.2$ mm has the most negative stiffness. Other combinations of t_r such as $t_w=t_f=0.8$ mm are not simulated since $t=1.2$ mm along with $t_r=1$ has the most desirable performance and will be used for optimization. Torsional stiffness is more negative with a smaller w_w . When $\Delta w_w=0$ mm, which means the T beam is not tapered and has a constant web width along the z -axis, has the most negative stiffness. It shows that the effect of l_g is negligible. For w_g and N , after reaching local extrema, stiffness becomes more negative with larger w_g and less negative with larger N . The result of w_f fluctuates, however, a slight trend of larger w_f resulting in more negative stiffness can still be observed.

Fig. 16b indicates that RoM increases with decreasing t , t_r , and w_w but with increasing w_g , l_g , w_f , and N have little influence on RoM. For Δw_w smaller than 30mm, RoM is larger with smaller Δw_w , however, it shows an opposite trend when Δw_w exceeds 30mm. This could be a consequence of the local buckling of the web.

In Fig. 16c, it is observed that maximum stress increases t and w_w . While w_f , l_g , and N are insignificant. Maximum stress decreases when t_r and w_g increase. The relation between Δw_w and maximum stress shows similarity with RoM but with very high sensitivity.

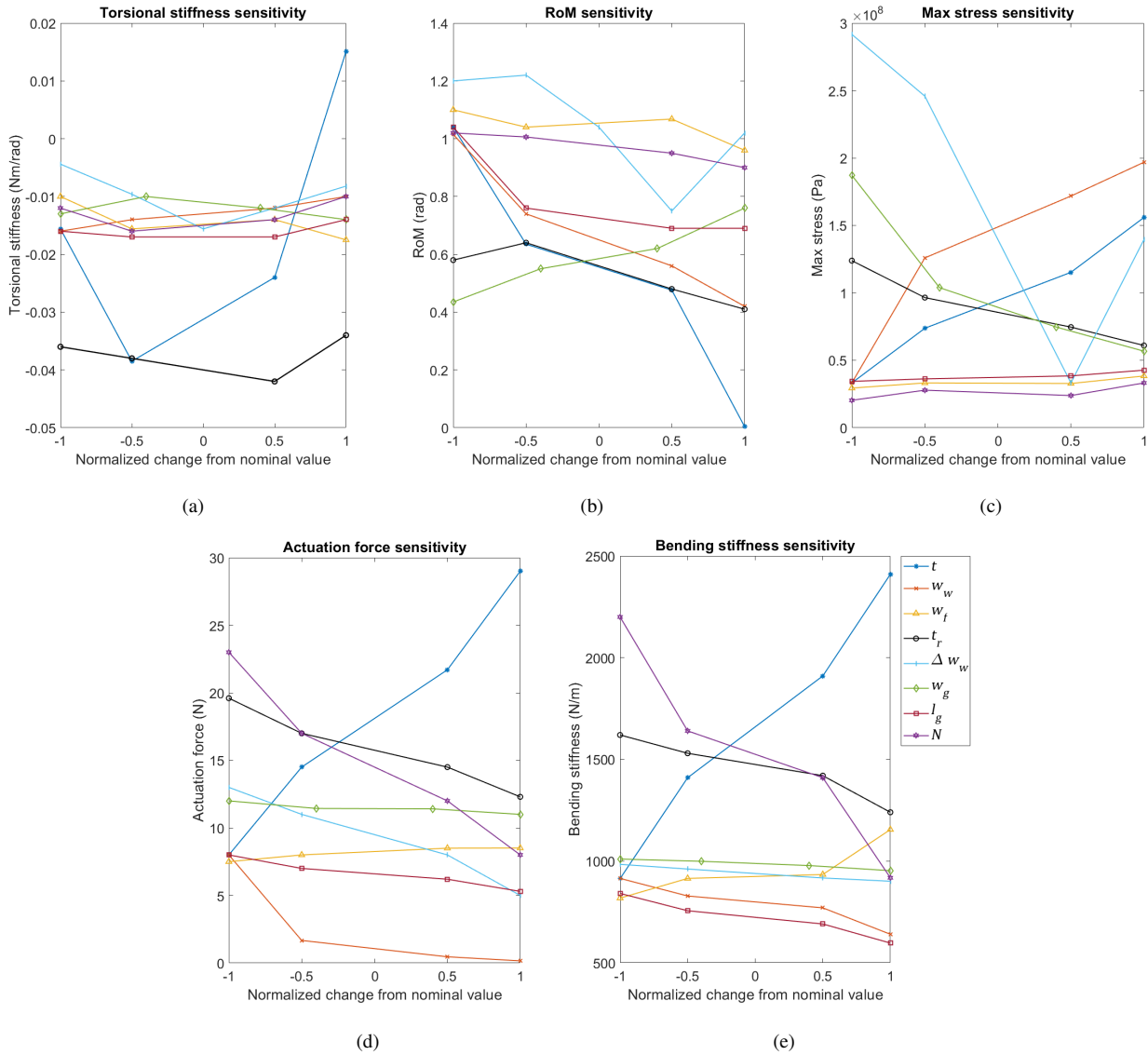


Fig. 16: Sensitivity analysis of T beam

Fig. 16d shows negative relations between actuation force and the parameters: t_r , Δw_w , and N . The actuation force remains nearly constant for different values of w_f , w_g , and l_g , indicating their insignificance. The deep positive slope of t shows the actuation force increases greatly with thickness. Lastly, while the actuation force decreases with increasing w_w , a saturation is spotted at larger w_w .

As can be seen in Fig. 16e, thickness-related parameters and N contributes substantially to bending stiffness. Although the other shows subtle positive and negative relations, they're considered irrelevant compared to the

other three.

In this sensitivity analysis, six parameters: t , w_w , w_f , Δw_w , w_g , and N are considered influential to the responses. However, only four parameters t , w_w , Δw_w , and N are identified as relevant factors for RSM analysis since the sensitivity trends of w_f , and w_g show that at $w_f > 9\text{mm}$ and $w_g = w_w$, the T beam has the best performance for all responses based on the optimization aim established in the project objectives. Hence, the four parameters are chosen to undergo a more thorough sensitivity analysis that investigates the interaction between parameters.

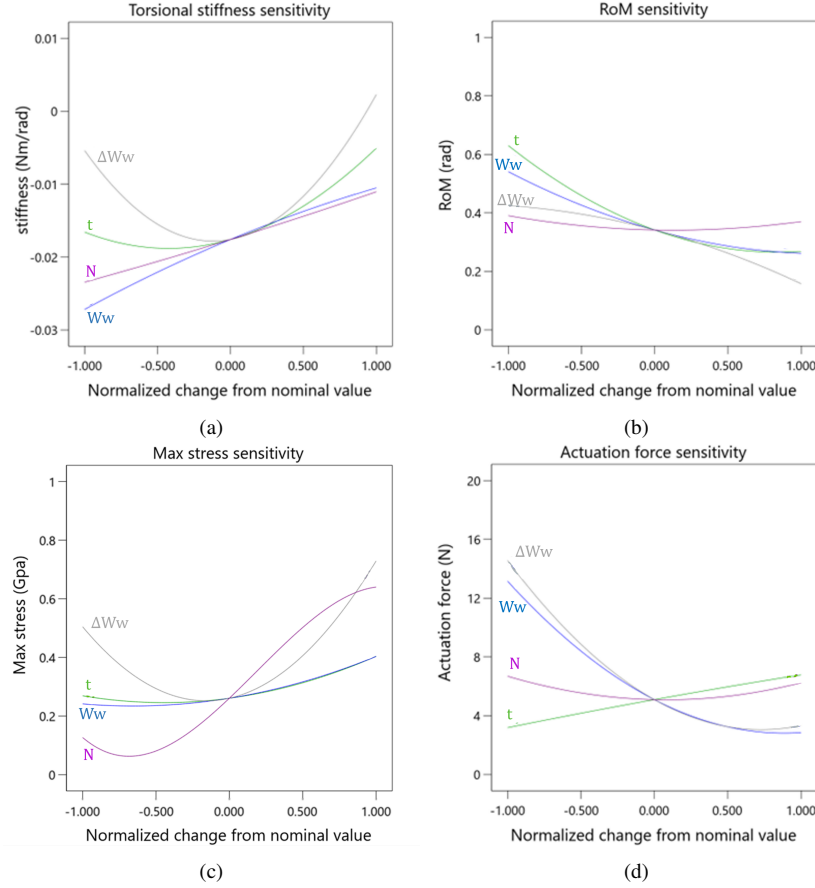


Fig. 17: RSM analysis of T beam parameters: t , w_w , Δw_w , N .

Parameter	Nominal value	Scaling factor
t (mm)	1.4	0.6
w_w (mm)	27.5	7.5
w_f (mm)	10.5	4.5
t_r	1.05	0.45
Δw_w (mm)	0	10
w_g (mm)	10	5
l_g (mm)	1.75	0.75
N	20	3

TABLE III: Normalization of T beam paramters.

b) RSM analysis: From the 55 factorial points (appendix C.1) generated by the four parameters: t , w_w , Δw_w , and N , and by utilizing RSM, regression models approximating the relations between the parameters and the responses are developed in appendix C.2. Fig. 17 (a)-(d) shows the sensitivities of each parameter with respect to distinct responses. Different from the sensitivity analysis conducted in the previous section, the interaction between the parameters is accounted for in

the RSM analysis, thus offering more accurate models for behavior prediction. Further details regarding the two-variable response surfaces can be referred to appendix C.3.

To analyze the accuracy of the predictive models, the factorial points are fed into the predictive models, and the obtained response values are compared with those from the actual FEM simulation as shown in appendix C.4. The results show that the quadratic model predicts the responses better.

With the response predictive models, the optimal shape of the T beam can be determined according to the target performance specified by designers. For the application of the proposed ball joint, the objective lies in maximizing the stiffness variation range and RoM, all while maintaining stress levels below the yield strength and minimizing actuation force. Fig. 18 summarizes the boundary conditions of the parameters as well as the target performance of the responses. The lower bound of t is limited by the manufacturing technique. As for w_w , small w_w can lead to reduced bending stiffness (supporting stiff-

ness) of the T beam, which is undesirable for ball joint application. Conversely, an overly large w_w transforms the webs into slender beams themselves, causing local buckling when the T beam is prestressed as demonstrated in Fig. 19. The same happens to the T beam with a high N , which indicates a shorter web length. Hence, the maximum N should be bounded to prevent local buckling. Table. 17 shows the optimal shape of the T beam, along with the performance predicted by the RSM model and results obtained through FEM.

Name	Goal	Lower Limit	Upper Limit
A:thickness	is in range	0.8	1.6
B:web width	is in range	15	35
C:web width difference	is in range	-10	10
D:web number	is in range	16	24
stiffness	minimize	-0.05	0.3
range of motion	maximize	0	1.5
stress	is in range	0	4.4E+07
force	minimize	0	55.8699

Fig. 18: Boundary condition for the T beam parameters.



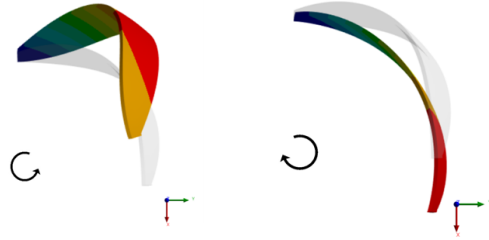
Fig. 19: Local buckling of the T beam.

Optimal shape	$t = 0.8\text{mm}$, $w_w = 15\text{mm}$, $w_f = 9\text{mm}$, $t_r = 1$, $\Delta w_w = 0.37\text{mm}$ $w_g = w_w$, $l_g = 1\text{mm}$, $N = 17$	
Performance	Predictive model	FEM
Stiffness	-0.029 Nm/rad	-0.03 Nm/rad
RoM	1.37 rad	1.08 rad
Max stress	4.4E+7 Pa	1.74E+8 Pa
Actuation force	9 N	16 N

TABLE IV: Optimal shape of the T beam and its performance.

2) *diagonal beam*: The influence of the four parameters on four responses is compared in Fig. 20 (a)-(d). The parameters are normalized using scaling factors as specified in Table. 18.

Given that the diagonal beam behaves differently when rotated clockwise (CW) and counterclockwise (CCW) as shown in Fig. 20, the sensitivity analyses are conducted separately. In Fig. 21, solid lines correspond to CCW rotation (push), while dashed lines indicate CW rotation (pull). Figures 21a and 21b reveal that, despite slight level differences, torsional stiffness and maximum stress demonstrate similar sensitivity trends in both pushing and pulling directions.



(a) The deformation of the diagonal beam when subjected to CCW moment (pushing direction).
(b) The deformation of the diagonal beam when subjected to CW moment (pulling direction).

Fig. 20: The deformation of the diagonal beam.

Parameter	Nominal value	Scaling factor
Δr (mm)	7.5	5
κ (mm)	4	2
α (deg)	60	30
t (mm)	0.9	0.1

TABLE V: Normalization of diagonal beam parameters.

The results also exhibit a consistent trend wherein torsional stiffness and actuation force demonstrate an increase across all parameters. While maximum stress increases with t and α , but decrease with Δr and κ . Nevertheless, the sensitivity of the maximum stress appears to be negligible when compared to the yield strength of PA12, which ranges from 20-60 MPa ([13] [14]).

An interesting behavior of RoM is observed in Fig. 21f. Due to the diagonal connection, the RoM of the diagonal beam is always equal to $\alpha/2$ in the pushing direction regardless of the values of the parameters. After the twisting angle exceeds $\alpha/2$, the moment either saturates or diminishes, resulting in either zero torsional stiffness or negative torsional stiffness, depending on κ as illustrated in Fig. 22

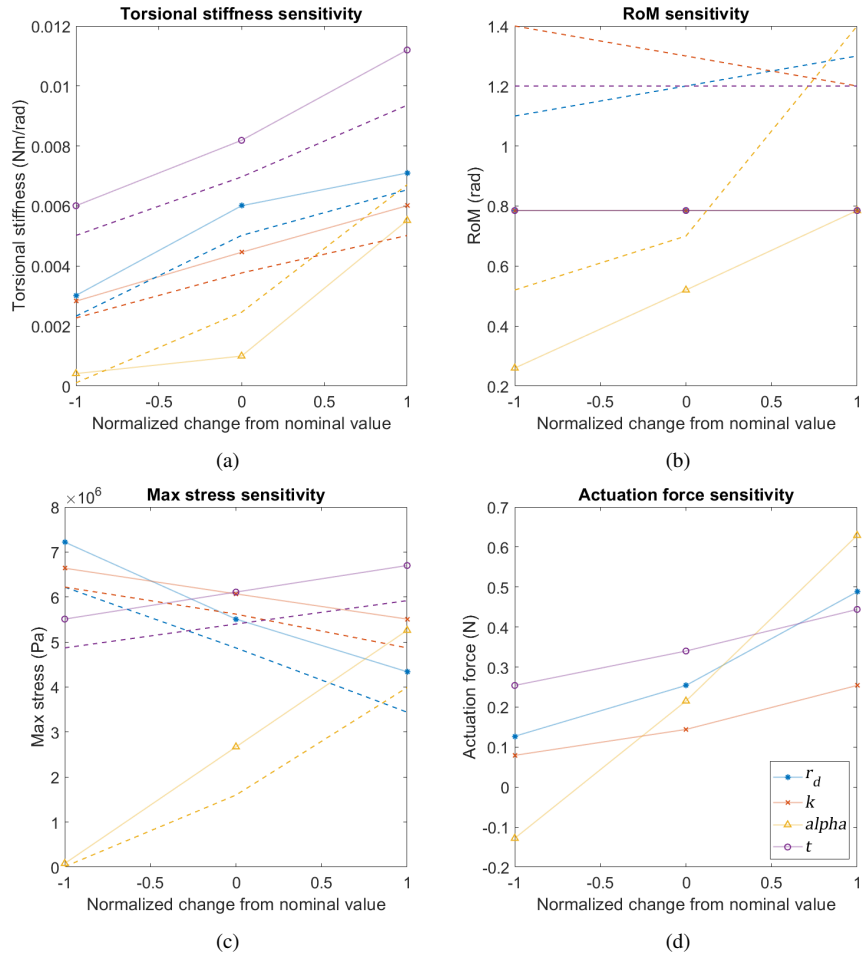


Fig. 21: Sensitivity analysis of diagonal beam.

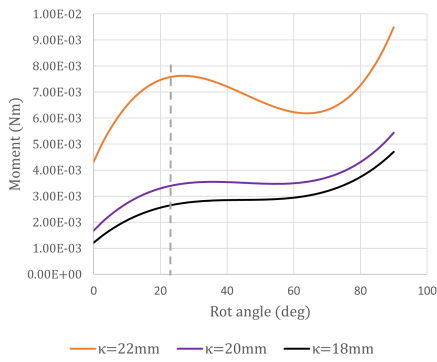


Fig. 22: Reaction moment of different κ ($\alpha = 45$ deg).

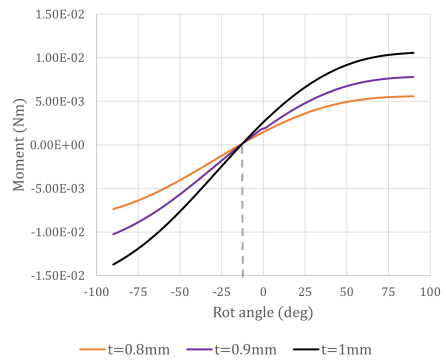


Fig. 23: Reaction moment shift due to the prestress of the diagonal beam ($\alpha = 90$ deg).

On the contrary, RoM is still dependent on Δr , κ , and α in the pulling direction. The results show RoM becomes larger as Δr and α increase, while the opposite holds true for κ . This indicates that a more slender and outwardly-bent diagonal beam possesses a greater RoM. This phenomenon is due to the diagonal beam undergoing bending deformation rather than contraction when subjected to a CCW moment or elongation under CW moment, providing a large elastic deformation range before the beam reaches its yield strength.

An undesirable behavior of the diagonal beam is captured in Figure 23. The prestressing of the diagonal beam not only results in a reaction force but also generates a reaction moment about the axis. Consequently, the moment at a 0-degree rotation angle deviates from zero, exhibiting an approximate shift of 10-15 degrees. A solution to this concern involves arranging two opposing diagonal beams, as depicted in Figure 11. By adopting this configuration, the moment shifts of the opposing diagonal beams cancel each other out, resulting in a VTS element with zero moment at a 0-degree rotation angle.

Fig. 24 shows how the prestress level affects the torsional stiffness and RoM of the diagonal beam. The axial prestress reduces the torsional stiffness along with the positive stiffness RoM in the pushing direction. The positive stiffness range is then followed by a zero/negative stiffness range, whose RoM (denoted with black lines) expands with the prestress. Regarding the pulling direction, the prestress leads to reduced torsional stiffness but an augmented RoM.

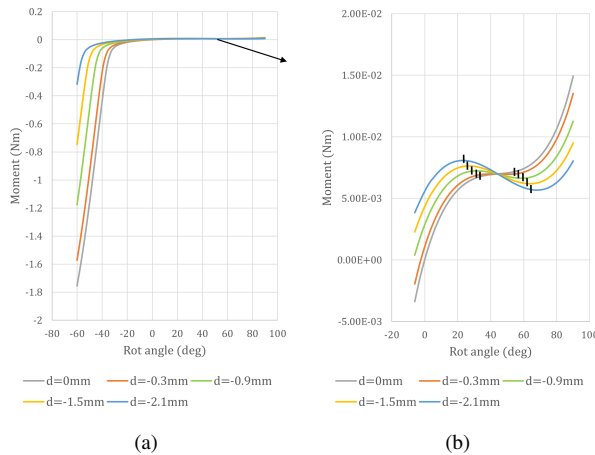


Fig. 24: Effect of displacement prestress level on the reaction moment of the diagonal beam. ($\alpha=45$ deg). (a) shows the Moment-Rot angle graph in both the CCW and CW direction and (b) shows the Moment-Rot angle graph in the CCW (pushing) direction, black lines denote the RoM.

3) *compliant VTS element*: In this section, the FEM-simulated torsional stiffness of the compliant VTS element is compared with the experimentally measured result. Fig. 25 illustrates the moment-rotation angle relationship of the VTS element under varying prestress levels. Dashed lines represent the FEM data, while solid lines represent the experimental data. The results reveal a consistent color order between the measured and simulated torsional stiffness, validating that an increase in prestress results in decreased torsional stiffness. However, a value discrepancy is observed between the FEM and experimental results. Moreover, the FEM result exhibits nonlinearity, whereas the experimental result is almost linear. This variation may be attributed to several factors, including differences in material properties, the 3D printing technique employed, and most importantly, the 3D printing infill percentage.

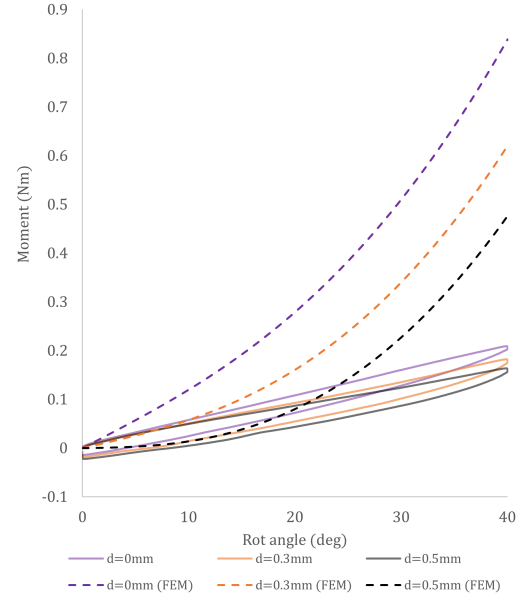


Fig. 25: Moment-rotation angle graph of the compliant VTS element. "d" represents the displacement of the prestress point.

In FEM simulation, the material is set to be isotropic. While in reality, the material exhibits slight differences in mechanical properties between different directions. Moreover, the choice of 3D printing technique significantly affects the stiffness. Unlike powder bed fusion technique that produces more homogeneous models, the FDM (Fused Deposition Modeling) printing technique used in this experiment results in reduced stiffness due to the relatively weak bond between deposited layers. To ensure axis symmetry, the VTS element must be printed in a vertical orientation, illustrated in Fig. 26a. This orientation implies that when subjected to a moment,

the VTS element deforms along the direction with the least robust material adhesion, which may lead to reduced torsional stiffness in comparison to the predictions from FEM simulations.

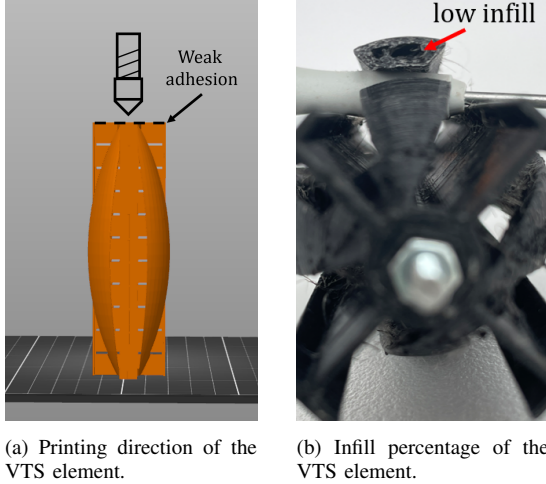


Fig. 26: Possible reasons for torsional stiffness discrepancy between FEM and experiment results.

The printing infill percentage is the most probable reason for the observed reduction in torsional stiffness in the experiment. In FEM, a solid element is used with an infill percentage of 100%. However, the element used in the experiment has a low infill percentage as shown in Fig. 26b.

In summary, despite the discrepancy, the experiment validates the anticipation of decreasing stiffness with increasing prestress.

IV. DISCUSSION

A. Performance of the VTS element

Table. 27 and Table. 28 conclude the sensitivity analysis of the T beam and the diagonal beam by classifying the influence of parameters into four levels: positive influence(+), negative(-) influence, insignificant(x), and fluctuating(F). 'Positive influence' signifies that the response increases with parameter value, while 'negative influence' denotes a response decrease with higher parameter values. 'Insignificant' implies the parameter has a negligible effect on the response, and 'fluctuating' indicates a non-quasi-linear relationship. The tables offer insights into the parameter-response dynamics, by manipulating the value of the parameters, the optimal shape of the VTS element that suffices the performance objectives and spatial constraints can be determined.

Since the VTS element comprises parallel-connected T beams and diagonal beams, its overall torsional stiffness

and actuation force are the superposition of the two beams, whereas the RoM is determined by the beam with the smaller RoM. To leverage the performance of both beams, it is essential to ensure their torsional stiffness values are comparable. However, when considering identical thickness and length, the torsional stiffness provided by the diagonal beam is an order of magnitude lower than that provided by the T beam. In order to match the level of the T beam, a substantial increase in the thickness of the diagonal beam is required. However, this implies diminished material efficiency and reduced strength-to-weight ratio.

On the other hand, unlike the T beam, whose RoM greatly relies upon the level of the prestress, the advantage of the diagonal beam is having a considerably larger and consistent RoM within the positive stiffness range (I) depicted in Fig. 27. The prestress has little impact on the positive stiffness RoM as can be seen in Fig. 24b. Originally, the purpose of the diagonal beam is to solely contribute positive torsional stiffness (I), compensating for the T beam's negative stiffness. However, beyond the positive stiffness range, the behavior of the diagonal beam starts to mirror that of the T beam(II). At a Rot angle = α deg, the moment-Rot angle behavior of the diagonal beam coincides with that of the T beam at a Rot angle = 0 deg. In other words, a α degree shift of the torsional stiffness and RoM behavior of the diagonal beam overlap with those of the T beam. This distinctive trait of the diagonal beam holds promising applications.

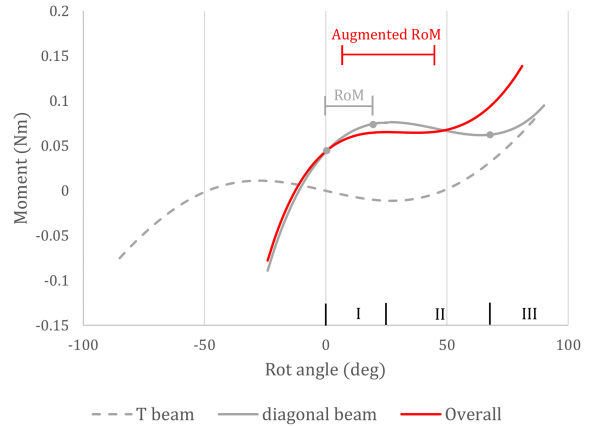


Fig. 27: Summation of T beam moment and diagonal beam moment at prestress $d = 2\text{mm}$. The dashed gray line represents the behavior of the T beam, whereas the solid gray line represents the diagonal beam. The combined moment of both beams is represented by the red line. ($\alpha = 45$ deg)

For instance, the diagonal beam itself can offer continuous variable torsional stiffness across both the positive

	Torsional stiffness	RoM	Max Stress	Actuation force	Bending stiffness
t	F	-	+	+	+
w_w	+	-	+	-	x
w_f	F	+	x	x	x
t_r	F	-	-	-	-
Δw_w	F	-	-	-	x
w_g	F	+	-	x	x
l_g	x	x	x	x	x
N	F	x	x	-	-

positive influence(+) / negative influence(-) / insignificant(x) / fluctuating(F)

TABLE VI: correlation of the T beam parameters and responses

	Torsional stiffness	RoM	Max Stress	Actuation force
	CCW/CW	CCW/CW	CCW/CW	
Δr	+/+	x/+	-/-	+
κ	+/+	x/-	-/-	+
α	+/+	x/+	+/+	+
t	+/+	x/x	+/+	+

positive influence(+) / negative influence(-) / insignificant(x) / fluctuating(F)

TABLE VII: correlation of the diagonal beam parameters and responses

stiffness range (I,III) and the zero/negative stiffness range (II), as shown in Fig. 27 denoted with the solid grey line. The potential energy minima at the junction point between II and III represents a stable position where the diagonal beam remains stationary without external energy input. Therefore, a possible application of the diagonal beam is to serve as a non-back-drivable mechanism that locks the rotational motion at this junction point. Moreover, when integrating the diagonal beam and the T beam, the former exhibits positive stiffness followed by negative stiffness, while the sequence reverses for the latter. Since the overall stiffness is the sum of the stiffness of two beams, a matching overall stiffness of I and II can be achieved by maneuvering the design parameters, resulting in augmented RoMs at specific torsional stiffness levels.

Although the diagonal beam itself offers the continuous variable torsional stiffness feature, making the incorporation of the T beam seems redundant. The downside of using a stand-alone diagonal beam is a lower stiffness variation gradient when compared to the T beam. As previously mentioned, when considering beams with equal thickness and length, the T beam outperforms the diagonal beam in both stiffness level and variation gradient by an order of magnitude. This not only underscores the superior material efficiency of the T beam but also highlights a crucial benefit: a slight axial displacement of the prestressed point generates a

much greater stiffness variation compared to the diagonal beam. This characteristic becomes particularly significant and advantageous in ball joint applications, as the axial displacement of the prestressed point induces undesired translational movement of the ball joint's end effector.

To achieve the equivalent stiffness variation as the T beam, the axial displacement of the diagonal beam's prestress point would need to be significantly larger. As a result, the role of the T beam becomes a coarse stiffness adjuster, while the diagonal beam excels in finer stiffness adjustments. In conclusion, the T beam provides high stiffness variation efficiency and ensures insignificant translational movement of the ball joint. Meanwhile the diagonal beam secures the stability of the ball joint throughout the stiffness adjustment process. Together the integration of the two beams facilitates a compliant ball joint with an expansive stiffness variation range, high stability, and precise motion control.

Apart from the symmetrical configuration of the VTS element as shown in Fig. 11, the behavior difference between the CCW(pushing) direction and CW(pulling) direction of the diagonal beam can be exploited for designing VTS elements with asymmetric torsional stiffness behavior as demonstrated in Fig. 28. so that the motion of the ball joint can also be customized in different directions.

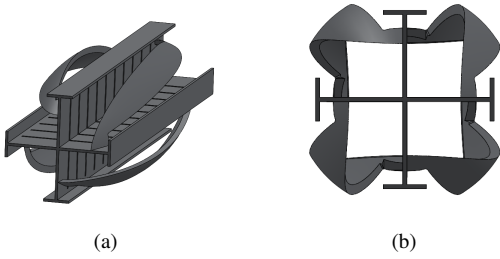


Fig. 28: Asymmetric configuration of the VTS element.

B. Compliant VS ball joint



Fig. 29: Fabricated compliant VS ball joint.

Compliant VS ball joint is fabricated with 3D printing technology as shown in Fig. 29. In this design, the prestress of VTS elements is done manually using threaded rods and nuts. However, adjustment of the prestress for the ball joint is impractical and imprecise. A more feasible approach involves active actuation methods such as electromagnetic, piezoelectric, and smart material actuation. These techniques offer precise control over prestress level and allow for miniaturization. However, a major drawback is the constant energy input for sustaining the structure at its prestressed state. To address this issue, non-back-drivable can be integrated into the VTS elements. Nevertheless, in cases where the need for adjusting prestress is frequent, the prestress(actuation) force level becomes critical, and the sensitivity study of actuation force provides a valuable criterion to improve energy efficiency.

The experimental validation for the accuracy of the ball joint's analytical model is absent due to the high complexity of the experimental setup. Nevertheless, various factors that affect the model's performance can be identified to reduce error. For instance, the introduction of prestress inevitably induces displacement at the axis-point of the VTS element, thereby resulting in translational

movement of the ball joint. To address this, designers can establish a threshold for permissible displacement, tailored to the specific application's demands. This trade-off facilitates a balance between mitigating translational movement and expanding the stiffness variation range of the ball joint.

Other factors encompass the weight of the structure, leading to unaccounted forces and moments that is excluded from the analytical model. The connectors' rigidity directly affects the overall compliance of the ball joint. Moreover, the presence of hysteresis within the elastic material introduces an irreversible deformation. Nonlinear deformations such as the shortening effect of the bending beam and the varying bending stiffness of the VTS element due to prestress. Taking these factors into consideration helps improve the precision and performance of the ball joint.

V. CONCLUSION

This paper accomplishes two breakthroughs in designing variable stiffness mechanisms. Firstly, it presents a novel compliant continuous variable torsional stiffness (VTS) element, where the stiffness spans from positive to zero. Secondly, by connecting the VTS element, a variable stiffness (VS) ball joint is created. The method used for tuning stiffness is by compressing the center axis of the VTS element. As the prestress increases, the torsional stiffness is gradually reduced.

After the configuration of the VTS element is decided, shape optimization is conducted for enhancing the performance of the ball joint, including maximizing the range of motion (RoM), expanding the stiffness variation range, and minimizing the actuation force. This shape optimization is achieved by a thorough investigation into the design parameters' sensitivity. The parametric analysis establishes predictive models to describe the quantitative relationship between design parameters and performance. With the predictive models, the optimal shape of the VTS element is determined. This optimized VTS element provides a 0.033 Nm/rad variable torsional stiffness range within a 0.2m x 0.04m x 0.04m space.

Next, in order to validate the FEM findings, an experiment is undertaken to measure the torsional stiffness of the VTS element. The results reveal that while there is a stiffness discrepancy between the FEM simulations and the experimental data, they consistently exhibit the same trend: an increase in prestress leads to a decrease in torsional stiffness.

In regard to the behavior of the ball joint, an analytical model is developed and implemented in MATLAB, constructing a graphical user interface (GUI) that allows users to easily predict the ball joint's reaction

force/moment when an input displacement of the end effector is applied. This analytical model accounts for both the torsional stiffness and support stiffness of the VTS element, ensuring its fidelity in representing the real-world ball joint. In the analytical model, the reaction force/moment is dependent on the known variables: stiffness and input displacement. As a result, future enhancements for the analytical model and GUI involve enabling users to directly specify the VTS element's shape, prestress level, and input displacement to obtain the reaction force/moment, eliminating the need for users to compute the VTS element's stiffness themselves.

In summary, this study unveils an innovative and promising potential in variable stiffness joints. The proposed compliant VS ball joint can be used in various applications such as exoskeleton joints, prostheses, and bio-mimicking. The variable stiffness characteristics equip the joint with high adaptability to multi-tasks and environmental changes. However, despite the comprehensive investigation into numerous factors affecting the performance, other factors such as material mass, the influence of prestress on the VTS element's bending stiffness, and web local buckling can be considered in future work to improve the prediction of the ball joint's behavior.

REFERENCES

- [1] J. Guo, "Conceptual mechanical design of antagonistic variable stiffness joint based on equivalent quadratic torsion spring," *Science Progress*, vol. 103, p. 003685042094129, 07 2020.
- [2] K. Kinnunen, S. Laine, T. Tiainen, R. Viitala, A. Seppänen, T. Turrin, P. Kiviluoma, and R. Viitala, "Coupling with adjustable torsional stiffness," *Proceedings of the Estonian Academy of Sciences*, vol. Volume 70, issue 4, p. 7, 2021.
- [3] J. M. Robinson, "A compliant mechanism-based variable-stiffness joint," 2015.
- [4] R. Van Ham, B. Vanderborght, M. Damme, B. Verrelst, and D. Lefeber, "Maccepa: The mechanically adjustable compliance and controllable equilibrium position actuator for 'controlled passive walking'," vol. 2006, pp. 2195 – 2200, 06 2006.
- [5] J. Guo, J.-H. Low, J. Liu, Y. Li, Z. Liu, and C.-H. Yeow, "Three-dimensional printable ball joints with variable stiffness for robotic applications based on soft pneumatic elastomer actuators," *Polymers*, vol. 14, no. 17, 2022.
- [6] Q. Boehler, M. Vedrines, S. Abdelaziz, P. Poignet, and P. Renaud, "Design and evaluation of a novel variable stiffness spherical joint with application to mr-compatible robot design," 05 2016.
- [7] P. Kuppens, M. Bessa, J. Herder, and J. Hopkins, "Monolithic binary stiffness building blocks for mechanical digital machines," *Extreme Mechanics Letters*, vol. 42, p. 101120, 2021.
- [8] S. Shimohara, R. Lee, and J. Hopkins, "Compliant mechanisms that achieve binary stiffness along multiple degrees of freedom. journal of composite materials," 2022.
- [9] Y. Yang, y. Chen, Y. Li, and M. Chen, "3d printing of variable stiffness hyper-redundant robotic arm," pp. 3871–3877, 05 2016.
- [10] G. R. Ali Amoozandeh Nobaveh, Just L. Herder, "Compliant variable negative to zero to positive stiffness twisting elements.," 2023.
- [11] H.-C. Tsai and J. M. Kelly, "Buckling of short beams with warping effect included," *International Journal of Solids and Structures*, vol. 42, no. 1, pp. 239–253, 2005.
- [12] StatEase, "Design-expert." <https://www.statease.com/docs/v12/>, 2023. Accessed: 20/09/2023.
- [13] P. McDonnell, K. McGarvey, L. Rochford, and C. . Brádaigh, "Processing and mechanical properties evaluation of a commingled

- carbon-fibre/pa-12 composite,” *Composites Part A: Applied Science and Manufacturing*, vol. 32, no. 7, pp. 925–932, 2001.
- [14] G. Salmoria, J. Leite, L. Vieira, A. Pires, and C. Roesler, “Mechanical properties of pa6/pa12 blend specimens prepared by selective laser sintering,” *Polymer Testing*, vol. 31, no. 3, pp. 411–416, 2012.

4

Conclusion

The contribution of this report is the presentation of a method for fulfilling the research gap identified in the literature review: To design a compliant variable stiffness ball joint.

In the literature review: "Review on methods of variable torsional stiffness", methods for achieving variable torsional stiffness are gathered and evaluated, and from there the method with the best overall performance is determined: Applying prestress to elastic elements to modify their stiffness. This chosen method is then implemented in designing the compliant variable torsional stiffness (VTS) element, which is later used for constructing the ball joint.

In the concept generation phase of the VTS element, three designs employing the prestress as the stiffness tuning method are developed. Concept III from A is selected to be the most suitable design for ball joint application due to its broad and continuous stiffness variation range, smooth rotational motion, and sufficient support stiffness ensuring precise control of the ball joint.

In the main paper: "Design of compliant variable stiffness ball joint", the development of the ball joint is elucidated. Starting from introducing the geometry detail and working principle of the VTS element. Then, the shape of the VTS element is optimized to meet the thesis objectives. Eventually, three optimized VTS element is connected to realize the compliant variable stiffness ball joint. The value of this paper is not limited to proposing a novel VTS design that improves the stiffness variability, strength-to-weight ratio, and scalability as compared to the existing VTS mechanisms, it also delves deep into the quantitative analysis of the ball joint's behavior.

In conclusion, the compliant variable stiffness ball joint achieves continuous stiffness variability, which has not been discovered in previous research. The stiffness variation range as well as the RoM are maximized, and the actuation force used for tuning the stiffness is minimized for energy efficiency concerns. In addition, an analytical model is derived for describing the ball joint's behavior. However, the verification of the accuracy of the ball joint's analytical model is omitted in this research due to the complex experimental setup. Therefore, future work involves considering additional factors that influence the ball joint's performance, selecting an appropriate actuation method, exploring scalability, and investigating the precision of the ball joint.

References

- [1] Giuseppe Radaelli Ali Amoozandeh Nobaveh Just L. Herder. “Compliant variable negative to zero to positive stiffness twisting elements.” In: (2023).
- [2] P.R. Kuppens et al. “Monolithic binary stiffness building blocks for mechanical digital machines”. In: *Extreme Mechanics Letters* 42 (2021), p. 101120. ISSN: 2352-4316. DOI: <https://doi.org/10.1016/j.eml.2020.101120>. URL: <https://www.sciencedirect.com/science/article/pii/S235243162030290X>.
- [3] S Shimohara, RH Lee, and JB Hopkins. “Compliant mechanisms that achieve binary stiffness along multiple degrees of freedom. *Journal of Composite Materials*”. In: (2022).
- [4] Jiaqi Zhang et al. “A lightweight variable stiffness knee exoskeleton driven by shape memory alloy”. In: *Industrial Robot: the international journal of robotics research and application* ahead-of-print (Feb. 2022). DOI: 10.1108/IR-11-2021-0262.

A

Concept generation- compliant VTS mechanism

A.1. Chapter Introduction

In this chapter, three concepts of compliant VTS mechanisms are introduced. Section: Concept Overview illustrates the working principles and geometrical details of these three designs. It is important to note that, during the concept generation phase, the primary objective is to generate multiple ideas and verify their feasibility. Therefore, this section does not delve into the dimensions or the quantitative performances of the designs as they are not the main focus of this investigation. Section: Performance comparison examines the behavior of each concept and their degree of match with the thesis objectives such that the most suitable design can be identified for further optimization.

According to the conclusion of the literature overview and the thesis objective, the most ideal way to tune the stiffness of compliant mechanisms is to apply different levels of prestress on elastic elements. By doing so, the potential energy stored in the elastic elements varies, leading to stiffness changes in certain directions. The following three designs all operate on the abovementioned working principle and a more thorough explanation is elaborated in the following section.

Before going through the details of the three concepts, several commonly used terms in compliant mechanisms are introduced to help picture a clearer view of the interaction between elements. First, the "ground" refers to the fixed reference point or base to which the compliant mechanism is attached or anchored. It serves as a stable and immovable foundation for the mechanism's operation. Second, the "end effector" refers to the component that directly interacts with the external environment, where normally the input force and moment are applied. Third, the "elastic elements" are the components that deflect under input force and moment. The stiffness of the elastic elements is the factor that determines the movement of the end effector.

A.2. Concept overview

A.2.1. Concept I

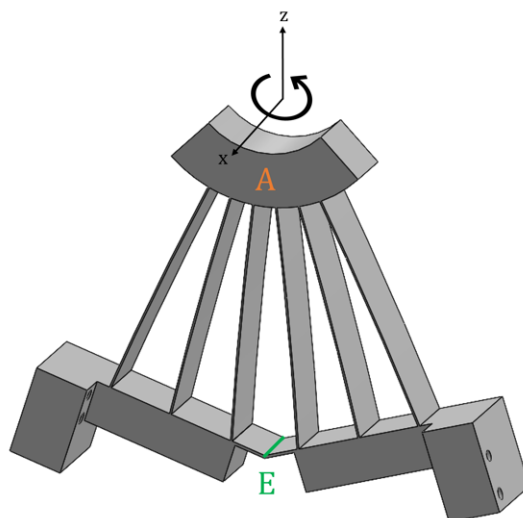


Figure A.1: VTS mechanism - Concept I

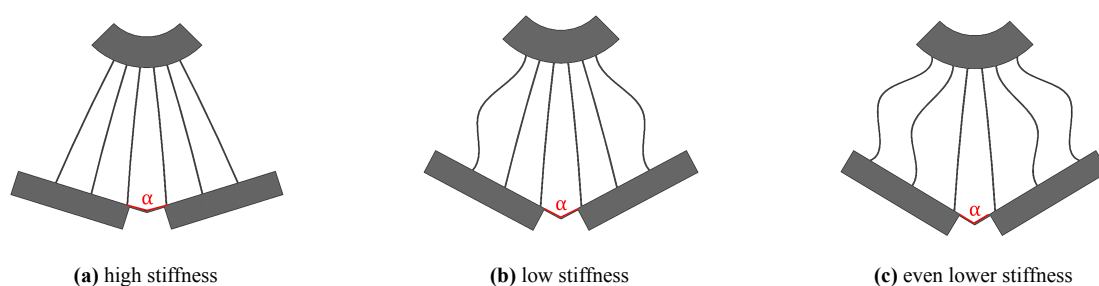


Figure A.2: Different stiffness states.

Concept I employed the concept of beam buckling used in [2]. In [2], the binary torsional stiffness of the rotary device is achieved by buckling and unbuckling beams. However, this limits the rotary device to provide only two extreme stiffness states. In order to augment the stiffness states, Concept I arranges more beams in a circular configuration as illustrated in Fig.A.1. The edge(denoted as E) connecting the two cuboids is the ground, the arc-shaped block on the top(denoted as A) is the end effector, and the beams in between are the elastic elements that determine the overall torsional stiffness of this design. When the two cuboids are pushed and rotated about E, the outermost beams start to buckle. These buckled beams exhibit negative stiffness that cancels out the positive stiffness of the unbuckled beams in the middle. The mathematical detail of stiffness value is not addressed here but can be found in [2]. As angle α becomes larger, more and more beams are buckled the and torsional stiffness of the mechanism decreases. The overall stiffness of the design is dependent on the rotation angle α , namely, the number of buckled beams.

A.2.2. Concept 2

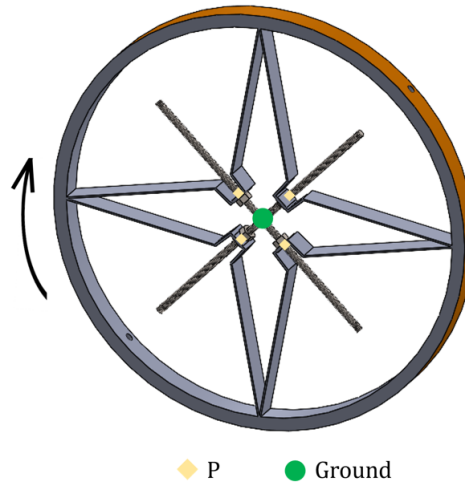


Figure A.3: VTS mechanism - Concept II

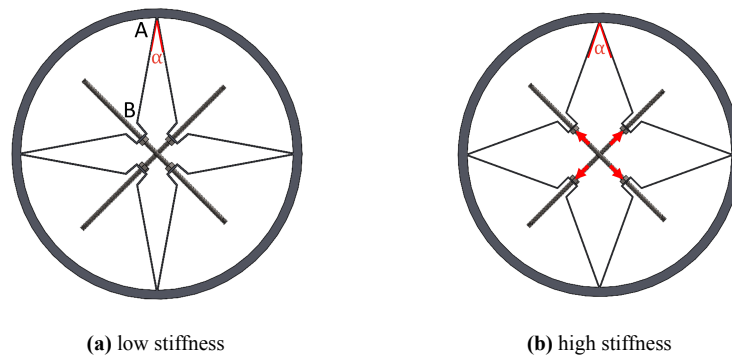


Figure A.4: Different stiffness states.

Concept II connects four pairs of slender beams in a circular arrangement to form a rotational element as shown in Fig.A.4. In this configuration, the center point is the designated ground. Noted that a rigid component (threaded rod) will be used to connect the center point and the four points which are collectively denoted as P in Fig.A.4. The outer ring is the end effector (colored in orange). As the outer ring experiences a moment and rotates, the slender beams bend and their stiffness determines the angular displacement of the outer ring. In other words, the overall torsional stiffness of the element is the sum of the bending stiffness of all slender beams.

To be able to tune the bending stiffness of the slender beam pair, the two slender beams within a pair are arranged in parallel with an angular offset α , forming a triangular shape. In theory, the bending stiffness of a slender beam AB reflected at point "A" is given by the equation:

$$k'_{AB} = k_{AB} \sin^2(\alpha/2)$$

Where k_{AB} is the bending stiffness of slender beam AB without angular offset. Therefore, by

varying the value of α , the bending stiffness of the beam pair reflected at the end effector can be altered. According to the equation, an increased value of α results in a higher bending stiffness of the beam pair.

In order to vary the value of α , two threaded rods are used to adjust the position of P. When the screw nuts push P outward, α becomes larger and consequently the torsional stiffness of the element increases. Fig.A.4a shows the original undeformed configuration and Fig.A.4b shows the deformed configuration with a larger α . In conclusion, by adjusting the position of P along the axial axis of the rods, the value of α varies thereby leading to a change in the bending stiffness of the beam pairs reflected at the end effector and the torsional stiffness of the element.

A.2.3. Concept 3

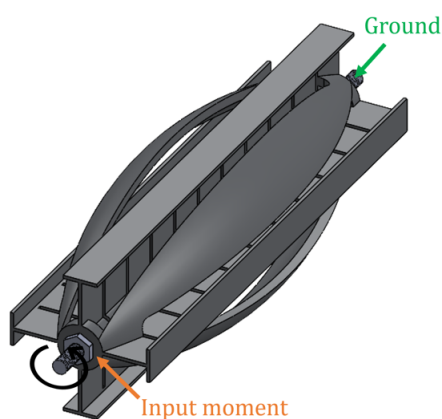


Figure A.5: VTS mechanism - Concept III

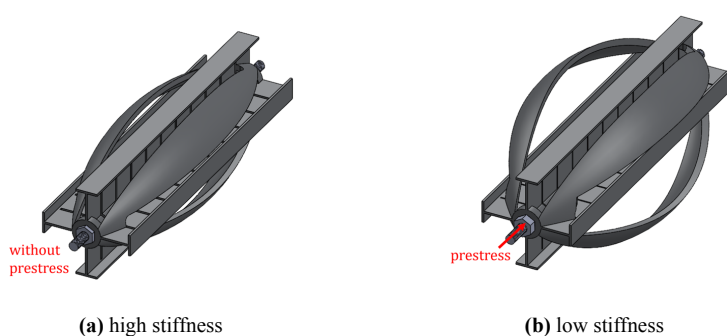


Figure A.6: Different stiffness states.

Based on [1], Concept III utilizes an axially prestressed crucified beam to achieve variable torsional stiffness. It is known when an open-section flanged beam such as I beam or crucified beam is compressed in the axial direction as shown in Fig.A.7, the resulting stress induces a twisting deformation, commonly referred to as warping. As the warping occurs, the torsional stiffness decreases. The higher the prestress, the lower the torsional stiffness.

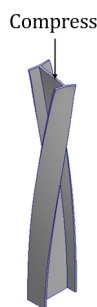


Figure A.7: I beam subjected to compression load.

During the compression, the torsional stiffness of the beam varies from positive to negative. However, negative stiffness implies the bistability of the structure. This bistability characteristic entails that the structure will not remain in its original state but deform to one of the stable equilibrium states. In this case, it is disadvantageous since these open-section beams twist during the stiffness-adjusting process, meaning that the variable stiffness joint will rotate before an external moment is applied to the VTS element.

To address this issue, one way is to tune the stiffness only in the positive range. However, given beam length = 0.18m and beam thickness = 0.8mm, the range of motion will be extremely small compared to the negative stiffness range. To increase the range of motion, the length should be increased or the thickness should be decreased. These two solutions are unfavorable since increasing the length leads to low space efficiency, while the thickness can only be decreased to a limited level, depending on the material and manufacturing technique.

Another way is to integrate a positive stiffness agent to compensate for the negative stiffness from the open-section beam. As long as the overall stiffness of the VTS element is above zero, the rotation will be constrained during the stiffness tuning process. Numerous positive stiffness structures are considered such as torsional springs, beams, and wires. Nevertheless, the torsional spring can only provide near-constant positive stiffness in one direction. When turned in the other direction, it tends to unwind and deform plastically, losing its initial stiffness characteristics. As for wires, the challenge is to integrate the wires into the open-section beam. The integration requires additional parts to clamp the wires at the center of the open-section beam, thereby rigidly connecting the wires and the open-section beam. Yet this additional clamping mechanism not only complicates the structure but also indicates that the VTS element is no longer monolithic.

Consequently, diagonal beams as shown in FigA.5 are chosen as the stiffness compensator. The elongated curved shape exhibits a relatively large range of motion and adequate torsional stiffness that matches the negative stiffness level of the T beam. Instead of connecting a beam at the center of the crucified beam, the diagonal beams are connected around the crucified beam in order to reduce the required actuation force for providing prestress (For more details refer to Chapter: Main paper.)

To sum up, in Concept III, the crucified beam is used to provide variable torsional stiffness characteristics. Whereas the diagonal beams are used for compensating the negative stiffness of the crucified beam, keeping the VTS element motionless during the stiffness tuning process. The overall structure offers the feature of variable torsional stiffness, in which the value ranges from positive to zero.

A.3. Performance Comparison

In this section, the three concepts are 3D printed and tested, after which their performances are evaluated.

Although Concept I is equipped with multiple stiffness states, two drawbacks are observed. Firstly, the thin plates buckle when they are axially prestressed. These buckled beams exhibit negative stiffness, introducing bistability in the transverse direction as depicted in Fig. A.8. Since the beams are bistable, the rotation of the end effector is not smooth but discontinuous and stepwise. While such switch-like behavior might hold utility in diverse applications, it falls short of fulfilling the fundamental goal of achieving continuous variable stiffness.



Figure A.8: Concept I configuration with prestress.

Another disadvantage pertains to the low torsional stiffness about the z-axis when the plates are in a buckled configuration. Since the VTS elements proposed in this research are used for ball joints, the stiffness of the VTS element should be substantial in all directions except for the intended rotational direction (rotation about the x-axis). This prevents the translational motion of the ball joint. As a result, the low torsional stiffness about the z-axis will induce displacement error in the end effector's positioning, thereby compromising precise motion control.

Next, in theory, Concept II should be able to provide continuous variable stiffness owing to the continuous alteration of α . However, practical implementation reveals an unexpected issue. When P is pushed outward, instead of adopting the anticipated configuration illustrated in Fig. A.6a, the slender beam pair exhibits bending as depicted in Fig. A.9b, making eq. [] not applicable to this design. Although the stiffness still varies with the prestress, the same predicament as stated in Concept I occurs: Bent slender beams exhibit bistable behavior which leads to stepwise rotation.

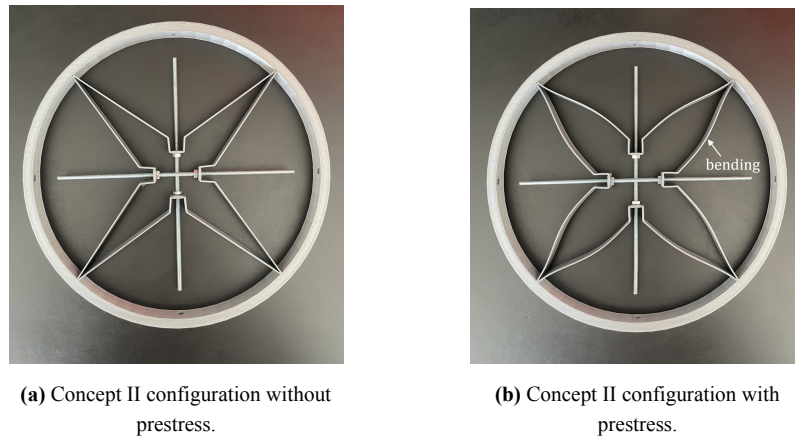


Figure A.9: The effect of prestress on Concept II leading to different stiffness states.

Finally, Concept III achieves continuous variable stiffness across positive to zero values. Nevertheless, as the stiffness of the crucified beam approaches zero, the range of motion of the VTS element becomes extremely small. It is important to note that in this context, the term "range of motion" refers to the motion range where within this range, the torsional stiffness change is less than 5 percent of the average value (as illustrated in Fig.A.10), rather than the maximum elastic deformation range of the VTS element.

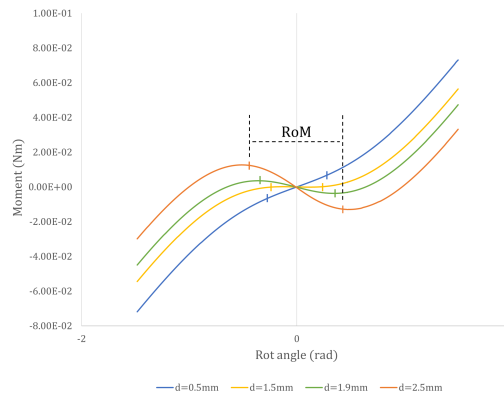


Figure A.10: Definition of RoM. "d" represents the displacement of the prestress point.

A.4. Summary

Each of the three concepts possesses the ability to achieve multiple stiffness states through the application of varying prestress levels. However, Concept I and Concept II display a notable drawback of discontinuous or stepwise rotation due to their utilization of bent beams as compliant elements. In contrast, Concept I exploits the torsional buckling of open-section beams, resulting not only in smooth rotation but also in the provision of continuous variability in stiffness.

Another criterion for performance comparison is the support stiffness. Support stiffness refers to the element stiffness in directions where the motion of the end effector should be confined. For instance, in this case, the VTS elements should allow only one rotational degree of freedom (DoF), meanwhile exhibiting high support stiffness in all other directions. Among the three concepts, Concept I displays

the worst performance in this regard, as it lacks a structure to constrain the end effector's rotation around the z-axis when the beams are buckled or bent. Concept II and Concept III on the other hand, provide adequate support stiffness to counteract unintended motion.

In regard to range of motion(RoM), Concept I offers relatively wide RoM throughout all stiffness states since both straight plate and bent plate have a large elastic deformation range. Although Concept II also utilizes thin plates(slender beams), the RoM of is much smaller than Concept I since its rotation axis is not situated at the intersection of the slender beam pair but rather at the center of the VTS element. Unlike Concept I, where torsional stiffness stems solely from the bending stiffness of the plates, in Concept II both tension stiffness and bending stiffness of the beams should be accounted for when computing the torsional stiffness of the VTS element. As for Concept III, its RoM greatly depends on the stiffness level of the open-section beam. The RoM decreases to infinitely small as the stiffness of the open-section beam approaches zero. Therefore, the VTS element has a larger operational RoM when the open-section beam's stiffness is more positive or more negative. This characteristic highlights the importance of the diagonal beam's stiffness level since it determines the VTS element's overall stiffness. If the designers aim to achieve a specified RoM at zero stiffness of the VTS element, the positive stiffness provided by the diagonal beam should match the open-section beam's negative stiffness level at that specified RoM.

Other criteria including space and material efficiency, stiffness magnitude, or actuation force which can be considered as the key determinant of energy efficiency are not investigated in the concept generation phase as Concept III outperforms the other two concepts in fulfilling the thesis objectives of achieving continuous variable torsional stiffness and exhibiting smooth rotation when subjected to external moment. As a result, Concept III is chosen as the foundational VTS element for constructing the compliant ball joint. A comprehensive research on Concept III is presented in paper:

B

Sensitivity Analysis

B.1. APDL code

In this section, the Ansys APDL code used for T beam FEM simulation is presented. The code can be input into the APDL command bar and it automatically generates the model, specified loads, and finally retrieve the FEM results.

```
1 ""
2 This code is for investigating the sensitivity of the following parameters: t, ww,
   wf, lg, N. By changing the value in the "Set design parameters" section, the
   code can model different shapes of the T beam and analyze their behavior under
   specific load steps.
3 ""
4
5 !! general inintialization
6 FINISH                                ! Finish previous analysis
7 /CLEAR,START                          ! Clear data and start new analysis
8 /CWD,'C:\Users\TZU\thesis_AnsysAPDL'  ! Location of this file
9 /FILENAME, APDLCOMMANDS               ! Set filename in ansys
10
11 !! Set design parameters
12 ww = 0.04                             !web width (in m)
13 wf = 0.009                            !flange width (in m)
14 t  = 0.0008                           !web and flange thickness (in m)
15 len = 0.00905                         !web length (in m)
16 slit = 0.11                           !gap length/web length (len)
17 Middle_BC = 'Yes'                     !having axissymmetric boundary conditions
   for middle points 'Yes' or 'No'
18 N_section = 20                        !number of sections (number of slits+1)
19 Density = 1010                         !material properties
20 Poisson = 0.38                         !0.35 for PLA          0.38 for PA12
21 Elastmod = 1.7e9                       !3.144e9 for PLA      1.7e9 for PA12
22 Prestress = -0.0028                    !displacement to tune torsional
   stiffness (in m)
23 perturbation = 0.01                    !perturbation moment to converge to one
   stable state
24 perturbation_ang = 1.5                  !perturbation angle in rad to converge
   to one stable state
25 time_step_prestress = 33                !Time steps for incremental prestressing
```

```

26 time_step_Rmoment = 170           !Time steps to evaluate reaction moment
    by a full reverse turn
27
28
29 !! Set properties
30 /PREP7
31 !element selection
32 ET, 1, shell281           ! defines a local element type from the library (ET,
    ITYPE, Ename, KOP1, KOP2)
33 mp, ex, 1, Elastmod       !Defines a linear material property as a constant
    or a function of temperature.
34 mp, nuxy, 1, Poisson
35 mp, dens,1, Density
36
37
38 sect,1,shell,,
39 secdata, t,1,0,3
40 secoffset,MID
41
42
43 !! Define keypoints SHAPE, the syntax is: K,*keypointnumber*,*Xcoord*,*Ycoord*,*
    Zcoord*
44     *DO,N_Node, 1, N_section, 1
45         N_K=10*(N_Node*2-1)
46
47         K,N_K,           0,           0,           (N_Node-1)*len
48         K,N_K+1,        ww/2,        0,           (N_Node-1)*len
49         K,N_K+2,        ww/2,        wf/2,        (N_Node-1)*len
50         K,N_K+3,        ww/2,        -wf/2,        (N_Node-1)*len
51
52
53         N_K=10*(N_Node*2)
54
55         K,N_K,           0,           0,           (N_Node-slit)*len
56         K,N_K+1,        ww/2,        0,           (N_Node-slit)*len
57         K,N_K+2,        ww/2,        wf/2,        (N_Node-slit)*len
58         K,N_K+3,        ww/2,        -wf/2,        (N_Node-slit)*len
59
60     *ENDDO
61
62
63     *DO,N_Line, 1, 2*N_section-1, 1
64
65         N_L=10*N_Line
66
67         !! Define lines crosssection
68         NUMSTR,LINE,N_L
69         L,N_L,N_L+1
70         L,N_L+1,N_L+2
71         L,N_L+1,N_L+3
72

```

```

73      !! define Lines SHAPE
74      NUMSTR,LINE,1000          ! controls the starting number for any
75      L,N_L,N_L+10
76
77      *ENDDO
78
79
80      *DO,N_Area, 1, N_section, 1
81
82      !! drag sectional lines
83      N_A= 20*N_Area-10
84      NUMSTR,AREA,N_Area*1000
85      ADRAG,N_A,, , , ,1000+2*(N_Area-1)
86      ADRAG,N_A+1,N_A+2, , , ,1000+2*(N_Area-1)
87
88      *IF, N_Area,LT,N_section,THEN
89      ADRAG,10+N_A+1,10+N_A+2, , , ,1001+2*(N_Area-1)
90
91      *ENDDO
92
93
94  NUMMRG,ALL          !Merges coincidents or equivalently defined items.
95
96      *DO,N_Mesh, 1, N_section, 1
97
98      !! Mesh Areas
99      ASEL, s, , , N_Mesh*1000, N_Mesh*1000+16,, 0
100     AATT, 1, , 1, 0, 1
101     AESIZE, all, 1E-3
102     AMESH, N_Mesh*1000,N_Mesh*1000+16
103
104     *ENDDO
105
106
107
108  !! Commands to visualize the elements.
109  /ESHAPE,1
110  /VIEW,1,1,1,1
111  eplot
112
113
114  !! SOLUTION
115  /SOLU
116  ANTYPE, 0          ! Static structural analysis
117  NLGEOM,ON         ! Set nonlinear geometry option on
118  EQSLV,SPARSE
119  autots,off
120  pstres,off
121  arclen,off
122  PRED,off

```

```

123 OUTRES,ALL,ALL
124
125
126 !! These are commands to assign ID's to the nodes that were meshed at the
      keypoints (Because these ID's are more easy to refer to when we apply the loads
      )
127 N_M_0 =          NODE(0,              0,              0)
      !Node on middle fixation side section
128 N_R_0 =          NODE(ww/4,          0,              0)
      !Node on middle fixation side section
129 N_M_I =          NODE(0,              0,              N_section*len-slit*len)
      !Node on middle actuation side section
130 N_R_I =          NODE(ww/4,          0,              N_section*len-slit*len)
      !Node on middle actuation side section
131
132
133 !! Apply constraints
134 D,N_M_I,,,,,,,,UX,UY,
135 D,N_M_0,,,,,,,,UX,UY,UZ,ROTZ
136 D,N_R_0,,,,,,,,UY,
137 CERIG, N_M_I, N_R_I,ROTZ          !this will keep the last section's web straight (
      input)
138 !CERIG, N_M_0, N_R_0,ROTZ          !this will keep the First section's web straight (
      output)
139
140
141
142 *IF, Middle_BC,EQ,'Yes',THEN
143     *DO,N_Node, 1, 50*N_section-1, 1
144
145         D,NODE(0,              0,              N_Node*len/50),,,,,Ux,UY,
146
147     *ENDDO
148 *ENDIF
149
150
151 !! Apply perturbation
152 !F,N_M_I,MZ,perturbation
153 D,N_M_I,ROTZ,perturbation_ang
154
155
156 ! Step 0-1 (Apply pretension)
157 /SOLU
158 KBC,0                                ! ramped
      loading
159 DELTIM, 1/time_step_prestress, 1E-3, 1, ON          ! Command to specify the
      number of steps in the analysis (this can be necessary for nonlinear systems
      where too big steps cause crashes)
160 D,N_M_I,UZ,Prestress
161 solve
162

```

```

163
164 FDELE, N_M_I,MZ ! deleting the perturbation load
165 DDELE, N_M_I,ROTZ ! deleting the
    perturbation angle
166
167
168 ! Step 1-2 (Update apdl registry to prevent crashes)
169 /SOLU
170 KBC,1 ! Apply this load step
    in a step
171 DELTIM, 1/2, 1E-2, 1, ON ! Command to specify
    the number of steps in the analysis (this can be necessary for nonlinear
    systems where too big steps cause crashes)
172 *GET, Rot_Ang_1, NODE, N_M_I, ROT, Z ! Figure out the rotation angle
173 D, N_M_I, ROTZ, Rot_Ang_1 ! Apply this rotation as a
    displacement to update the registry in APDL (in reality this point is already
    at this location, APDL just doesn't know that yet)
174 solve
175
176
177 ! Step 2-3 (Apply rotation and measuring the moment)
178 /SOLU
179 OUTRES, , ALL ! After this
    command, loadstep data is saved for every substep (normally it is only saved at
    the end of each loadstep)
180 KBC, 0 ! ramped
    loading
181 DELTIM, 1/time_step_Rmoment, 1E-4, 1, ON ! Command to specify the
    number of steps in the analysis (this can be necessary for nonlinear systems
    where too big steps cause crashes)
182 D, N_M_I, ROTZ, -Rot_Ang_1
183 solve
184
185
186 !! Commands to plot force-displacement output and save results
187 *GET, N_steps, active, 0, solu, NCMSS ! Count the number of
    substeps to size the table correctly
188 /POST26 ! Go to
    postprocessor menu
189 TIMERANGE, 0, 1 ! Plot data from
    loadstep 0-1 only
190 NSOL, 2, N_M_I, U, Z, displacement ! Get the displacment
    data of the node with N_M_I
191 RFORCE, 3, N_M_0, F, Z, Rforce ! Get the reaction
    force
192 /AXLAB, X, displacement in m
193 /AXLAB, Y, force in N
194 XVAR, 2 ! Put the
    displacment on the X axis in the plot
195 PLVAR, 3 ! Plot the reaction force on
    the Y axis

```

```

196
197 !! The commands below are to save force-displacement plot in a .txt file
198 *CREATE,scratch,gui
199     *DEL,VAR_export
200     *DIM,VAR_export,TABLE,N_steps,3           ! Set size of the table
           for results export
201     VGET,VAR_export(1,0),1
202     VGET,VAR_export(1,1),2
203     VGET,VAR_export(1,2),3
204     /OUTPUT,'RESULTS_force-displacement','txt','C:\Users\TZU\thesis_AnsysAPDL' !
           In this line you specify the location to export results
205     *VWRITE,VAR_export(1,0),VAR_export(1,1),VAR_export(1,2)
206     %G, %G, %G
207     /OUTPUT,TERM
208     *END
209     /INPUT,scratch,gui
210
211 !! Commands to plot moment-angle output and save results
212 *GET, N_steps, active, 0, solu, ncmss       ! Count the number of substeps
           to size the table correctly
213 /POST26                                     ! Go to postprocessor
           menu
214 TIMERANGE,2,3                               ! Plot data from
           loadstep 2-3 only
215 NSOL,2,N_M_I,ROT,Z,Rotation                 ! Get the angle data of
           the node with N_M_I
216 RFORCE,3,N_M_I,M,Z,RMoment                 ! Get the reaction
           moment
217 /AXLAB, X, Angle in rad
218 /AXLAB, Y, Reaction moment in N.m
219 XVAR,2                                       ! Put the angle on the
           X axis in the plot
220 PLVAR,3                                     ! Plot the reaction
           moment on the Y axis
221
222 !! The commands below are to save the plot in a .txt file
223 *CREATE,scratch,gui
224     *DEL,VAR_export
225     *DIM,VAR_export,TABLE,N_steps,3       ! Set size of the
           table for results export
226     VGET,VAR_export(1,0),1
227     VGET,VAR_export(1,1),2
228     VGET,VAR_export(1,2),3
229     /OUTPUT,'RESULTS_moment_angle','txt','C:\Users\TZU\thesis_AnsysAPDL' ! In this
           line you specify the location to export results
230     *VWRITE,VAR_export(1,0),VAR_export(1,1),VAR_export(1,2)
231     %G, %G, %G
232     /OUTPUT,TERM
233     *END
234     /INPUT,scratch,gui
235

```

```

236
237 !! Commands to retrieve maximum stress value and its location
238 /POST1
239 PLNSOL,S,EQV,1                !Display stress contour
240 *GET,MaxStress,PLNSOL,0,MAX    !Get maximum value of stress in contour
    display
241 *GET,AvgStress,PLNSOL,0,MAX
242 *GET,MinStress,PLNSOL,0,MIN   !Get minimum value of stress in contour
    display
243
244 PLNSOL,EPT0,EQV,1            !Display stress contour
245 *GET,MaxStrain,PLNSOL,0,MAX   !Get maximum value of strain in contour
    display
246 *GET,MinStrain,PLNSOL,0,MIN  !Get minimum value of strain in contour
    display
247
248
249 !! The commands below are to save the value in a .txt file
250 *CREATE,scratch,gui
251 /OUTPUT,'RESULTS_maximum stress and strain','txt','C:\Users\TZU\thesis_AnsysAPDL
    ! In this line you specify the location to export results
252 *VWRITE,MaxStress,MinStress,MaxStrain,MinStrain
253   %G, %G, %G %G
254   /OUTPUT,TERM
255   *END
256   /INPUT,scratch,gui

1  """
2  This code is for investigating the sensitivity of the following parameter: tr. By
   changing the value in the "Set design parameters" section, the code can model
   different shapes of the T beam and analyze their behavior under specific load
   steps.
3  """
4
5  !! general initialization
6  FINISH                        ! Finish previous analysis
7  /CLEAR,START                  ! Clear data and start new analysis
8  /CWD,'C:\Users\TZU\thesis_AnsysAPDL' ! Location of this file
9  /FILENAME, APDLCOMMANDS      ! Set filename in ansys
10
11 !! Set design parameters
12 ww = 0.04                     !web width (in m)
13 wf = 0.009                    !flange width (in m)
14 tw = 0.0012                   !web thickness (in m)
15 tf = 0.0015                   !flange thickness (in m)
16 len = 0.00905                 !web length (in m)
17 slit = 0.11                   !gap length/web length (len)
18 Middle_BC = 'Yes'            !having axissymmetric boundary conditions
    for middle points 'Yes' or 'No'
19 N_section = 20                !number of sections (number of slits+1)
20 Density = 1010                !material properties

```

```

21 Poisson = 0.38 !0.35 for PLA 0.38 for PA12
22 Elastmod = 1.7e9 !3.144e9 for PLA 1.7e9 for PA12
23 Prestress = -0.0028 !displacement to tune torsional
    stiffness (in m)
24 perturbation = 0.01 !perturbation moment to converge to one
    stable state
25 perturbation_ang = 1.5 !perturbation angle in rad to converge
    to one stable state
26 time_step_prestress = 33 !Time steps for incremental prestressing
27 time_step_Rmoment = 170 !Time steps to evaluate reaction moment
    by a full reverse turn
28
29
30 !! Set properties
31 /PREP7
32 !element selection
33 ET, 1, shell281 !shell181! SOLSH190 !shell181 !beam188 ! defines
    a local element type from the library (ET, ITYPE, Ename, KOP1, KOP2)
34
35
36 mp, ex, 1, Elastmod !Defines a linear material property as a constant
    or a function of temperature.
37 mp, nuxy, 1, Poisson
38 mp, dens,1, Density
39
40
41
42 !! Define keypoints SHAPE, the syntax is: K,*keypointnumber*,*Xcoord*,*Ycoord*,*
    Zcoord*
43 *DO,N_Node, 1, N_section, 1
44     N_K=10*(N_Node*2-1)
45
46     K,N_K, 0, 0, (N_Node-1)*len
47     K,N_K+1, ww/2, 0, (N_Node-1)*len
48     K,N_K+2, ww/2, wf/2, (N_Node-1)*len
49     K,N_K+3, ww/2, -wf/2, (N_Node-1)*len
50
51
52     N_K=10*(N_Node*2)
53
54     K,N_K, 0, 0, (N_Node-slit)*len
55     K,N_K+1, ww/2, 0, (N_Node-slit)*len
56     K,N_K+2, ww/2, wf/2, (N_Node-slit)*len
57     K,N_K+3, ww/2, -wf/2, (N_Node-slit)*len
58
59 *ENDDO
60
61
62 *DO,N_Line, 1, 2*N_section-1, 1
63
64     N_L=10*N_Line

```

```

65
66         !! Define lines crosssection
67         NUMSTR,LINE,N_L
68         L,N_L,N_L+1
69         L,N_L+1,N_L+2
70         L,N_L+1,N_L+3
71
72
73         !! define Lines SHAPE
74         NUMSTR,LINE,1000 ! controls the starting number for any
75         subsequently created lines.
76         L,N_L,N_L+10
77
78         *ENDDO
79
80         *DO,N_Area, 1, N_section, 1
81
82         !! drag sectional lines
83         N_A= 20*N_Area-10
84         NUMSTR,AREA,N_Area*1000
85         ADRAG,N_A,, , , ,1000+2*(N_Area-1)
86         ADRAG,N_A+1,N_A+2, , , ,1000+2*(N_Area-1)
87
88
89         *IF, N_Area,LT,N_section,THEN
90         ADRAG,10+N_A+1,10+N_A+2, , , ,1001+2*(N_Area-1)
91
92         *ENDDO
93
94
95
96 *DIM,TK,table,3,3,1,x,y !Define a table to specified thickness
97         at different location
98 *taxis,TK(1,1,1),1,0,ww/2*0.99,ww/2
99 *taxis,TK(1,1,1),2,-wf/2,0,wf/2
100
101
102 TK(1,1,1)= tw,tw,tf
103 TK(1,2,1)= tw,tw,tf
104 TK(1,3,1)= tw,tw,tf
105
106 sect,1,shell,, !Web
107 secfunction,%TK%,
108 secoff,mid
109
110
111 NUMMRG,ALL !Merges coincidents or
112         equivalently defined items.

```

```

113      *DO,N_Mesh, 1, N_section, 1
114
115      !! Mesh Areas
116      ASEL, s, , , N_Mesh*1000, N_Mesh*1000+16,, 0      ! Mesh webs
117      AATT, 1, , 1, 0, 1
118      AESIZE, all, 5E-4
119      AMESH, N_Mesh*1000,N_Mesh*1000+16
120      *ENDDO
121
122
123
124
125  !! Commands to visualize the elements.
126  /ESHAPE,1
127  /VIEW,1,1,1,1
128  eplot
129
130
131  !! SOLUTION
132  /SOLU
133  ANTYPE, 0                ! Static structural analysis
134  NLGEOM,ON                ! Set nonlinear geometry option on
135  EQSLV,SPARSE
136  autots,off
137  pstres,off
138  arclen,off
139  PRED,off
140  OUTRES,ALL,ALL
141
142
143  !! These are commands to assign ID's to the nodes that were meshed at the
      keypoints (Because these ID's are more easy to refer to when we apply the loads
      )
144  N_M_0 =      NODE(0,                0,                0)
      !Node on middle fixation side section
145  N_R_0 =      NODE(ww/4,            0,                0)
      !Node on middle fixation side section
146  N_M_I =      NODE(0,                0,                N_section*len-slit*len)
      !Node on middle actuation side section
147  N_R_I =      NODE(ww/4,            0,                N_section*len-slit*len)
      !Node on middle actuation side section
148
149
150  !! Apply constraints
151  D,N_M_I,,,,,UX,UY,
152  D,N_M_0,,,,,UX,UY,UZ,ROTZ
153  D,N_R_0,,,,,UY,
154  CERIG, N_M_I, N_R_I,ROTZ          !this will keep the last section's web straight (
      input)
155  !CERIG, N_M_0, N_R_0,ROTZ        !this will keep the First section's web straight (
      output)

```

```

156
157
158
159 *IF, Middle_BC,EQ,'Yes',THEN
160     *DO,N_Node, 1, 50*N_section-1, 1
161
162         D,NODE(0,                0,                N_Node*len/50),,,,,,Ux,UY,
163
164     *ENDDO
165 *ENDIF
166
167
168 !! Apply perturbation
169 !F,N_M_I,MZ,perturbation
170 D,N_M_I,ROTZ,perturbation_ang
171
172
173 ! Step 0-1 (Apply pretension)
174 /SOLU
175 KBC,0                                ! ramped
    loading
176 DELTIM, 1/time_step_prestress, 1E-3, 1, ON      ! Command to specify the number of
    steps in the analysis (this can be necessary for nonlinear systems where too
    big steps cause crashes)
177 D,N_M_I,UZ,Prestress
178 solve
179
180
181 FDELE, N_M_I,MZ                        ! deleting the perturbation load
182 DDELE, N_M_I,ROTZ                      ! deleting the perturbation angle
183
184
185 ! Step 1-2 (Update apdl registry to prevent crashes)
186 /SOLU
187 KBC,1                                ! Apply this load step
    in a step
188 DELTIM, 1/2, 1E-2, 1, ON              ! Command to specify
    the number of steps in the analysis (this can be necessary for nonlinear
    systems where too big steps cause crashes)
189 *GET,Rot_Ang_1,NODE,N_M_I,ROT,Z        ! Figure out the rotation angle
190 D,N_M_I,ROTZ,Rot_Ang_1                ! Apply this rotation as a
    displacement to update the registry in APDL (in reality this point is already
    at this location, APDL just doesn't know that yet)
191 solve
192
193
194 ! Step 2-3 (Apply rotation and measuring the moment)
195 /SOLU
196 OUTRES,,ALL
    ! After this command, loadstep data is saved for every substep (normally it is
    only saved at the end of each loadstep)

```

```

197 KBC,0
    ! ramped loading
198 DELTIM, 1/time_step_Rmoment, 1E-4, 1, ON          ! Command to specify the number
    of steps in the analysis (this can be necessary for nonlinear systems where too
    big steps cause crashes)
199 D,N_M_I,ROTZ,-Rot_Ang_1
200 solve
201
202
203 !! Commands to plot force-displacement output and save results
204 *GET, N_steps, active, 0, solu, NCMSS              ! Count the number of
    substeps to size the table correctly
205 /POST26                                           ! Go to
    postprocessor menu
206 TIMERANGE,0,1                                    ! Plot data from
    loadstep 0-1 only
207 NSOL,2,N_M_I,U,Z,displacement                    ! Get the displacment
    data of the node with N_M_I
208 RFORCE,3,N_M_0,F,Z,Rforce                        ! Get the reaction
    force
209 /AXLAB, X, displacement in m
210 /AXLAB, Y, force in N
211 XVAR,2                                           ! Put the
    displacment on the X axis in the plot
212 PLVAR,3                                           ! Plot the reaction force on
    the Y axis
213
214 !! The commands below are to save force-displacement plot in a .txt file
215 *CREATE,scratch,gui
216 *DEL,VAR_export
217 *DIM,VAR_export,TABLE,N_steps,3                  ! Set size of the table
    for results export
218 VGET,VAR_export(1,0),1
219 VGET,VAR_export(1,1),2
220 VGET,VAR_export(1,2),3
221 /OUTPUT,'RESULTS_force-displacement','txt','C:\Users\TZU\thesis_AnsysAPDL    !
    In this line you specify the location to export results
222 *VWRITE,VAR_export(1,0),VAR_export(1,1),VAR_export(1,2)
223 %G, %G, %G
224 /OUTPUT,TERM
225 *END
226 /INPUT,scratch,gui
227
228 !! Commands to plot moment-angle output and save results
229 *GET, N_steps, active, 0, solu, ncmss            ! Count the number of substeps
    to size the table correctly
230 /POST26                                           ! Go to postprocessor
    menu
231 TIMERANGE,2,3                                    ! Plot data from
    loadstep 2-3 only
232 NSOL,2,N_M_I,ROT,Z,Rotation                      ! Get the angle data of

```

```

    the node with N_M_I
233 RFORCE,3,N_M_I,M,Z,RMoment           ! Get the reaction
    moment
234 /AXLAB, X, Angle in rad
235 /AXLAB, Y, Reaction moment in N.m
236 XVAR,2                               ! Put the angle on the
    X axis in the plot
237 PLVAR,3                               ! Plot the reaction
    moment on the Y axis
238
239 !! The commands below are to save the plot in a .txt file
240 *CREATE,scratch,gui
241 *DEL,VAR_export
242 *DIM,VAR_export,TABLE,N_steps,3       ! Set size of the
    table for results export
243 VGET,VAR_export(1,0),1
244 VGET,VAR_export(1,1),2
245 VGET,VAR_export(1,2),3
246 /OUTPUT,'RESULTS_moment_angle','txt','C:\Users\TZU\thesis_AnsysAPDL' ! In this
    line you specify the location to export results
247 *VWRITE,VAR_export(1,0),VAR_export(1,1),VAR_export(1,2)
248 %G, %G, %G
249 /OUTPUT,TERM
250 *END
251 /INPUT,scratch,gui
252
253
254 !! Commands to retrieve maximum stress value and its location
255 /POST1
256 PLNSOL,S,EQV,1                         !Display stress contour
257 *GET,MaxStress,PLNSOL,0,MAX            !Get maximum value of stress in contour
    display
258 *GET,AvgStress,PLNSOL,0,MAX
259 *GET,MinStress,PLNSOL,0,MIN           !Get minimum value of stress in contour
    display
260
261 PLNSOL,EPT0,EQV,1                       !Display stress contour
262 *GET,MaxStrain,PLNSOL,0,MAX           !Get maximum value of strain in contour
    display
263 *GET,MinStrain,PLNSOL,0,MIN          !Get minimum value of strain in contour
    display
264
265
266 !! The commands below are to save the value in a .txt file
267 *CREATE,scratch,gui
268 /OUTPUT,'RESULTS_maximum stress and strain','txt','C:\Users\TZU\thesis_AnsysAPDL
    ! In this line you specify the location to export results
269 *VWRITE,MaxStress,MinStress,MaxStrain,MinStrain
270 %G, %G, %G %G
271 /OUTPUT,TERM
272 *END

```

```

273 /INPUT,scratch,gui

1  """
2  This code is for investigating the sensitivity of the following parameter:  $\Delta w$ . By
   changing the value in the "Set design parameters" section, the code can model
   different shapes of the T beam and analyze their behavior under specific load
   steps.
3  """
4
5  !! general initialization
6  FINISH ! Finish previous analysis
7  /CLEAR,START ! Clear data and start new analysis
8  /CWD,'C:\Users\TZU\thesis_AnsysAPDL' ! Location of this file
9  /FILENAME, APDLCOMMANDS ! Set filename in ansys
10
11 !! Set design parameters
12 ww = 0.04 !web width (in m)
13 wf = 0.009 !flange width (in m)
14 wb = 0.025 !web width actuation side(in m)
15 t = 0.0008 !web and flange thickness (in m)
16 len = 0.00905 !web length (in m)
17 slit = 0.11 !gap length/web length (len)
18 Middle_BC = 'Yes' !having axissymmetric boundary conditions
   for middle points 'Yes' or 'No'
19 N_section = 20 !number of sections (number of slits+1)
20 Density = 1010 !material properties
21 Poisson = 0.38 !0.35 for PLA 0.38 for PA12
22 Elastmod = 1.7e9 !3.144e9 for PLA 1.7e9 for PA12
23 Prestress = -0.0028 !displacement to tune torsional
   stiffness (in m)
24 perturbation = 0.01 !perturbation moment to converge to one
   stable state
25 perturbation_ang = 1.5 !perturbation angle in rad to converge
   to one stable state
26 time_step_prestress = 33 !Time steps for incremental prestressing
27 time_step_Rmoment = 170 !Time steps to evaluate reaction moment
   by a full reverse turn
28
29
30 !! Set properties
31 /PREP7
32 !element selection
33 ET, 1, shell281 !shell181! SOLSH190 !shell181 !beam188 ! defines
   a local element type from the library (ET, ITYPE, Ename, KOP1, KOP2)
34
35 mp, ex, 1, Elastmod !Defines a linear material property as a constant
   or a function of temperature.
36 mp, nuxy, 1, Poisson
37 mp, dens,1, Density
38
39

```

```

40 sect,1,shell,, !Web
41 secdata, t,1,0,3
42 secoffset,MID
43
44
45 !! Define keypoints SHAPE, the syntax is: K,*keypointnumber*,*Xcoord*,*Ycoord*,*
    Zcoord*
46     *DO,N_Node, 1, N_section+1, 1
47         N_K=10*(N_Node*2-1)
48
49         K,N_K,          0,          0,          (N_Node-1)*len
50         K,N_K+1,      ww/2-(N_Node-1)*len*((ww/2-wb)/(N_section*len-slit
    *len)),          0,          (N_Node-1)*len
51         K,N_K+2,      ww/2-(N_Node-1)*len*((ww/2-wb)/(N_section*len-slit
    *len)),          wf/2,          (N_Node-1)*len
52         K,N_K+3,      ww/2-(N_Node-1)*len*((ww/2-wb)/(N_section*len-slit
    *len)),          -wf/2,          (N_Node-1)*len
53
54     *ENDDO
55
56     *DO,N_Node, 1, N_section, 1
57         N_K=10*(N_Node*2)
58
59         K,N_K,          0,          0,          (N_Node-slit)*len
60         K,N_K+1,      ww/2-(N_Node-slit)*len*((ww/2-wb)/(N_section*len-
    slit*len)),          0,          (N_Node-slit)*len
61         K,N_K+2,      ww/2-(N_Node-slit)*len*((ww/2-wb)/(N_section*len-
    slit*len)),          wf/2,          (N_Node-slit)*len
62         K,N_K+3,      ww/2-(N_Node-slit)*len*((ww/2-wb)/(N_section*len-
    slit*len)),          -wf/2,          (N_Node-slit)*len
63
64     *ENDDO
65
66
67
68
69     *DO,N_Line, 1, 2*N_section, 1
70
71         N_L=10*N_Line
72
73         !! Define lines crosssection
74         NUMSTR,LINE,N_L
75
76         L,N_L,N_L+1
77         L,N_L+1,N_L+2
78         L,N_L+1,N_L+3
79
80
81         !! define Lines SHAPE
82         NUMSTR,LINE,10000 ! controls the starting number for any
    subsequently created lines.

```

```

83         L,N_L,N_L+10
84         L,N_L+1,N_L+10+1
85         L,N_L+2,N_L+10+2
86         L,N_L+3,N_L+10+3
87
88
89
90     *ENDDO
91
92
93
94     *DO,N_Area, 1, N_section, 1
95
96
97         !! drag sectional lines
98         N_A= 10*N_Area
99         NUMSTR,AREA,10000*N_Area
100        AL, 2*N_A-10,2*N_A,10000+8*(N_Area-1),10001+8*(N_Area-1)
101        AL, 2*N_A-10+1,2*N_A+1,10001+8*(N_Area-1),10002+8*(N_Area-1)
102        AL, 2*N_A-10+2,2*N_A+2,10001+8*(N_Area-1),10003+8*(N_Area-1)
103        AL, 2*N_A+1,2*N_A+10+1,10005+8*(N_Area-1),10006+8*(N_Area-1)
104        AL, 2*N_A+2,2*N_A+10+2,10005+8*(N_Area-1),10007+8*(N_Area-1)
105
106
107
108     *ENDDO
109
110
111
112 NUMMRG,ALL,                                !Merges coincidents or
        equivalently defined items.
113
114
115     *DO,N_Mesh, 1, N_section, 1
116
117         !! Mesh Areas
118         ASEL, s, , , N_Mesh*10000, N_Mesh*10000+16,, 0 ! Mesh webs
119         AATT, 1, , 1, 0, 1
120     !AESIZE, all, 1E-3
121     AMESH, N_Mesh*10000,N_Mesh*10000+16
122
123     *ENDDO
124
125
126
127 !! Commands to visualize the elements.
128 /ESHAPE,1
129 /VIEW,1,1,1,1
130 eplot
131
132

```

```

133 !! SOLUTION
134 /SOLU
135 ANTYPE, 0           ! Static structural analysis
136 NLGEOM,ON         ! Set nonlinear geometry option on
137 EQSLV,SPARSE
138 autots,off
139 pstres,off
140 arclen,off
141 PRED,off
142 OUTRES,ALL,ALL
143
144
145 !! These are commands to assign ID's to the nodes that were meshed at the
      keypoints (Because these ID's are more easy to refer to when we apply the loads
      )
146 N_M_0 =           NODE(0,           0,           0)
      !Node on middle fixation side section
147 N_R_0 =           NODE(wb/2,       0,           0)
      !Node on middle fixation side section
148 N_M_I =           NODE(0,           0,           N_section*len-slit*len)
      !Node on middle actuation side section
149 N_R_I =           NODE(ww/4,       0,           N_section*len-slit*len)
      !Node on middle actuation side section
150
151
152 !! Apply constraints
153 D,N_M_I,,,,,UX,UY,
154 D,N_M_0,,,,,UX,UY,UZ,ROTZ
155 D,N_R_0,,,,,UY,
156 CERIG, N_M_I, N_R_I,ROTZ           !this will keep the last section's web straight (
      input)
157 !CERIG, N_M_0, N_R_0,ROTZ           !this will keep the First section's web straight (
      output)
158
159
160
161 *IF, Middle_BC,EQ,'Yes',THEN
162     *DO,N_Node, 1, 50*N_section-1, 1
163
164         D,NODE(0,           0,           N_Node*len/50),,,,,Ux,UY,
165
166     *ENDDO
167 *ENDIF
168
169
170 !! Apply perturbation
171 !F,N_M_I,MZ,perturbation
172 D,N_M_I,ROTZ,perturbation_ang
173
174
175 ! Step 0-1 (Apply pretension)

```

```

176 /SOLU
177 KBC,0                                ! ramped
      loading
178 DELTIM, 1/time_step_prestress, 1E-3, 1, ON      ! Command to specify the number of
      steps in the analysis (this can be necessary for nonlinear systems where too
      big steps cause crashes)
179 D,N_M_I,UZ,Prestress
180 solve
181
182
183 FDELE, N_M_I,MZ                        ! deleting the perturbation load
184 DDELE, N_M_I,ROTZ                      ! deleting the perturbation angle
185
186
187 ! Step 1-2 (Update apdl registry to prevent crashes)
188 /SOLU
189 KBC,1                                ! Apply this load step
      in a step
190 DELTIM, 1/2, 1E-2, 1, ON              ! Command to specify
      the number of steps in the analysis (this can be necessary for nonlinear
      systems where too big steps cause crashes)
191 *GET, Rot_Ang_1, NODE, N_M_I, ROT, Z    ! Figure out the rotation angle
192 D, N_M_I, ROTZ, Rot_Ang_1              ! Apply this rotation as a
      displacement to update the registry in APDL (in reality this point is already
      at this location, APDL just doesn't know that yet)
193 solve
194
195
196 ! Step 2-3 (Apply rotation and measuring the moment)
197 /SOLU
198 OUTRES, , ALL
      ! After this command, loadstep data is saved for every substep (normally it is
      only saved at the end of each loadstep)
199 KBC,0
      ! ramped loading
200 DELTIM, 1/time_step_Rmoment, 1E-5, 1E-2, ON    ! Command to specify the number
      of steps in the analysis (this can be necessary for nonlinear systems where too
      big steps cause crashes)
201 D, N_M_I, ROTZ, -Rot_Ang_1
202 solve
203
204
205 !! Commands to plot force-displacement output and save results
206 *GET, N_steps, active, 0, solu, NCMSS          ! Count the number of
      substeps to size the table correctly
207 /POST26                                     ! Go to
      postprocessor menu
208 TIMERANGE, 0, 1                             ! Plot data from
      loadstep 0-1 only
209 NSOL, 2, N_M_I, U, Z, displacement           ! Get the displacement
      data of the node with N_M_I

```

```

210 RFORCE,3,N_M_0,F,Z,Rforce           ! Get the reaction
      force
211 /AXLAB, X, displacement in m
212 /AXLAB, Y, force in N
213 XVAR,2                               ! Put the
      displacment on the X axis in the plot
214 PLVAR,3                             ! Plot the reaction force on
      the Y axis
215
216 !! The commands below are to save force-displacement plot in a .txt file
217 *CREATE,scratch,gui
218   *DEL,VAR_export
219   *DIM,VAR_export,TABLE,N_steps,3     ! Set size of the table
      for results export
220   VGET,VAR_export(1,0),1
221   VGET,VAR_export(1,1),2
222   VGET,VAR_export(1,2),3
223 /OUTPUT,'RESULTS_force-displacement','txt','C:\Users\TZU\thesis_AnsysAPDL   !
      In this line you specify the location to export results
224 *VWRITE,VAR_export(1,0),VAR_export(1,1),VAR_export(1,2)
225 %G, %G, %G
226 /OUTPUT,TERM
227 *END
228 /INPUT,scratch,gui
229
230 !! Commands to plot moment-angle output and save results
231 *GET, N_steps, active, 0, solu, ncmss   ! Count the number of substeps
      to size the table correctly
232 /POST26                               ! Go to postprocessor
      menu
233 TIMERANGE,2,3                         ! Plot data from
      loadstep 2-3 only
234 NSOL,2,N_M_I,ROT,Z,Rotation           ! Get the angle data of
      the node with N_M_I
235 RFORCE,3,N_M_I,M,Z,RMoment           ! Get the reaction
      moment
236 /AXLAB, X, Angle in rad
237 /AXLAB, Y, Reaction moment in N.m
238 XVAR,2                               ! Put the angle on the
      X axis in the plot
239 PLVAR,3                             ! Plot the reaction
      moment on the Y axis
240
241 !! The commands below are to save the plot in a .txt file
242 *CREATE,scratch,gui
243   *DEL,VAR_export
244   *DIM,VAR_export,TABLE,N_steps,3     ! Set size of the
      table for results export
245   VGET,VAR_export(1,0),1
246   VGET,VAR_export(1,1),2
247   VGET,VAR_export(1,2),3

```

```

248 /OUTPUT,'RESULTS_moment_angle','txt','C:\Users\TZU\thesis_AnsysAPDL' ! In this
      line you specify the location to export results
249 *VWRITE,VAR_export(1,0),VAR_export(1,1),VAR_export(1,2)
250 %G, %G, %G
251 /OUTPUT,TERM
252 *END
253 /INPUT,scratch,gui
254
255
256 !! Commands to retrieve maximum stress value and its location
257 /POST1
258 PLNSOL,S,EQV,1 !Display stress contour
259 *GET,MaxStress,PLNSOL,0,MAX !Get maximum value of stress in contour
      display
260 *GET,AvgStress,PLNSOL,0,MAX
261 *GET,MinStress,PLNSOL,0,MIN !Get minimum value of stress in contour
      display
262
263 PLNSOL,EPTO,EQV,1 !Display stress contour
264 *GET,MaxStrain,PLNSOL,0,MAX !Get maximum value of strain in contour
      display
265 *GET,MinStrain,PLNSOL,0,MIN !Get minimum value of strain in contour
      display
266
267
268 !! The commands below are to save the value in a .txt file
269 *CREATE,scratch,gui
270 /OUTPUT,'RESULTS_maximum stress and strain','txt','C:\Users\TZU\thesis_AnsysAPDL
      ! In this line you specify the location to export results
271 *VWRITE,MaxStress,MinStress,MaxStrain,MinStrain
272 %G, %G, %G %G
273 /OUTPUT,TERM
274 *END
275 /INPUT,scratch,gui

```

```

1 ""
2 This code is for investigating the sensitivity of the following parameter: wg. By
      changing the value in the "Set design parameters" section, the code can model
      different shapes of the T beam and analyze their behavior under specific load
      steps.
3 ""
4
5 !! general initialization
6 FINISH ! Finish previous analysis
7 /CLEAR,START ! Clear data and start new analysis
8 /CWD,'C:\Users\TZU\thesis_AnsysAPDL' ! Location of this file
9 /FILENAME, APDLCOMMANDS ! Set filename in ansys
10
11 !! Set design parameters
12 ww = 0.04 !web width (in m)
13 wf = 0.009 !flange width (in m)

```

```

14 ws = 0.008 !gap width (in m)
15 t = 0.0008 !web and flange thickness (in m)
16 len = 0.00905 !web length (in m)
17 slit = 0.11 !gap length/web length (len)
18 Middle_BC = 'Yes' !having axissymmetric boundary conditions
    for middle points 'Yes' or 'No'
19 N_section = 20 !number of sections (number of slits+1)
20 Density = 1010 !material properties
21 Poisson = 0.38 !0.35 for PLA 0.38 for PA12
22 Elastmod = 1.7e9 !3.144e9 for PLA 1.7e9 for PA12
23 Prestress = -0.0028 !displacement to tune torsional
    stiffness (in m)
24 perturbation = 0.01 !perturbation moment to converge to one
    stable state
25 perturbation_ang = 1.5 !perturbation angle in rad to converge
    to one stable state
26 time_step_prestress = 33 !Time steps for incremental prestressing
27 time_step_Rmoment = 170 !Time steps to evaluate reaction moment
    by a full reverse turn
28
29
30 !! Set properties
31 /PREP7
32 !element selection
33 ET, 1, shell281 !shell181! SOLSH190 !shell181 !beam188 ! defines
    a local element type from the library (ET, ITYPE, Ename, KOP1, KOP2)
34
35 mp, ex, 1, Elastmod !Defines a linear material property as a constant
    or a function of temperature.
36 mp, nuxy, 1, Poisson
37 !mp, gxy, 1, Gmod
38 mp, dens,1, Density
39
40
41 sect,1,shell,, !Web
42 secdata, t,1,0,3
43 secoffset,MID
44
45
46 !! Define keypoints SHAPE, the syntax is: K,*keypointnumber*,*Xcoord*,*Ycoord*,*
    Zcoord*
47 *DO,N_Node, 1, N_section, 1
48 N_K=10*(N_Node*2-1)
49
50 K,N_K, 0, 0, (N_Node-1)*len
51
52 *IF, N_K, LT, 10*(N_section*2), AND, N_K, GT, 10, THEN
53 K,N_K+1, ws, 0, (N_Node-1)*len
54 *ENDIF
55
56 K,N_K+2, ww/2, 0, (N_Node-1)*len

```

```

57         K,N_K+3,      ww/2,  wf/2,  (N_Node-1)*len
58         K,N_K+4,      ww/2,  -wf/2,  (N_Node-1)*len
59
60
61         N_K=10*(N_Node*2)
62
63         K,N_K,         0,          0,          (N_Node-slit)*len
64
65         *IF, N_K, LT, 10*(N_section*2),THEN
66             K,N_K+1,    ws,    0,          (N_Node-slit)*len
67         *ENDIF
68
69         K,N_K+2,      ww/2,  0,          (N_Node-slit)*len
70         K,N_K+3,      ww/2,  wf/2,  (N_Node-slit)*len
71         K,N_K+4,      ww/2,  -wf/2,  (N_Node-slit)*len
72
73     *ENDDO
74
75
76     *DO,N_Line, 1, N_section*2-1, 1
77
78         N_L=10*N_Line
79
80         !! Define lines crosssection
81         NUMSTR,LINE,N_L
82
83         *IF, N_L, EQ, 10, THEN
84             L,N_L,N_L+2
85             L,N_L+2,N_L+3
86             L,N_L+2,N_L+4
87         *ELSE
88             L,N_L,N_L+1
89         L,N_L+1,N_L+2
90             L,N_L+2,N_L+3
91             L,N_L+2,N_L+4
92         *ENDIF
93
94
95
96         !! define Lines SHAPE
97         NUMSTR,LINE,1000 ! controls the starting number for any
98             subsequently created lines.
99         L,N_L,N_L+10
100
101     *ENDDO
102
103     *DO,N_Area, 1, N_section, 1
104
105         !! drag sectional lines
106         N_A= 20*N_Area-10

```

```

107         NUMSTR,AREA,N_Area*1000
108
109         *IF, N_A, EQ, 10, THEN
110             ADRAG,N_A,, , , , ,1000+2*(N_Area-1)
111             ADRAG,N_A+1,N_A+2, , , , ,1000+2*(N_Area-1)
112
113         *ELSE
114             ADRAG,N_A,N_A+1, , , , ,1000+2*(N_Area-1)
115             ADRAG,N_A+2,N_A+3, , , , ,1000+2*(N_Area-1)
116         *ENDIF
117
118         *IF, N_Area,LT,N_section,THEN
119             ADRAG,10+N_A+1, , , , , ,1001+2*(N_Area-1)
120             ADRAG,10+N_A+2,10+N_A+3, , , , ,1001+2*(N_Area-1)
121
122         *ENDDO
123
124
125 NUMMRG,ALL                                     !Merges coincidents or
        equivalently defined items.
126
127         *DO,N_Mesh, 1, N_section, 1
128
129         !! Mesh Areas
130         ASEL, s, , , N_Mesh*1000, N_Mesh*1000+16,, 0      ! Mesh webs
131         AATT, 1, , 1, 0, 1
132         AMESH, N_Mesh*1000,N_Mesh*1000+16
133
134         *ENDDO
135
136
137
138 !! Commands to visualize the elements.
139 /ESHAPE,1
140 /VIEW,1,1,1,1
141 eplot
142
143
144 !! SOLUTION
145 /SOLU
146 ANTYPE, 0                                     ! Static structural analysis
147 NLGEOM,ON                                     ! Set nonlinear geometry option on
148 EQSLV,SPARSE
149 autots,off
150 pstres,off
151 arclen,off
152 PRED,off
153 OUTRES,ALL,ALL
154
155
156 !! These are commands to assign ID's to the nodes that were meshed at the

```

```

    keypoints (Because these ID's are more easy to refer to when we apply the loads
    )
157 N_M_0 =          NODE(0,          0,          0)
           !Node on middle fixation side section
158 N_R_0 =          NODE(ww/4,      0,          0)
           !Node on middle fixation side section
159 N_M_I =          NODE(0,          0,          N_section*len-slit*len)
           !Node on middle actuation side section
160 N_R_I =          NODE(ww/4,      0,          N_section*len-slit*len)
           !Node on middle actuation side section
161
162
163 !! Apply constraints
164 D,N_M_I,,,,,UX,UY,
165 D,N_M_0,,,,,UX,UY,UZ,ROTZ
166 D,N_R_0,,,,,UY,
167 CERIG, N_M_I, N_R_I,ROTZ          !this will keep the last section's web straight (
           input)
168 !CERIG, N_M_0, N_R_0,ROTZ          !this will keep the First section's web straight (
           output)
169
170
171
172 *IF, Middle_BC,EQ,'Yes',THEN
173     *DO,N_Node, 1, 50*N_section-1, 1
174
175         D,NODE(0,          0,          N_Node*len/50),,,,,Ux,UY,
176
177     *ENDDO
178 *ENDIF
179
180
181 !! Apply perturbation
182 !F,N_M_I,MZ,perturbation
183 D,N_M_I,ROTZ,perturbation_ang
184
185
186 ! Step 0-1 (Apply pretension)
187 /SOLU
188 KBC,0                                ! ramped
           loading
189 DELTIM, 1/time_step_prestress, 1E-3, 1, 0N          ! Command to specify the number of
           steps in the analysis (this can be necessary for nonlinear systems where too
           big steps cause crashes)
190 D,N_M_I,UZ,Prestress
191 solve
192
193
194 FDELE, N_M_I,MZ                        ! deleting the perturbation load
195 DDELE, N_M_I,ROTZ                      ! deleting the perturbation angle
196

```

```

197
198 ! Step 1-2 (Update apdl registry to prevent crashes)
199 /SOLU
200 KBC,1                                     ! Apply this load step
      in a step
201 DELTIM, 1/2, 1E-2, 1, ON                 ! Command to specify
      the number of steps in the analysis (this can be necessary for nonlinear
      systems where too big steps cause crashes)
202 *GET, Rot_Ang_1, NODE, N_M_I, ROT, Z      ! Figure out the rotation angle
203 D, N_M_I, ROTZ, Rot_Ang_1                ! Apply this rotation as a
      displacement to update the registry in APDL (in reality this point is already
      at this location, APDL just doesn't know that yet)
204 solve
205
206
207 ! Step 2-3 (Apply rotation and measuring the moment)
208 /SOLU
209 OUTRES, , ALL
      ! After this command, loadstep data is saved for every substep (normally it is
      only saved at the end of each loadstep)
210 KBC,0
      ! ramped loading
211 DELTIM, 1/time_step_Rmoment, 1E-4, 1, ON ! Command to specify the number
      of steps in the analysis (this can be necessary for nonlinear systems where too
      big steps cause crashes)
212 D, N_M_I, ROTZ, -Rot_Ang_1
213 solve
214
215
216 !! Commands to plot force-displacement output and save results
217 *GET, N_steps, active, 0, solu, NCMSS    ! Count the number of
      substeps to size the table correctly
218 /POST26                                  ! Go to
      postprocessor menu
219 TIMERANGE, 0, 1                          ! Plot data from
      loadstep 0-1 only
220 NSOL, 2, N_M_I, U, Z, displacement        ! Get the displacment
      data of the node with N_M_I
221 RFORCE, 3, N_M_I, F, Z, Rforce           ! Get the reaction
      force
222 /AXLAB, X, displacement in m
223 /AXLAB, Y, force in N
224 XVAR, 2                                   ! Put the
      displacment on the X axis in the plot
225 PLVAR, 3                                  ! Plot the reaction force on
      the Y axis
226
227 !! The commands below are to save force-displacement plot in a .txt file
228 *CREATE, scratch, gui
229 *DEL, VAR_export
230 *DIM, VAR_export, TABLE, N_steps, 3     ! Set size of the table

```

```

    for results export
231   VGET,VAR_export(1,0),1
232   VGET,VAR_export(1,1),2
233   VGET,VAR_export(1,2),3
234   /OUTPUT,'RESULTS_force-displacement','txt','C:\Users\TZU\thesis_AnsysAPDL' !
      In this line you specify the location to export results
235   *VWRITE,VAR_export(1,0),VAR_export(1,1),VAR_export(1,2)
236   %G, %G, %G
237   /OUTPUT,TERM
238   *END
239   /INPUT,scratch,gui
240
241 !! Commands to plot moment-angle output and save results
242 *GET, N_steps, active, 0, solu, ncmss           ! Count the number of substeps
      to size the table correctly
243 /POST26                                     ! Go to postprocessor
      menu
244 TIMERANGE,2,3                               ! Plot data from
      loadstep 2-3 only
245 NSOL,2,N_M_I,ROT,Z,Rotation                 ! Get the angle data of
      the node with N_M_I
246 RFORCE,3,N_M_I,M,Z,RMoment                 ! Get the reaction
      moment
247 /AXLAB, X, Angle in rad
248 /AXLAB, Y, Reaction moment in N.m
249 XVAR,2                                       ! Put the angle on the
      X axis in the plot
250 PLVAR,3                                     ! Plot the reaction
      moment on the Y axis
251
252 !! The commands below are to save the plot in a .txt file
253 *CREATE,scratch,gui
254   *DEL,VAR_export
255   *DIM,VAR_export,TABLE,N_steps,3           ! Set size of the
      table for results export
256   VGET,VAR_export(1,0),1
257   VGET,VAR_export(1,1),2
258   VGET,VAR_export(1,2),3
259   /OUTPUT,'RESULTS_moment_angle','txt','C:\Users\TZU\thesis_AnsysAPDL' ! In this
      line you specify the location to export results
260   *VWRITE,VAR_export(1,0),VAR_export(1,1),VAR_export(1,2)
261   %G, %G, %G
262   /OUTPUT,TERM
263   *END
264   /INPUT,scratch,gui
265
266
267 !! Commands to retrieve maximum stress value and its location
268 /POST1
269 PLNSOL,S,EQV,1                               !Display stress contour
270 *GET,MaxStress,PLNSOL,0,MAX                 !Get maximum value of stress in contour

```

```

    display
271 *GET,AvgStress,PLNSOL,0,MAX
272 *GET,MinStress,PLNSOL,0,MIN           !Get minimum value of stress in contour
    display
273
274 PLNSOL,EPTO,EQV,1                   !Display stress contour
275 *GET,MaxStrain,PLNSOL,0,MAX         !Get maximum value of strain in contour
    display
276 *GET,MinStrain,PLNSOL,0,MIN       !Get minimum value of strain in contour
    display
277
278
279 !! The commands below are to save the value in a .txt file
280 *CREATE,scratch,gui
281 /OUTPUT,'RESULTS_maximum stress and strain','txt','C:\Users\TZU\thesis_AnsysAPDL
    ! In this line you specify the location to export results
282 *VWRITE,MaxStress,MinStress,MaxStrain,MinStrain
283   %G, %G, %G %G
284   /OUTPUT,TERM
285   *END
286   /INPUT,scratch,gui

```

```

1  ""
2  This code is for investigating the sensitivity of the x-axis bending stiffness.
   The code for modeling the shape of the I beam is similar to the previous code
   which models the T beam. While the applied loads are changed. Therefore, not
   all bending stiffness sensitivity analysis code (8 parameters) is listed here.
3  ""
4
5  !!Bending stiffness along x
6  !!Tzu Lee 20230514
7  !! general initialization
8  FINISH           ! Finish previous analysis
9  /CLEAR,START    ! Clear data and start new analysis
10 /CWD,'C:\Users\TZU\thesis_AnsysAPDL' ! Location of this file
11 /FILENAME, APDLCOMMANDS ! Set filename in ansys
12
13 !! Set design parameters
14 ww = 0.04           !web width (in m)
15 wf = 0.009         !flange width (in m)
16 t   = 0.0008       !web and flange thickness
   (in m)
17 len = 0.00905      !web length (in m)
18 slit = 0.11        !gap length/web length (len)
19 Middle_BC = 'Yes'  !having axissymmetric boundary conditions
   for middle points 'Yes' or 'No'
20 N_section = 20     !number of sections (number of slits+1)
21 Density = 1010     !material properties
22 Poisson = 0.38     !0.35 for PLA           0.38 for PA12
23 Elastmod = 1.7e9   !3.144e9 for PLA       1.7e9 for PA12
24 Load = -5          !Bending force

```

```

25 time_step_load = 33          !Time steps for incremental loading
26
27
28
29 !! Set properties
30 /PREP7
31 !element selection
32 ET, 1, shell281             !shell181!          SOLSH190 !shell181 !beam188      ! defines
    a local element type from the library (ET, ITYPE, Ename, KOP1, KOP2)
33
34 mp, ex, 1, Elastmod         !Defines a linear material property as a constant
    or a function of temperature.
35 mp, nuxy, 1, Poisson
36 !mp, gxy, 1, Gmod
37 mp, dens,1, Density
38
39
40 sect,1,shell,, !Web
41 secdata, t,1,0,3
42 secoffset,MID
43
44
45 !! Define keypoints SHAPE, the syntax is: K,*keypointnumber*,*Xcoord*,*Ycoord*,*
    Zcoord*
46     *DO,N_Node, 1, N_section, 1
47         N_K=10*(N_Node*2-1)
48
49         K,N_K,          0,          0,          (N_Node-1)*len
50         K,N_K+1,        ww/2,    0,          (N_Node-1)*len
51         K,N_K+2,        ww/2,    wf/2,    (N_Node-1)*len
52         K,N_K+3,        ww/2,    -wf/2,    (N_Node-1)*len
53
54
55         N_K=10*(N_Node*2)
56
57         K,N_K,          0,          0,          (N_Node-slit)*len
58         K,N_K+1,        ww/2,    0,          (N_Node-slit)*len
59         K,N_K+2,        ww/2,    wf/2,    (N_Node-slit)*len
60         K,N_K+3,        ww/2,    -wf/2,    (N_Node-slit)*len
61
62     *ENDDO
63
64
65     *DO,N_Line, 1, 2*N_section-1, 1
66
67         N_L=10*N_Line
68
69         !! Define lines crosssection
70         NUMSTR,LINE,N_L
71         L,N_L,N_L+1
72         L,N_L+1,N_L+2

```

```

73         L,N_L+1,N_L+3
74
75         !! define Lines SHAPE
76         NUMSTR,LINE,1000 ! controls the starting number for any
           subsequently created lines.
77         L,N_L,N_L+10
78
79         *ENDDO
80
81
82         *DO,N_Area, 1, N_section, 1
83
84         !! drag sectional lines
85         N_A= 20*N_Area-10
86         NUMSTR,AREA,N_Area*1000
87         ADRAG,N_A,, , , ,1000+2*(N_Area-1)
88         ADRAG,N_A+1,N_A+2, , , ,1000+2*(N_Area-1)
89
90         *IF, N_Area,LT,N_section,THEN
91         ADRAG,10+N_A+1,10+N_A+2, , , ,1001+2*(N_Area-1)
92
93         *ENDDO
94
95
96 ARSYM,X,ALL, , , ,0,0 ! Reflect all areas to get a symmetric I
           beam for bending stiffness analysis
97 NUMMRG,ALL !Merges coincidents or
           equivalently defined items.
98
99         *DO,N_Mesh, 1, N_section, 1
100
101         !! Mesh Areas
102         ASEL, s, , , N_Mesh*1000, N_Mesh*1000+100,, 0 ! Mesh webs
103         AATT, 1, , 1, 0, 1
104         AMESH, N_Mesh*1000,N_Mesh*1000+100
105
106         *ENDDO
107
108
109
110
111 !! Commands to visualize the elements.
112 /ESHAPE,1
113 /VIEW,1,1,1,1
114 eplot
115
116
117 !! SOLUTION
118 /SOLU
119 ANTYPE, 0 ! Static structural analysis
120 NLGEOM,ON ! Set nonlinear geometry option on

```

```

121 EQSLV,SPARSE
122 autots,off
123 pstres,off
124 arclen,off
125 PRED,off
126 OUTRES,ALL,ALL
127
128
129 !! These are commands to assign ID's to the nodes that were meshed at the
      keypoints (Because these ID's are more easy to refer to when we apply the loads
      )
130 N_M_0 =      NODE(-ww/4,      0,      0)
      !Node on middle fixation side section
131 N_R_0 =      NODE(ww/4,      0,      0)
      !Node on middle fixation side section
132 N_M_I =      NODE(0,      0,      N_section*len-slit*len)
      !Node on middle actuation side section
133 N_R_I =      NODE(ww/4,      0,      N_section*len-slit*len)
      !Edge node on actuation side section
134
135
136 !! Apply constraints
137 D,N_M_0,,,,,UX,UY,UZ,ROTX,ROTY,ROTZ
138 D,N_R_0,,,,,UX,UY,UZ,ROTX,ROTY,ROTZ
139
140
141 ! Step 0-1 (Apply Load)
142 /SOLU
143 KBC,0                                     ! ramped
      loading
144 DELTIM, 1/time_step_load, 1E-3, 1, ON    ! Command to specify the number of steps
      in the analysis (this can be necessary for nonlinear systems where too big
      steps cause crashes)
145 F,N_M_I,FX,Load
146 solve
147
148
149 !! Commands to plot output and save results
150 *GET, N_steps, active, 0, solu, ncmss    ! Count the number of
      substeps to size the table correctly
151 /POST26                                     ! Go to
      postprocessor menu
152 NSOL,2,N_M_I,U,X,Deflection              ! Get the deflection data
      of the node with N_R_I
153 RFORCE,3,N_R_0,F,X,RForce              ! Get the reaction
      force
154 /AXLAB, X, Deflection in mm
155 /AXLAB, Y, Force in N
156 XVAR,2
      ! Put the deflection on the X axis in the plot
157 PLVAR,3

```

```
! Plot the reaction force on the Y axis
158
159 !! The commands below are to save the plot in a .txt file
160 *CREATE,scratch,gui
161   *DEL,VAR_export
162   *DIM,VAR_export,TABLE,N_steps,3           ! Set size of the table
        for results export
163   VGET,VAR_export(1,0),1
164   VGET,VAR_export(1,1),2
165   VGET,VAR_export(1,2),3
166 /OUTPUT,'RESULTS_Bending_stiffness_x_untwist','txt','C:\Users\TZU\
        thesis_AnsysAPDL' ! In this line you specify the location to export results
167 *VWRITE,VAR_export(1,0),VAR_export(1,1),VAR_export(1,2)
168 %G, %G, %G
169 /OUTPUT,TERM
170 *END
171 /INPUT,scratch,gui
```

B.2. Sensitivity analysis results

In this section, the FEM results are plotted and compared between different parameter values.

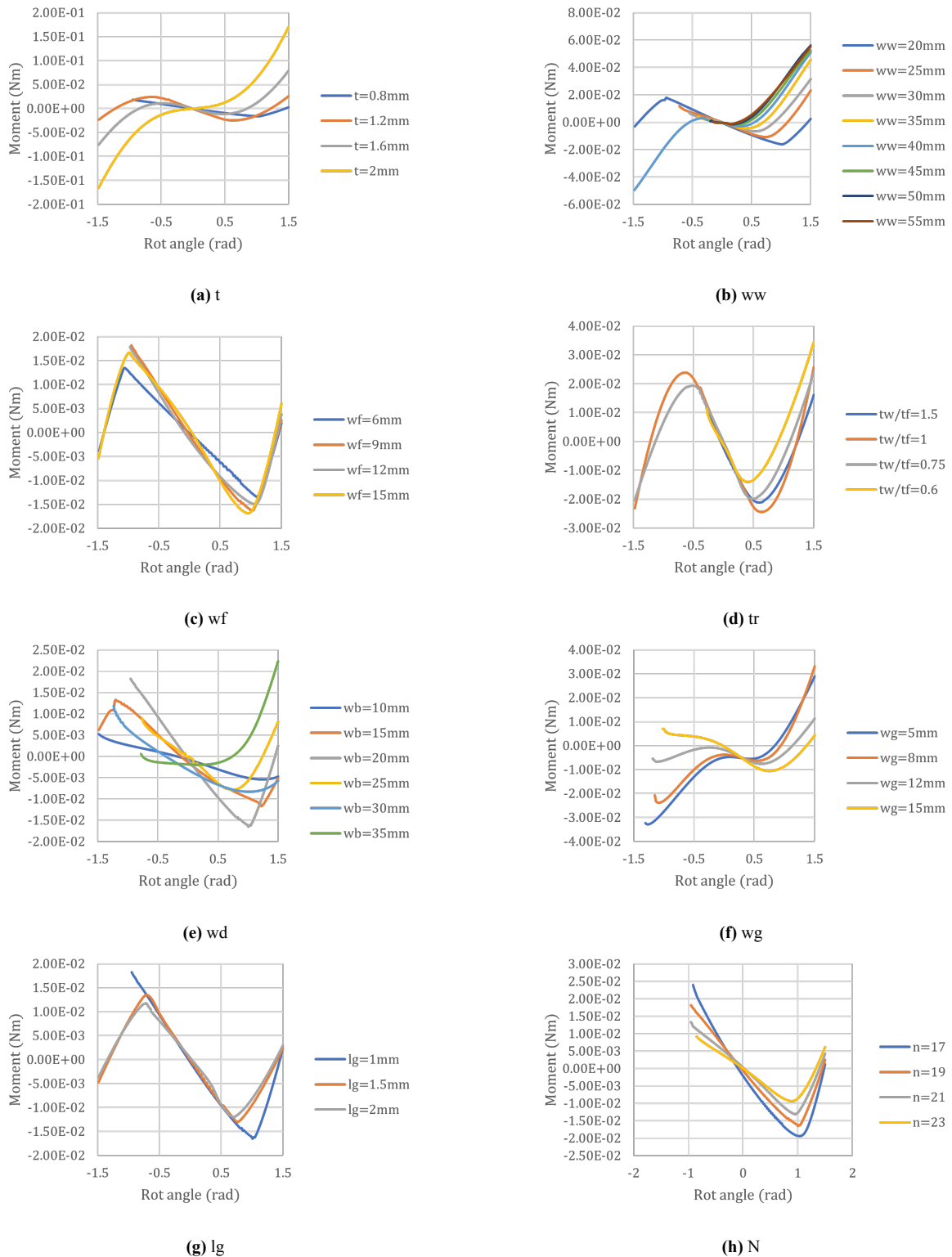
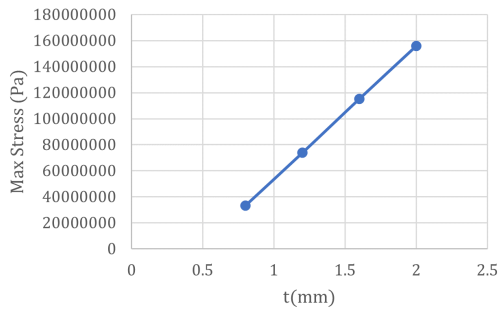
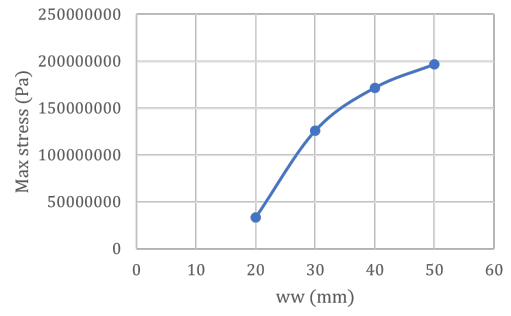


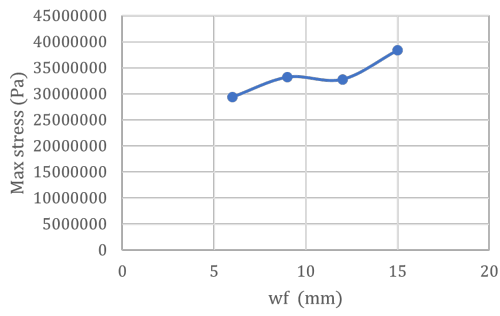
Figure B.1: Moment-Rot angle diagram



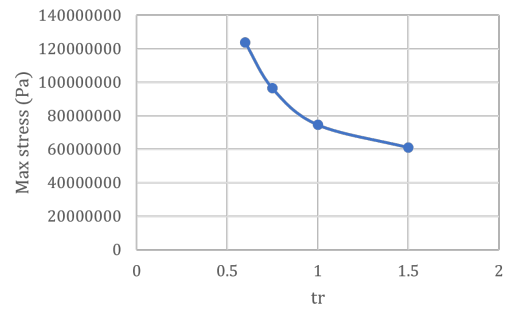
(a) t



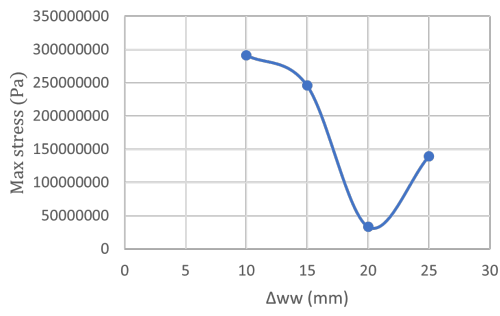
(b) ww



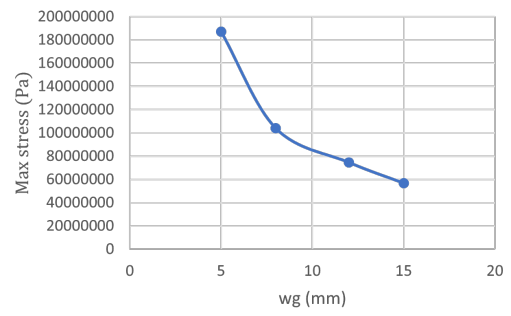
(c) wf



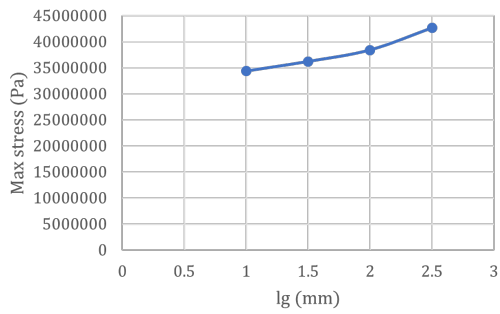
(d) tr



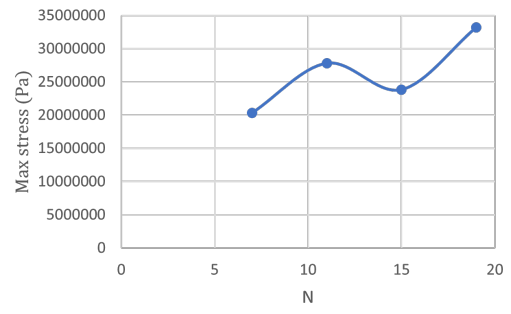
(e) Δww



(f) wg



(g) lg



(h) N

Figure B.2: Maximum stress diagram

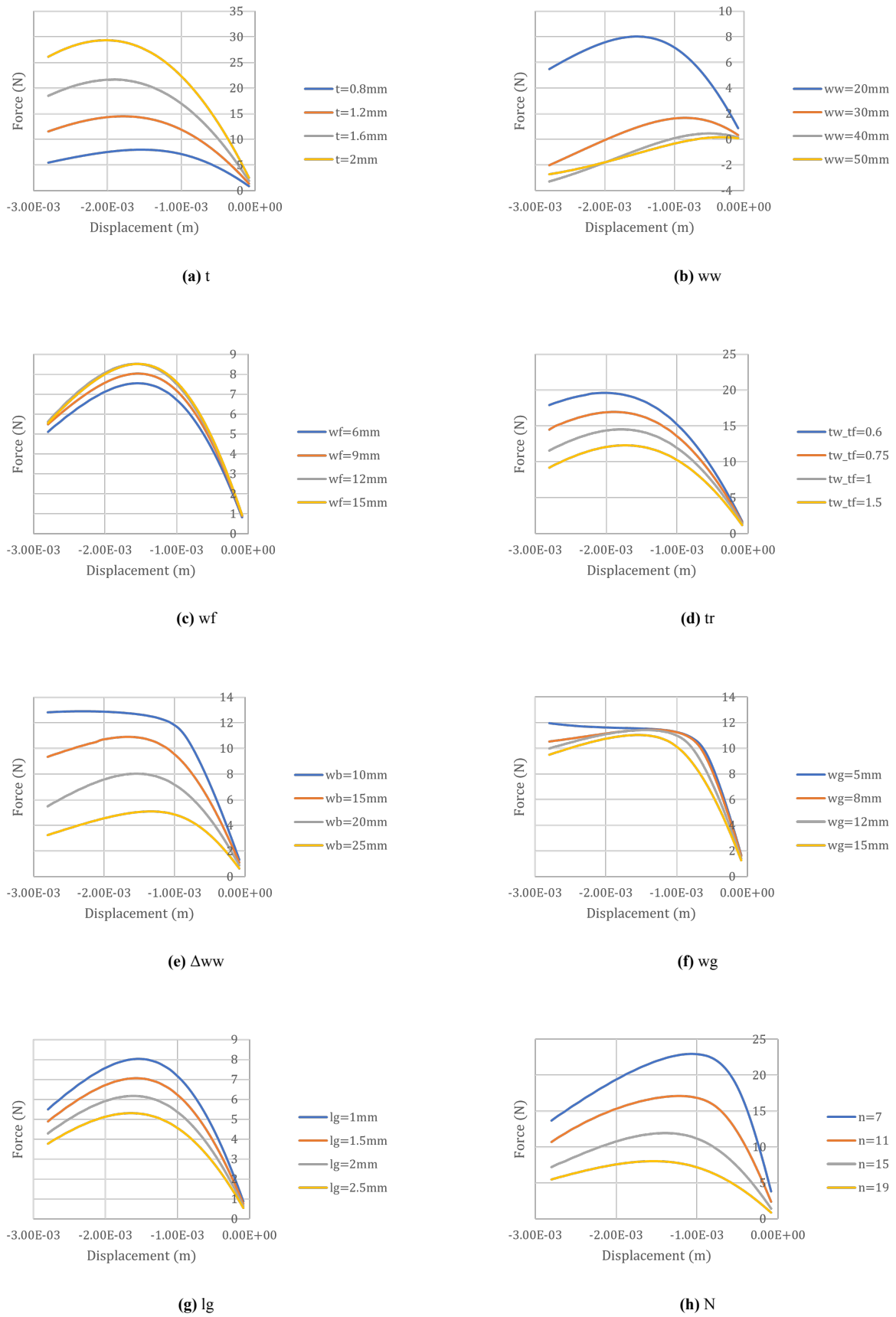


Figure B.3: Actuation force-displacement diagram

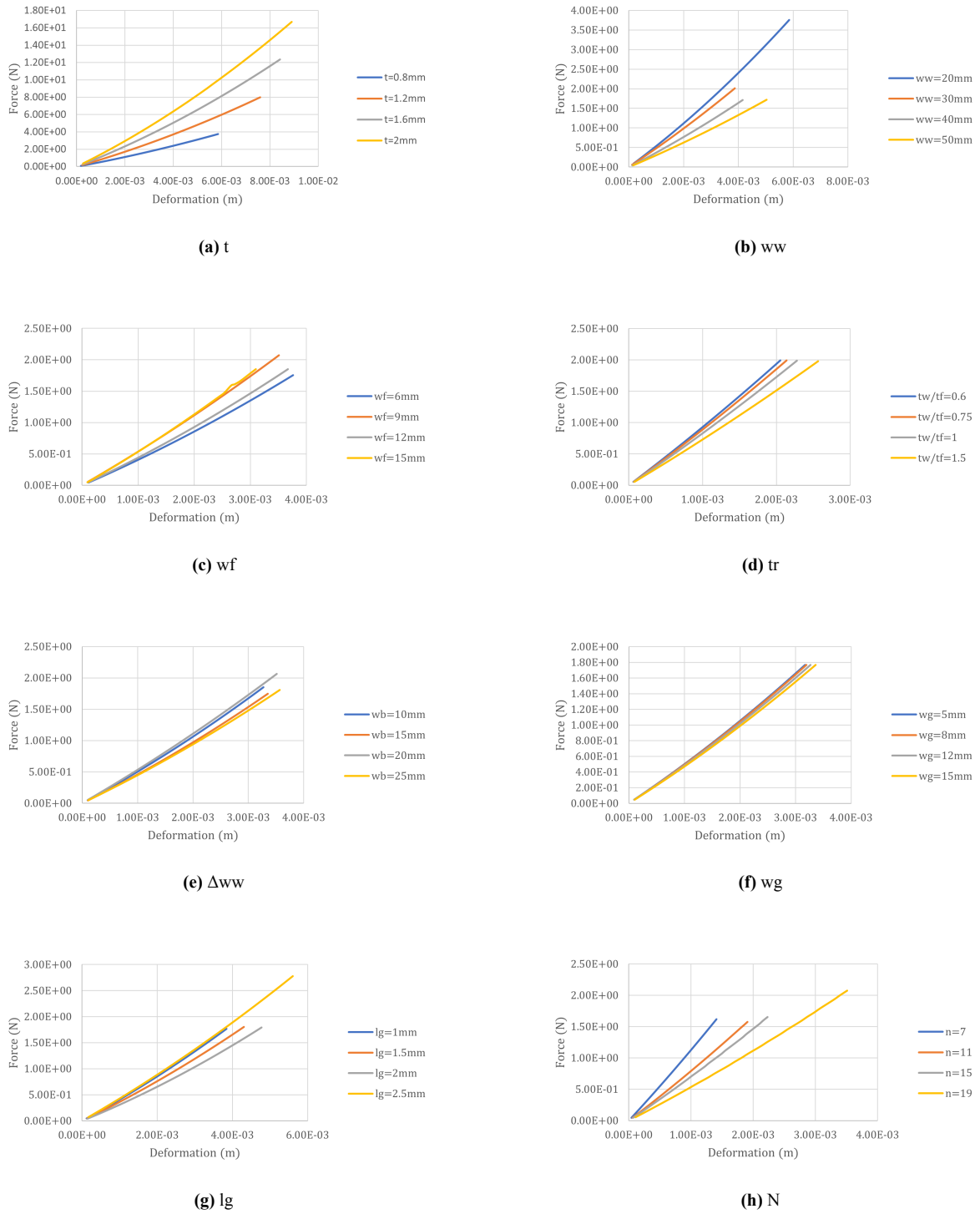


Figure B.4: Bending stiffness diagram (X-axis)

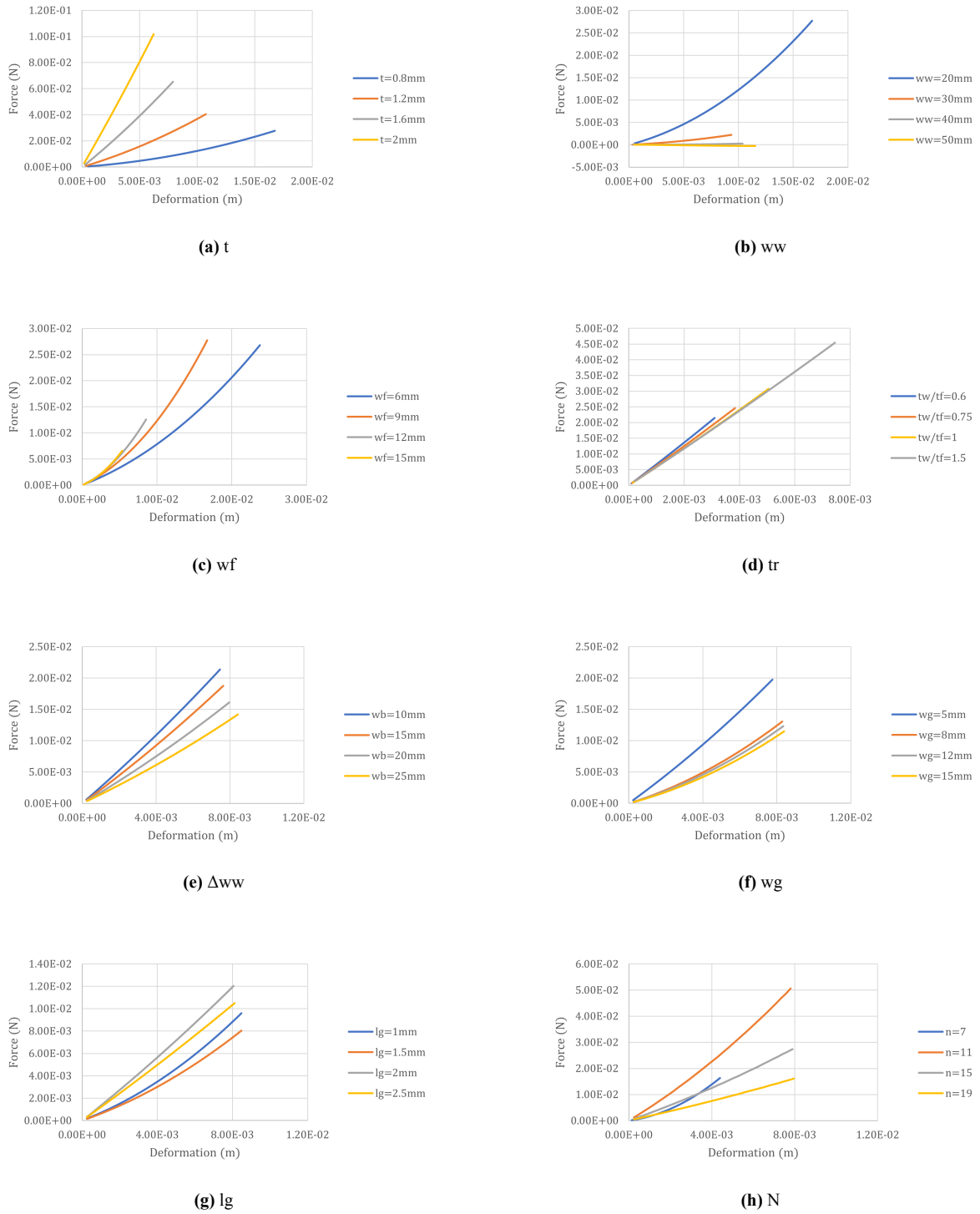


Figure B.5: Bending stiffness diagram (Y-axis)

C.1. Factorial point

Run number	Factor A:t(mm)	Factor B:Ww(mm)	Factor C:ΔWw(mm)	Factor D:Web number	Response 1: Stiffness(Nm/rad)	Response 2: RoM(rad)	Response 3: Max stress(Pa)	Response 4: Actuation force(N)
1	0.8	20	-10	17	-0.005743853	1.18235294	609680768	14.2835403
2	0.8	20	-10	19	-0.003744793	1.233333333	291654656	12.8975972
3	0.8	20	-10	23	-0.003497939	1.30588235	382283968	14.0541163
4	0.8	20	0	17	-0.018905168	1.02352941	25656734	9.85459319
5	0.8	20	0	19	-0.016408106	1.00588235	33195712	8.03170403
6	0.8	20	0	23	-0.010328693	0.9	46244752	5.43067535
7	0.8	20	10	23	-0.003199987	0.741176471	441560928	4.58132607
8	0.8	25	-10	17	-0.006203529	0.795	728340864	7.36531979
9	0.8	25	-10	19	-0.004697872	0.783333333	558631168	6.61614456
10	0.8	25	0	17	-0.016546961	0.847058824	88070824	4.45657862
11	0.8	25	0	19	-0.014465021	0.74	99956832	3.41206905
12	0.8	25	0	23	-0.008638593	0.585	82861328	2.21811512
13	0.8	25	10	17	-0.005327173	0.39	400560416	2.32757226
14	0.8	25	10	19	-0.002106667	0.375	157624256	1.81362684
15	0.8	30	-10	17	-0.005376672	0.555	371822656	3.96932068
16	0.8	30	-10	19	-0.003041667	0.48	298447648	3.25102216
17	0.8	30	-10	23	-0.003447383	0.688235294	238608896	4.3873447
18	0.8	30	0	17	-0.015567205	0.635294118	126847416	2.11439996
19	0.8	30	0	19	-0.011719136	0.56	27761.5312	1.66898561
20	0.8	30	0	23	-0.00737	0.39	66251860	1.02612171
21	0.8	30	10	23	-0.000359729	0.617647059	100290848	1.46850925
22	1.2	20	-10	17	-0.010627323	0.84	128000000	34.5600331
23	1.2	20	-10	19	-0.007773333	0.75	302216224	31.2520725
24	1.2	20	-10	23	-0.00555	0.758823529	521918048	34.2637333
25	1.2	20	0	17	-0.055336508	0.57	522915840	17.5679457
26	1.2	20	0	19	-0.038480888	0.635294118	73757168	14.5398393
27	1.2	20	10	17	-0.008815378	0.45	340158336	8.27676093
28	1.2	20	10	19	-0.00423	0.333333333	153801072	6.46960479
29	1.2	25	-10	17	-0.00670922	0.670588235	367544992	18.0091992
30	1.2	25	-10	19	-0.005950835	0.456	752968640	13.4772458
31	1.2	25	0	17	-0.021654297	0.405	551001856	8.55378172
32	1.2	25	0	19	-0.029319054	0.458823529	76881888	5.90727172
33	1.2	25	10	17	-0.007189048	0.255	114000000	4.55472755
34	1.2	25	10	19	-0.002591883	0.123529412	299997056	3.41921095
35	1.2	30	-10	19	-0.003787037	0.228	383875264	6.69879981
36	1.2	30	0	17	-0.013226779	0.3	885809536	4.47658803
37	1.2	30	0	19	-0.019298253	0.335294118	153510368	2.903539
38	1.2	30	10	19	-0.003403196	0.105882353	105000000	2.11900443
39	1.6	20	-10	17	-0.021063481	0.465	133000000	55.8698833
40	1.6	20	-10	19	-0.026630494	0.416666667	330938400	49.8902451
41	1.6	20	0	17	-0.045928251	0.564705882	81699672	25.6614716
42	1.6	20	0	19	-0.02367308	0.476470588	115209976	21.6630318
43	1.6	20	10	19	-0.002824419	0.133333333	439493856	9.81235264
44	1.6	25	-10	19	-0.00670922	0.670588235	367544992	18.0091992
45	1.6	25	0	17	-0.029501104	0.345	829148224	13.2734327
46	1.6	25	0	19	-0.008672512	0.229411765	165977856	8.65200884
47	1.6	25	10	19	0.0179	0.105882353	111000000	5.19440383
48	1.6	30	0	19	0.01632	0.264705882	195502240	4.29083544
49	1.2	25	0	21	-0.016113119	0.388235294	124279904	4.86271193
50	0.8	25	0	21	-0.012888531	0.494117647	581672768	2.91112743
51	1.2	30	0	21	-0.009863417	0.211764706	896222720	2.76275005
52	1.2	20	0	21	-0.024894779	0.504	763864768	12.6784934
53	1.2	25	-10	21	0.00359	0.247058824	605755072	18.0061958
54	0.8	20	-10	21	-0.002003448	0.847058824	444914176	10.4850744
55	1.6	30	-10	21	0.0213	0.247058824	957614144	8.09927106

C.2. Predictive model of responses

Stiffness =		RoM =		Max stress =		Force =	
+0.173538		+9.84481		+7.11E+09		+68.15	
-0.299581	t	-3.19309	t	+1.26E+09	t	+102.32	t
-0.000314	w_w	-0.216051	w_w	+3.88E+07	w_w	-3.02	w_w
-0.001642	Δw_w	-0.064035	Δw_w	-1.20E+08	Δw_w	-1.27	Δw_w
-0.006786	N	-0.421709	N	-8.46E+08	N	-6.93	N
+0.003986	$t*w_w$	+0.042186	$t*w_w$	+5.45E+07	$t*w_w$	-2.66	$t*w_w$
+0.000952	$t*\Delta w_w$	+0.004595	$t*\Delta w_w$	+2.04E+07	$t*\Delta w_w$	-1.34	$t*\Delta w_w$
+0.005640	$t*N$	+0.003382	$t*N$	-1.27E+07	$t*N$	-0.733	$t*N$
+4.23E-06	$w_w*\Delta w_w$	+0.001276	$w_w*\Delta w_w$	+2.42E+06	$w_w*\Delta w_w$	+0.094	$w_w*\Delta w_w$
-0.000014	w_w*N	+0.000896	w_w*N	-5.17E+05	w_w*N	-0.024	w_w*N
+0.000039	Δw_w*N	+0.000665	Δw_w*N	+1.85E+06	Δw_w*N	-0.0108	Δw_w*N
+0.042311	t^2	+0.674626	t^2	-7.79E+08	t^2	-4.119	t^2
-0.000050	w_w^2	+0.002392	w_w^2	-1.44E+06	w_w^2	+0.105	w_w^2
+0.000160	Δw_w^2	-0.000504	Δw_w^2	+2.74E+06	Δw_w^2	+0.027	Δw_w^2
+0.000087	N^2	+0.009757	N^2	+2.14E+07	N^2	+0.196	N^2

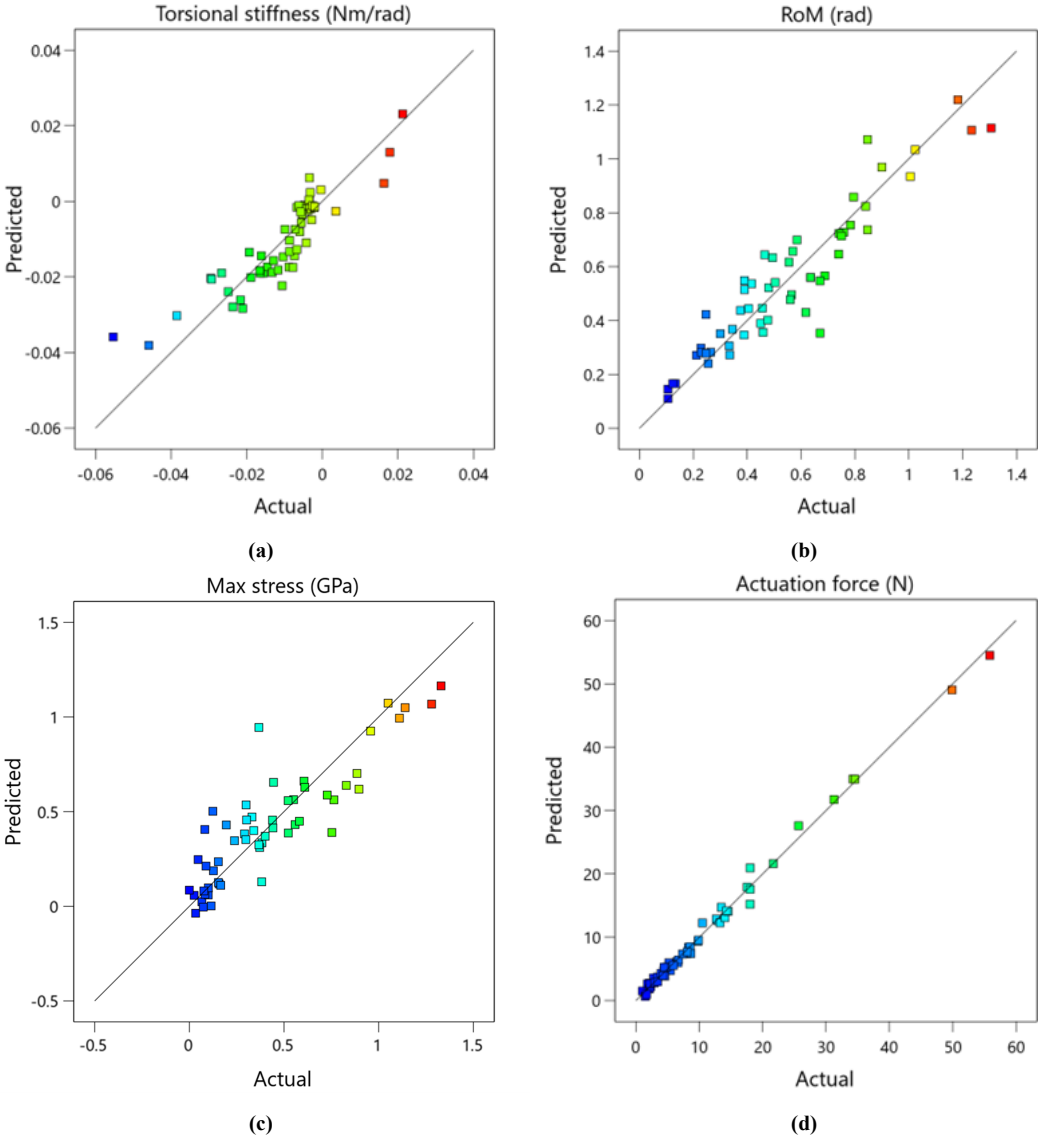
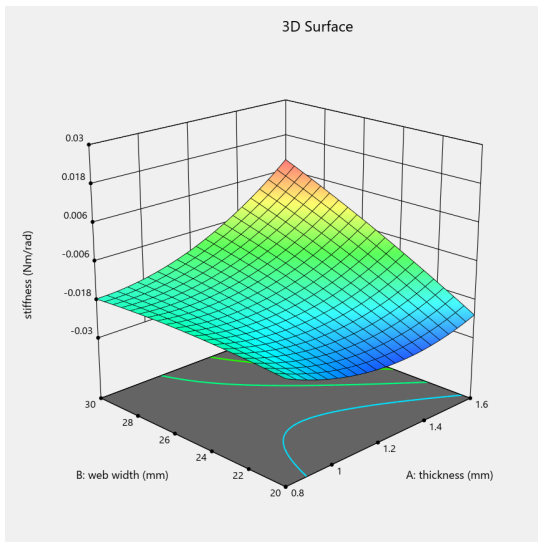
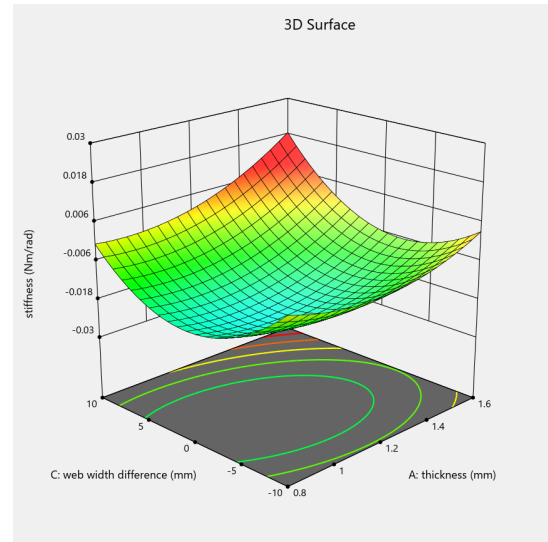


Figure C.1: Regressive models for predicting four responses.

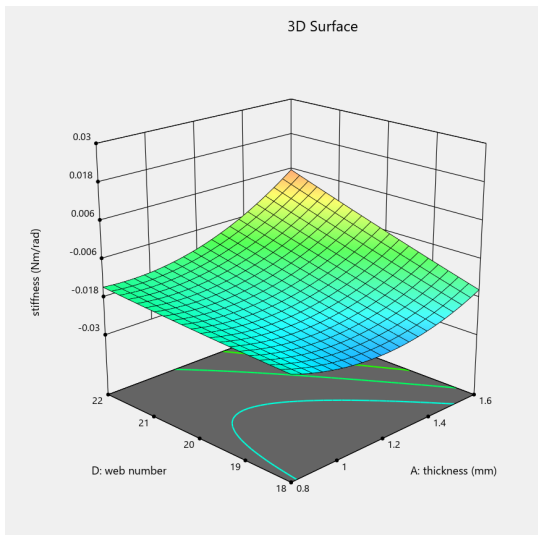
C.3. Response surfaces



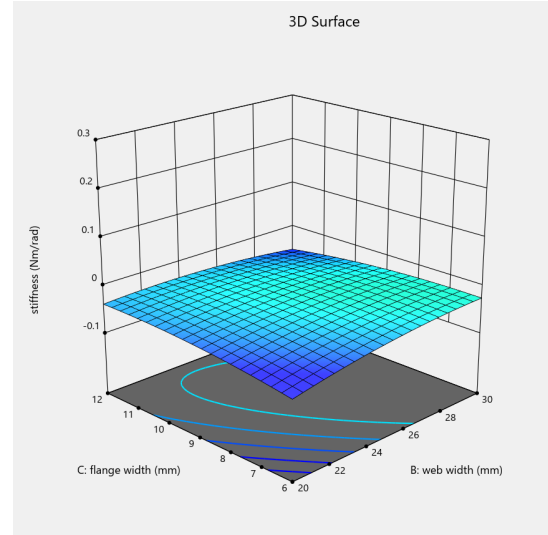
(a) AB



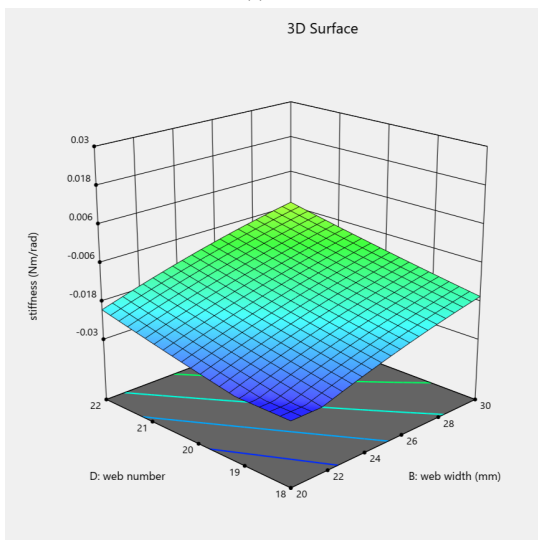
(b) AC



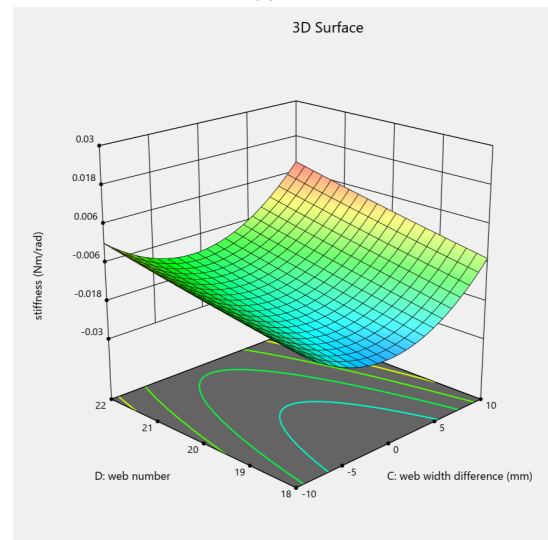
(c) AD



(d) BC

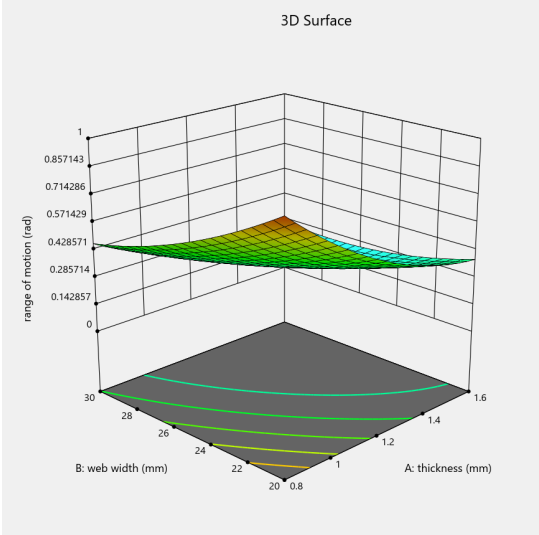


(e) BD

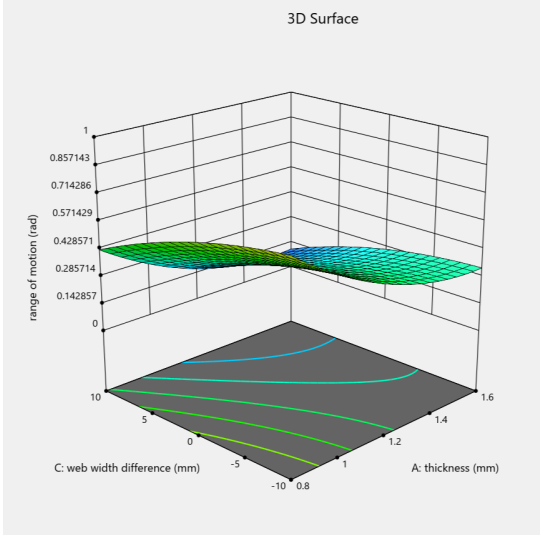


(f) CD

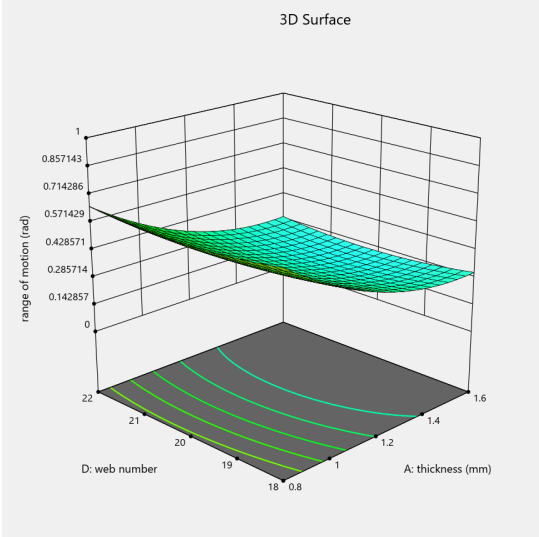
Figure C.2: 2 variable response surface - Stiffness



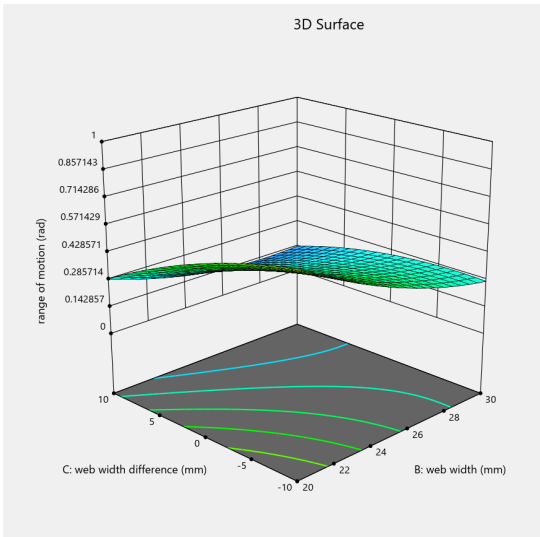
(a) AB



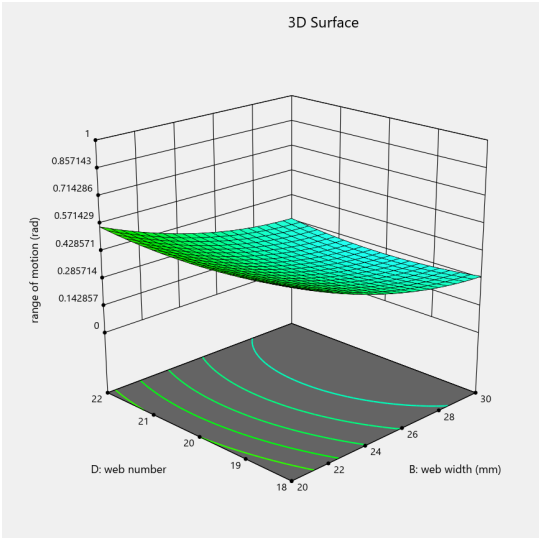
(b) AC



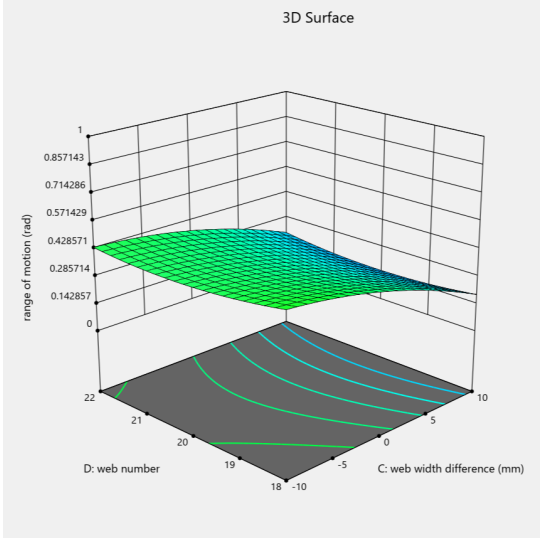
(c) AD



(d) BC

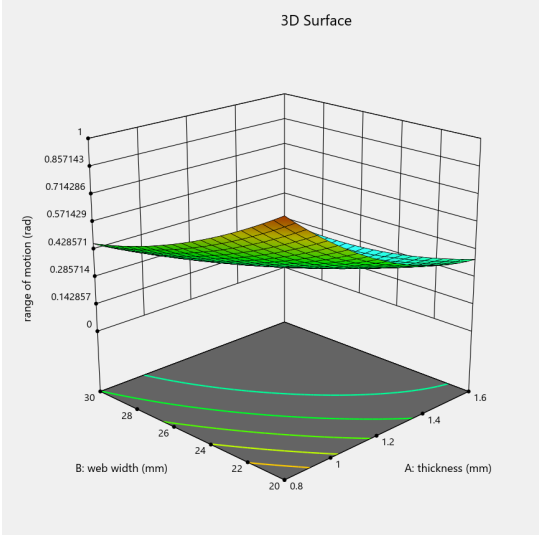


(e) BD

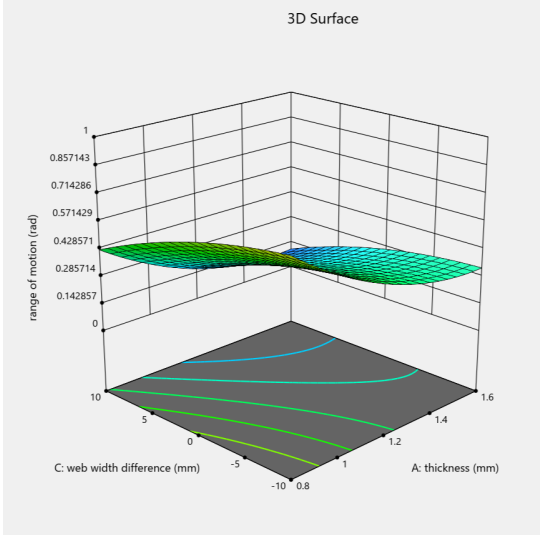


(f) CD

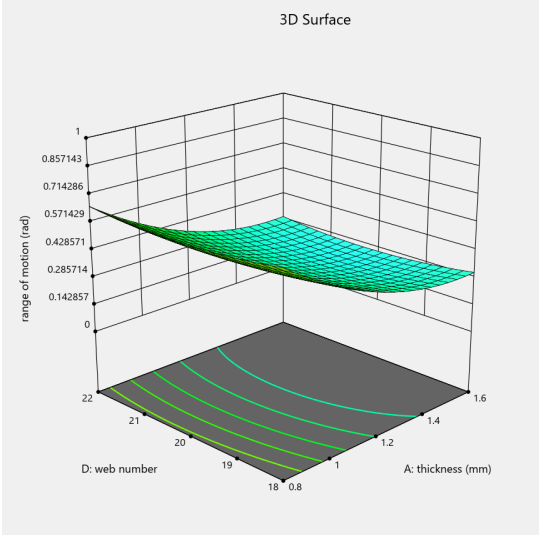
Figure C.3: 2 variable response surface - RoM



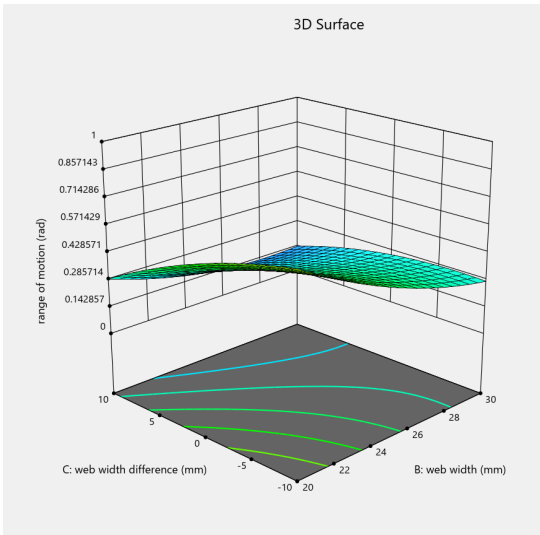
(a) AB



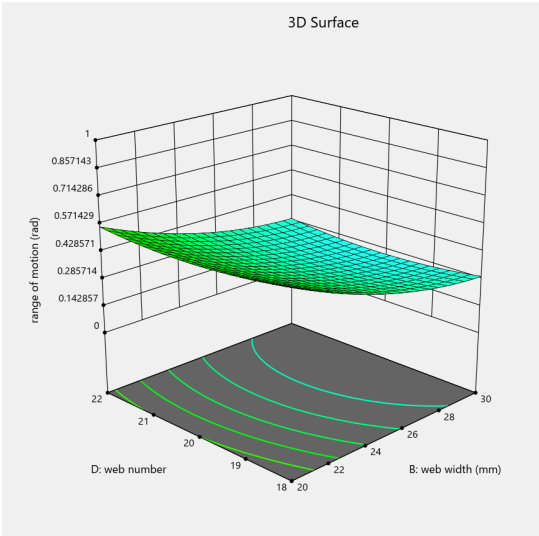
(b) AC



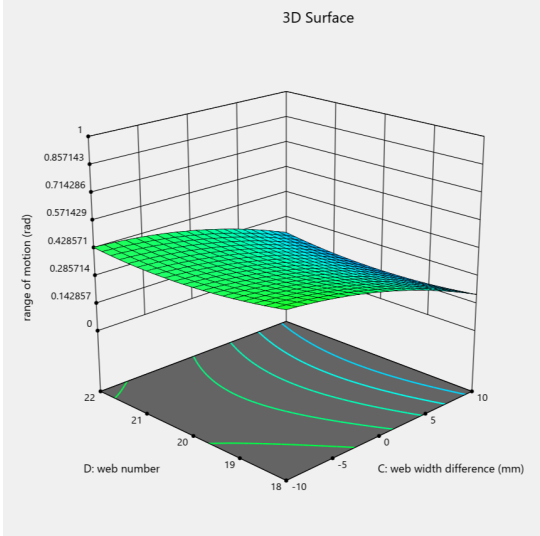
(c) AD



(d) BC

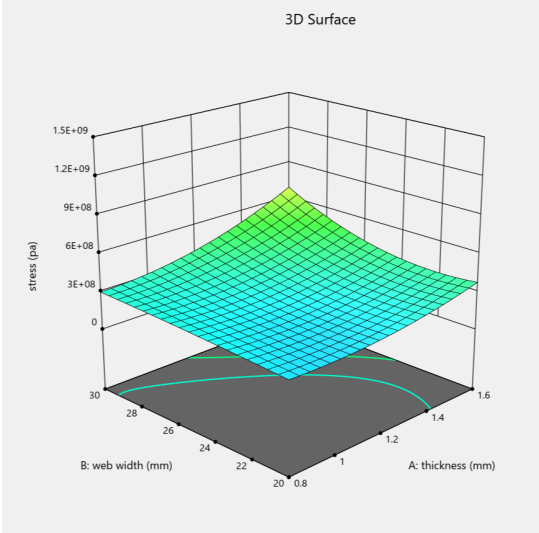


(e) BD

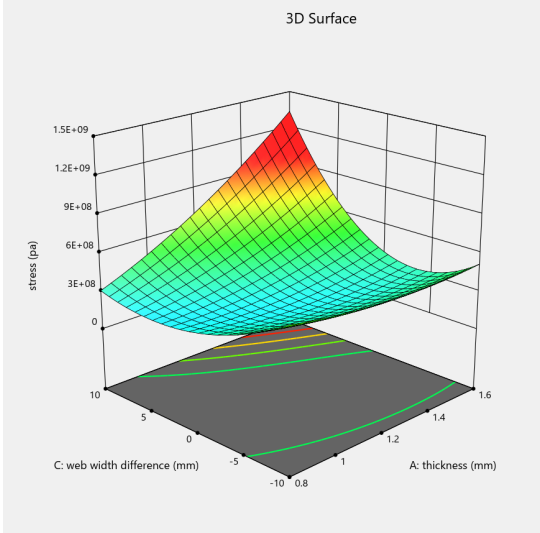


(f) CD

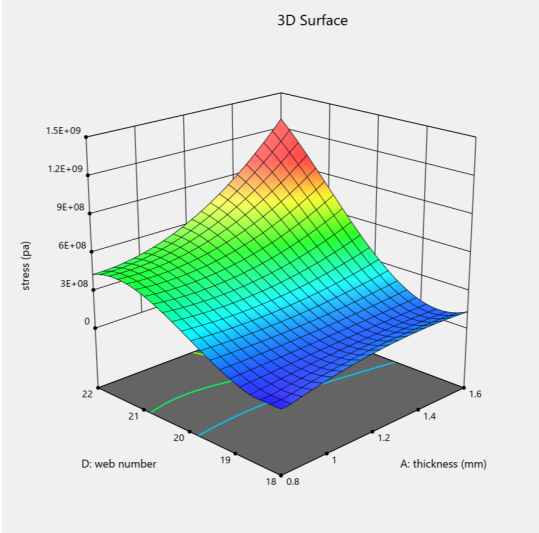
Figure C.4: 2 variable response surface - RoM



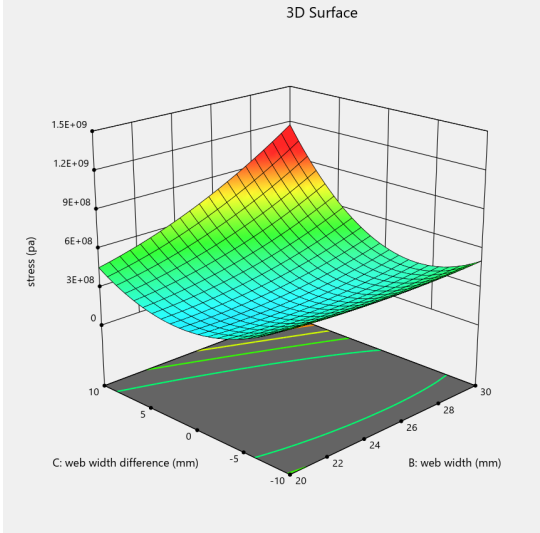
(a) AB



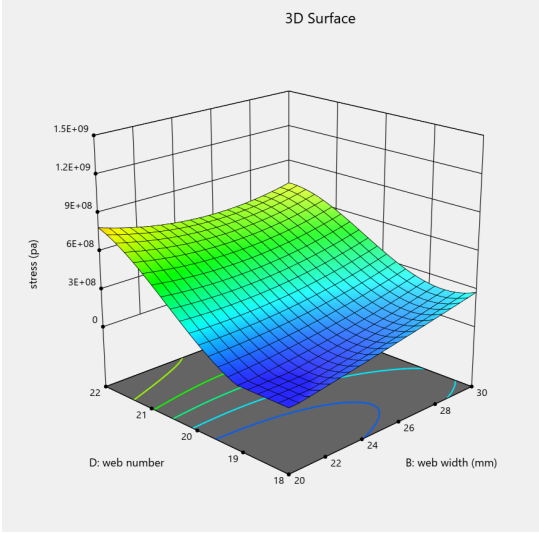
(b) AC



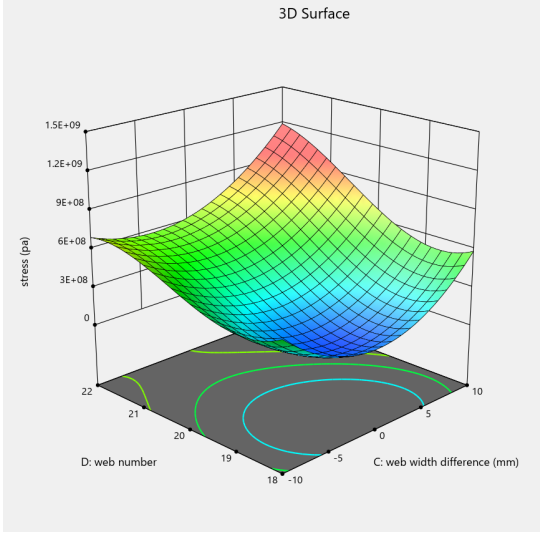
(c) AD



(d) BC

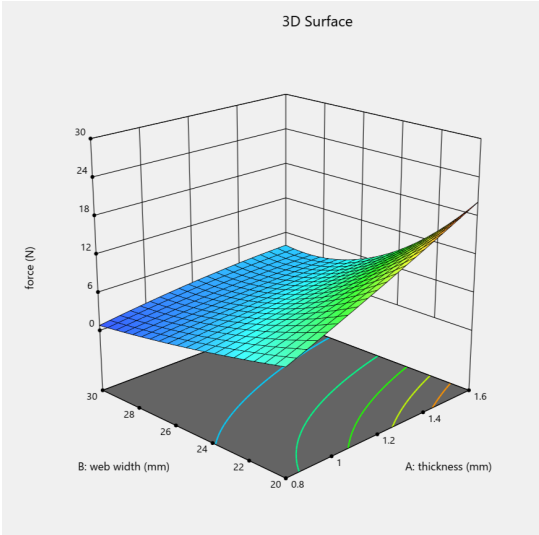


(e) BD

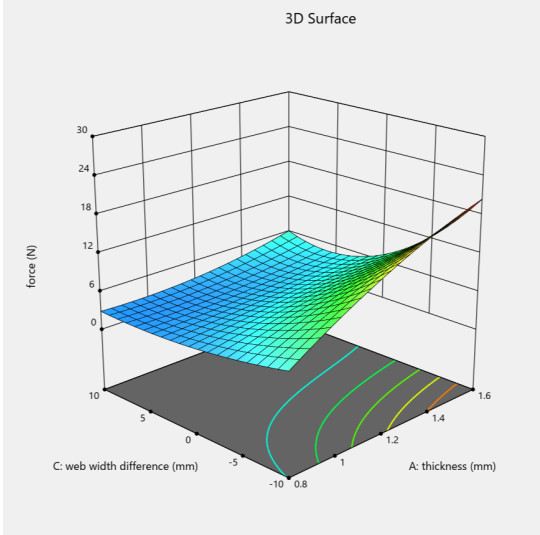


(f) CD

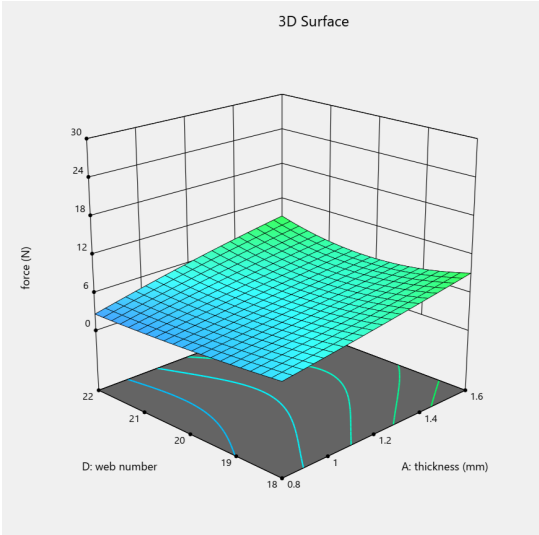
Figure C.5: 2 variable response surface - Max stress



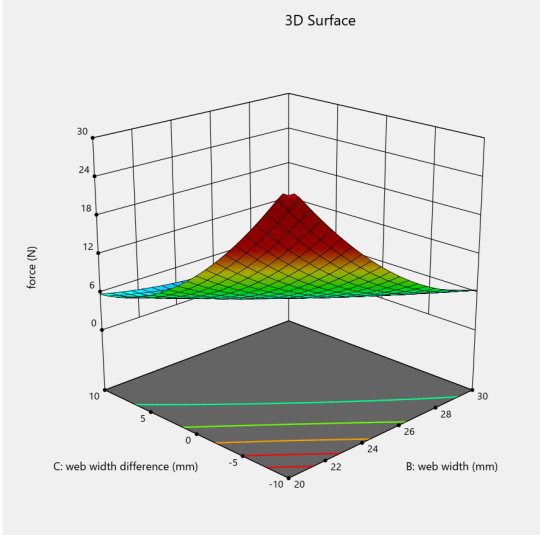
(a) AB



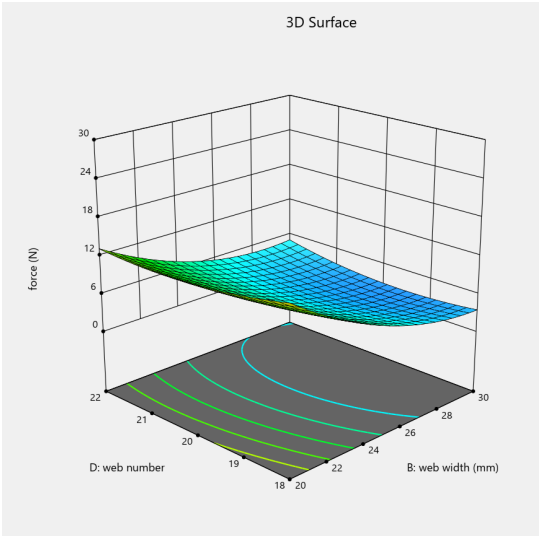
(b) AC



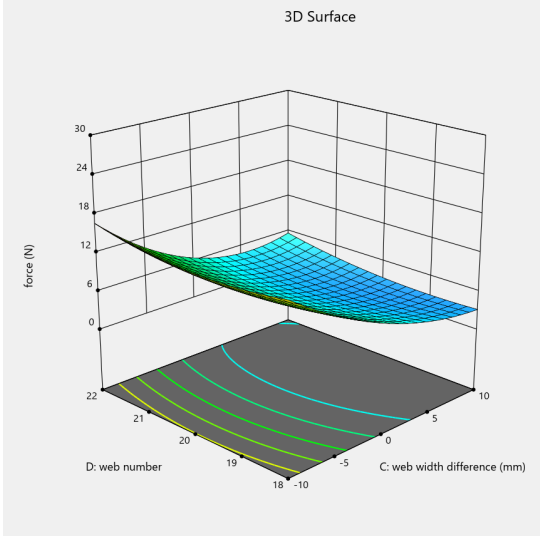
(c) AD



(d) BC



(e) BD



(f) CD

Figure C.6: 2 variable response surface - Actuation force

C.4. Predictive model vs FEM data

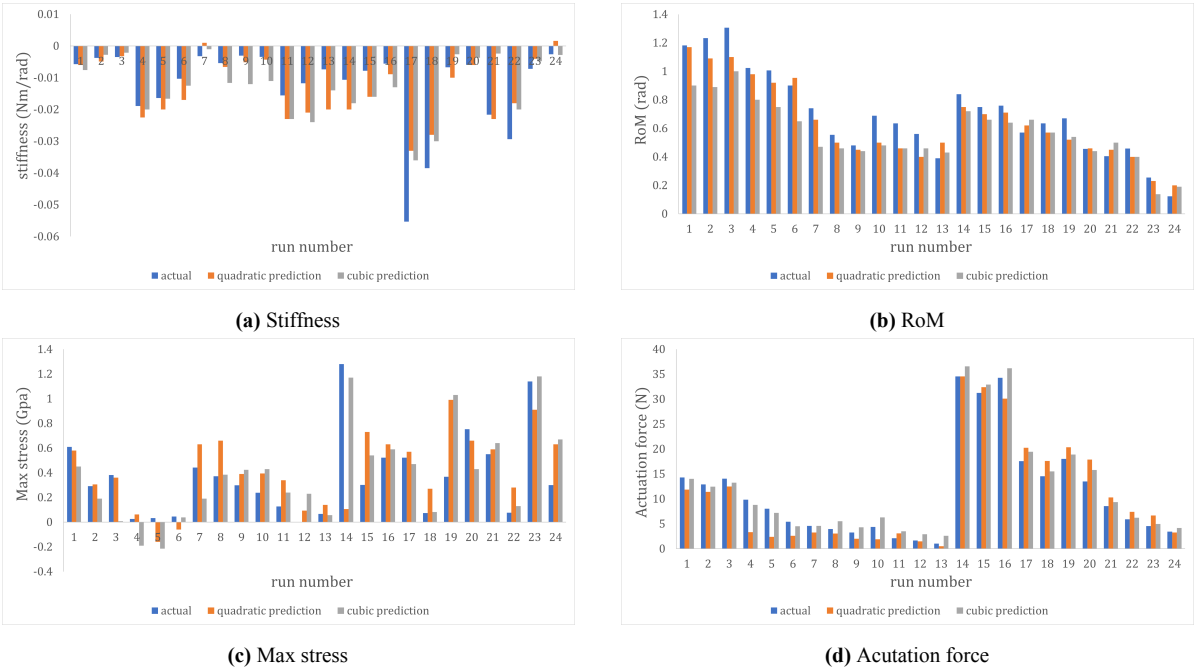
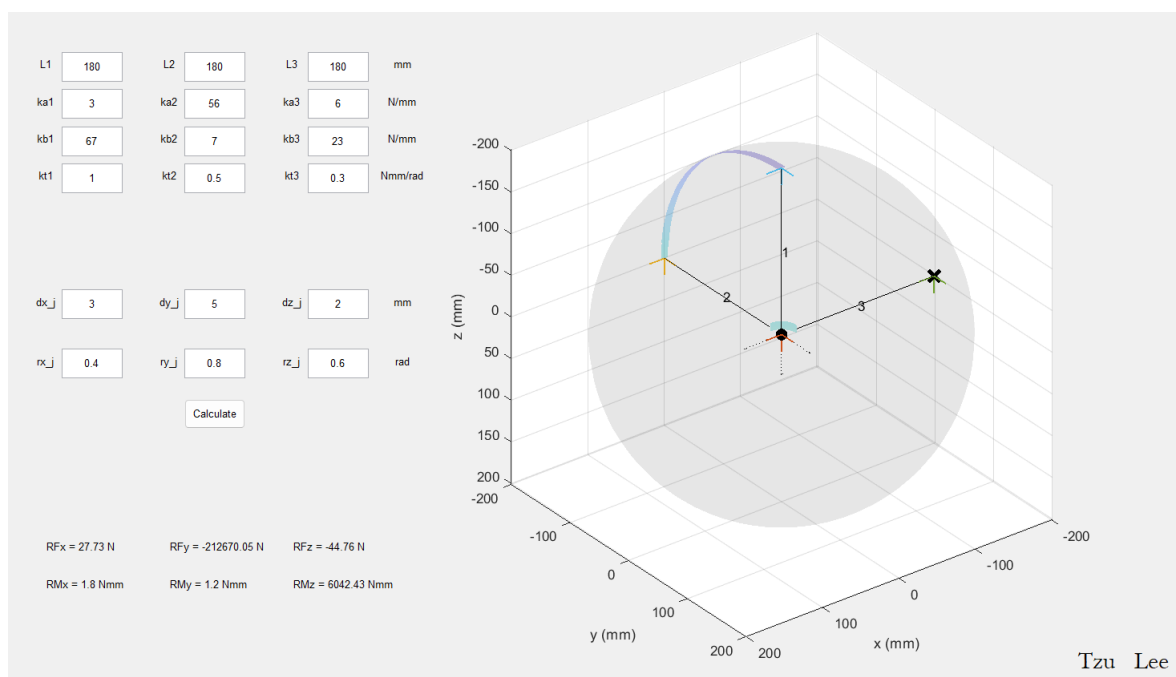


Figure C.7: Comparison of the predictive model and FEM data

D GUI

D.1. GUI layout



D.2. GUI matlab code

```
1  ""  
2  This code is for generating the GUI in matlab.  
3  ""  
4  function calculate()  
5  clc  
6  clear  
7  close all  
8  
9  %figure object that contains GUI.  
10 L = 200; %beam length  
11 f = figure('units','normalized');  
12
```

```
13 X_1 = [0;0;0];
14 Y_1 = [0;0;0];
15 Z_1 = [0;0;0];
16
17 X_2 = [-L;-L;-L];
18 Y_2 = [0;0;0];
19 Z_2 = [0;0;0];
20
21 X_3 = [0;0;0];
22 Y_3 = [-L;-L;-L];
23 Z_3 = [0;0;0];
24
25 X_4 = [0;0;0];
26 Y_4 = [0;0;0];
27 Z_4 = [-L;-L;-L];
28
29 P = [0;0;0];
30 U = [1;0;0];
31 V = [0;1;0];
32 W = [0;0;1];
33
34 quiver3(X_1,Y_1,Z_1,U,V,W,20,'Color','#D95319','linewidth',1);
35 hold on
36 quiver3(X_2,Y_2,Z_2,U,V,W,20,'Color','#77AC30','linewidth',1);
37 quiver3(X_3,Y_3,Z_3,U,V,W,20,'Color','#EDB120','linewidth',1);
38 quiver3(X_4,Y_4,Z_4,U,V,W,20,'Color','#4DBEEE','linewidth',1);
39 quiver3([20;0;0],[0;20;0],[0;0;20],U,V,W,1.5,'k:');
40
41 plot3(-L,0,0,'kx','LineWidth',12,'MarkerSize',3)
42 plot3(0,0,0,'k.','MarkerSize',30)
43
44 beam_1 = quiver3(X_2,Y_2,Z_2,U,P,P,180,'k');
45 beam_1.ShowArrowHead = 'off';
46
47 beam_2 = quiver3(X_3,Y_3,Z_3,P,V,P,180,'k');
48 beam_2.ShowArrowHead = 'off';
49
50 beam_3= quiver3(X_4,Y_4,Z_4,P,P,W,200,'k');
51 beam_3.ShowArrowHead = 'off';
52
53 beam_1_number = 3;
54 text(0.5*X_2(3),0.5*Y_2(3),0.5*Z_2(3), num2str(beam_1_number),'FontSize',10)
55 beam_2_number = 2;
56 text(0.5*X_3(3),0.5*Y_3(3),0.5*Z_3(3), num2str(beam_2_number),'FontSize',10)
57 beam_3_number = 1;
58 text(0.5*X_4(3),0.5*Y_4(3),0.5*Z_4(3), num2str(beam_3_number),'FontSize',10)
59
60 % draw connector 1
61 [X,Y,Z] = sphere(200) ;
62 c1_zlim = 5;
63 r_c1 = 20 ;
```

```

64 c1_X1 = r_c1*X ; c1_Y1 = r_c1*Y ; c1_Z1 = r_c1*Z ;
65 c1_X1(abs(c1_Z1)>c1_zlim | c1_X1>0) = NaN ; c1_Y1(abs(c1_Z1)>c1_zlim | c1_Y1>0) =
    NaN ; c1_Z1(abs(c1_Z1)>c1_zlim) = NaN ;
66 c1 = surf(c1_X1,c1_Y1,c1_Z1,'FaceColor','k', 'FaceAlpha',0.3) ;
67 axis equal
68 shading interp
69
70 % draw connector 2
71 [X,Y,Z] = sphere(2000) ;
72 c2_xlim = 5;
73 r_c2 = 200 ;
74 c2_X1 = r_c2*X ; c2_Y1 = r_c2*Y ; c2_Z1 = r_c2*Z ;
75 c2_X1(abs(c2_X1)>c2_xlim) = NaN ; c2_Y1(abs(c2_X1)>c2_xlim | c2_Y1>0) = NaN ;
    c2_Z1(abs(c2_X1)>c2_xlim | c2_Z1>0) = NaN ;
76 c2 = surf(c2_X1,c2_Y1,c2_Z1,'FaceColor','k','FaceAlpha',0.3) ;
77 axis equal
78 shading interp
79
80 % draw sphere
81 r = L+1;
82 [x,y,z] = sphere(50);
83 x = r*x;
84 y = r*y;
85 z = r*z;
86 workingspace = surf(x,y,z);
87 axis equal
88 shading interp
89 set(workingspace, 'FaceColor','k','FaceAlpha',0.05);
90 set(gca, 'XDir','reverse')
91 set(gca, 'YDir','reverse')
92 set(gca, 'ZDir','reverse')
93 xlabel('x (mm)')
94 ylabel('y (mm)')
95 zlabel('z (mm)')
96
97 %Uicontrols devoted to static text(Stiffness number):
98 Author = uicontrol('Parent',f,'units','normalized','Style','Text','FontName','
    Garamond','FontSize',18,'position',[0.7, 0.015, 0.08, 0.08],'String','Tzu Lee
    ');
99
100 L1_text = uicontrol('Parent',f,'units','normalized','Style','Text');
101 L2_text = uicontrol('Parent',f,'units','normalized','Style','Text');
102 L3_text = uicontrol('Parent',f,'units','normalized','Style','Text');
103
104 ka1_text = uicontrol('Parent',f,'units','normalized','Style','Text');
105 ka2_text = uicontrol('Parent',f,'units','normalized','Style','Text');
106 ka3_text = uicontrol('Parent',f,'units','normalized','Style','Text');
107 kb1_text = uicontrol('Parent',f,'units','normalized','Style','Text');
108 kb2_text = uicontrol('Parent',f,'units','normalized','Style','Text');
109 kb3_text = uicontrol('Parent',f,'units','normalized','Style','Text');
110 kt1_text = uicontrol('Parent',f,'units','normalized','Style','Text');

```

```

111 kt2_text = uicontrol('Parent',f,'units','normalized','Style','Text');
112 kt3_text = uicontrol('Parent',f,'units','normalized','Style','Text');
113
114 %Uicontrols devoted to editable fields(Stiffness value):
115 L1_edit = uicontrol('Parent',f,'units','normalized','Style','edit');
116 L2_edit = uicontrol('Parent',f,'units','normalized','Style','edit');
117 L3_edit = uicontrol('Parent',f,'units','normalized','Style','edit');
118
119 ka1_edit = uicontrol('Parent',f,'units','normalized','Style','edit');
120 ka2_edit = uicontrol('Parent',f,'units','normalized','Style','edit');
121 ka3_edit = uicontrol('Parent',f,'units','normalized','Style','edit');
122 kb1_edit = uicontrol('Parent',f,'units','normalized','Style','edit');
123 kb2_edit = uicontrol('Parent',f,'units','normalized','Style','edit');
124 kb3_edit = uicontrol('Parent',f,'units','normalized','Style','edit');
125 kt1_edit = uicontrol('Parent',f,'units','normalized','Style','edit');
126 kt2_edit = uicontrol('Parent',f,'units','normalized','Style','edit');
127 kt3_edit = uicontrol('Parent',f,'units','normalized','Style','edit');
128
129 %Uicontrols devoted to static text(Unit):
130 L_text = uicontrol('Parent',f,'units','normalized','Style','Text');
131 ka_text = uicontrol('Parent',f,'units','normalized','Style','Text');
132 kb_text = uicontrol('Parent',f,'units','normalized','Style','Text');
133 kt_text = uicontrol('Parent',f,'units','normalized','Style','Text');
134 d_text = uicontrol('Parent',f,'units','normalized','Style','Text');
135 r_text = uicontrol('Parent',f,'units','normalized','Style','Text');
136
137 %input displacement and rotation angle
138 dx_joint_text = uicontrol('Parent',f,'units','normalized','Style','Text');
139 dy_joint_text = uicontrol('Parent',f,'units','normalized','Style','Text');
140 dz_joint_text = uicontrol('Parent',f,'units','normalized','Style','Text');
141 rx_joint_text = uicontrol('Parent',f,'units','normalized','Style','Text');
142 ry_joint_text = uicontrol('Parent',f,'units','normalized','Style','Text');
143 rz_joint_text = uicontrol('Parent',f,'units','normalized','Style','Text');
144
145 dx_joint_edit = uicontrol('Parent',f,'units','normalized','Style','edit');
146 dy_joint_edit = uicontrol('Parent',f,'units','normalized','Style','edit');
147 dz_joint_edit = uicontrol('Parent',f,'units','normalized','Style','edit');
148 rx_joint_edit = uicontrol('Parent',f,'units','normalized','Style','edit');
149 ry_joint_edit = uicontrol('Parent',f,'units','normalized','Style','edit');
150 rz_joint_edit = uicontrol('Parent',f,'units','normalized','Style','edit');
151
152 % MLG Cell array strat.
153 k_texts = {L1_text,L2_text,L3_text,ka1_text,ka2_text,ka3_text,kb1_text,kb2_text,
            kb3_text,kt1_text,...
154            kt2_text,kt3_text,dx_joint_text,dy_joint_text,dz_joint_text,...
155            rx_joint_text,ry_joint_text,rz_joint_text};
156 strings_k = {'L1','L2','L3','ka1','ka2','ka3','kb1','kb2','kb3','kt1','kt2','kt3',
            '...',
157            'dx_j','dy_j','dz_j','rx_j','ry_j','rz_j'};
158 input_edits = {L1_edit,L2_edit,L3_edit,ka1_edit,ka2_edit,ka3_edit,kb1_edit,
            kb2_edit,kb3_edit,kt1_edit,...

```

```

159     kt2_edit,kt3_edit,dx_joint_edit,dy_joint_edit,dz_joint_edit,...
160     rx_joint_edit,ry_joint_edit,rz_joint_edit});
161 % defaults =
162     {'0','0','0','0','0','0','0','0','0','0','0','0','0','0','0','0','0','0'};
163 defaults =
164     {'180','180','180','3','56','6','67','7','23','1','0.5','0.3','3','5','2',...
165     '0.4','0.8','0.6'};
166
167 unit_texts = {L_text,ka_text,kb_text,kt_text,d_text,r_text};
168 strings_unit = {'mm','N/mm','N/mm','Nmm/rad','mm','rad'};
169
170 xi = 0.02; %X-coordinate of Bottom-Left corner.
171 yi = 0.85; %Y-coordinate of Bottom-Left corner.
172 width = 0.04; %Width of object.
173 height = 0.04; %Height of object
174 deltaH = 0.08; %Horizontal Spacing between objects.
175 deltaV = -0.05; %Vertical Spacing between objects.
176 deltaVD = -0.08;
177
178 offsetx = 0.03;
179 offsety = 0.008;
180 rows = 6; %Number of rows.
181 cols = 3; %Number of columns.
182 k = 0; % Counter for number of uicontrols that populate grid pattern.
183
184 for i = 1:rows
185     for j = 1:cols
186         k = k + 1;
187         if k <= length(k_texts)
188             if i >= 5
189                 x = xi + deltaH*(j-1);
190                 y = yi + deltaVD*(i-1);
191                 xo = x + offsetx; %horizontally offset the editable field.
192                 yo = y + offsety;
193                 set(k_texts{k},'Position',[x, y, width, height],'String',strings_k{k})
194                 set(input_edits{k},'Position',[xo, yo, width, height],'String',
195                     defaults{k})
196             else
197                 x = xi + deltaH*(j-1);
198                 y = yi + deltaV*(i-1);
199                 xo = x + offsetx; %horizontally offset the editable field.
200                 yo = y + offsety;
201                 set(k_texts{k},'Position',[x, y, width, height],'String',strings_k{k})
202                 set(input_edits{k},'Position',[xo, yo, width, height],'String',
203                     defaults{k})
204             end
205         end
206     end
207 end

```

```
206 end
207
208
209 unit_rows = 6;
210 k = 0;
211 for i = 1:unit_rows
212     k = k + 1;
213     if k <= length(unit_texts)
214         if i >= 5
215             x = xi + deltaH*2.9;
216             y = yi + deltaVD*(i-1);
217             set(unit_texts{k},'Position',[x, y, width, height],'String',
                strings_unit{k})
218
219         else
220             x = xi + deltaH*2.9;
221             y = yi + deltaV*(i-1);
222             set(unit_texts{k},'Position',[x, y, width, height],'String',
                strings_unit{k})
223         end
224     end
225 end
226
227 %Uicontrol for output object:
228 RFx= uicontrol('Parent',f,'Style','text','units','normalized','HorizontalAlignment
    ', 'left');
229 RFy= uicontrol('Parent',f,'Style','text','units','normalized','HorizontalAlignment
    ', 'left');
230 RFz= uicontrol('Parent',f,'Style','text','units','normalized','HorizontalAlignment
    ', 'left');
231 RMx= uicontrol('Parent',f,'Style','text','units','normalized','HorizontalAlignment
    ', 'left');
232 RMy= uicontrol('Parent',f,'Style','text','units','normalized','HorizontalAlignment
    ', 'left');
233 RMz= uicontrol('Parent',f,'Style','text','units','normalized','HorizontalAlignment
    ', 'left');
234 output_texts = {RFx,RFy,RFz,RMx,RMy,RMz};
235 out_strings = {'RFx','RFy','RFz','RMx','RMy','RMz'};
236
237
238 out_rows = 2; %Number of rows.
239 out_cols = 3; %Number of columns.
240 k = 0; % Counter for number of uicontrols that populate grid pattern.
241
242 for i = 1:out_rows
243     for j = 1:out_cols
244         k = k + 1;
245         if k <= length(output_texts)
246
247             out_x = 2*xi + deltaH*(j-1);
248             out_y = yi + deltaV*(i+12);
```

```

249         set(output_texts{k},'Position',[out_x, out_y, 2*width, height],'String
           ',out_strings{k})
250
251
252     end
253 end
254 end
255
256 %Uicontrol for button execution:
257
258 exe = uicontrol('Parent',f,'Style','pushbutton','units','normalized',...
259     'position',[xo-deltaH,y+1.2*deltaV,width,height],'String','Calculate',...
260     'Callback',@result);
261
262 %function
263 function result(hObject,eventdata,handles)
264 global dx_joint dy_joint dz_joint rx_joint ry_joint rz_joint ka1 ka2 ka3 kb1 kb2
           kb3 kt1 kt2 kt3 L1 L2 L3
265
266 dx_joint = str2double(get(input_edits{13},'String')); dy_joint = str2double(get(
           input_edits{14},'String')); dz_joint = str2double(get(input_edits{15},'String')
           );
267 ka1 = str2double(get(input_edits{4},'String')); ka2 = str2double(get(input_edits
           {5},'String')); ka3 = str2double(get(input_edits{6},'String'));
268 kb1 = str2double(get(input_edits{7},'String')); kb2 = str2double(get(input_edits
           {8},'String')); kb3 = str2double(get(input_edits{9},'String'));
269 L1 = str2double(get(input_edits{1},'String')); L2 = str2double(get(input_edits
           {2},'String')); L3 = str2double(get(input_edits{3},'String'));
270
271 rx_joint = str2double(get(input_edits{16},'String')); ry_joint = str2double(get(
           input_edits{17},'String')); rz_joint = str2double(get(input_edits{18},'String'))
           ;
272 kt1 = str2double(get(input_edits{10},'String')); kt2 = str2double(get(input_edits
           {11},'String')); kt3 = str2double(get(input_edits{12},'String'));
273
274
275 % the reaction force/moment at ground
276 % displacement of joint inducing force
277 z1 = (dz_joint-(kt3/kb2*L2)*rx_joint-(kt2/kb3*L3)*ry_joint)/(1+ka1/kb2+ka1/kb3-ka1
           /kb2); % dz_joint = z1 + Delta_z2 + Delta_z3 + 2 end shortening + 2 torque
           bending
278 Fz = z1*ka1; %Fz = 1 axial force + 2 bending force + 1
           torsional force
279 Fz_endeffector = Fz*dz_joint*(dz_joint^-1);
280 Fz_endeffector(isnan(Fz_endeffector))=0;
281
282 y2 = (dy_joint-(kt3/kb1*L1)*(rx_joint-ka1*L2*z1/kt3)-kt1*rz_joint/(kb3*L3))/(1+ka2
           /kb1+ka2/kb3);
283 Fy = y2*ka2; %Fy = 1 axial force + 2 bending force
284 Fy_endeffector = Fy*dy_joint*(dy_joint^-1);
285 Fy_endeffector(isnan(Fy_endeffector))=0;

```

```

286
287 x3 = (dx_joint-(kt2/(kb1*L1))*ry_joint-(kt1/(kb2*L2))*rz_joint)/(1+ka3/kb2+ka3/kb1
    );           %total displacement = 1 axial + 2 bending + 2 end shortening(
    ignore) + 2 torque bending
288 Fx = x3*ka3;           %Fx = 1 axial force + 2 bending force
289 Fx_endeffector = Fx*dx_joint*(dx_joint^-1);
290 Fx_endeffector(isnan(Fx_endeffector))=0;
291
292
293 % rotation angle of joint inducing torque
294 % 1-the following model is for ignorable translational deflection
295
296 rz1 = rz_joint;           % rotation of beam 3 can be triggered by Tx and
    Fz
297 Tx = rz1*kt1;
298 Tx_endeffector = Tx*rx_joint*(rx_joint^-1);
299 Tx_endeffector(isnan(Tx_endeffector))=0;
300
301 ry2 = ry_joint;
302 Ty = ry2*kt2;
303 Ty_endeffector = Ty*ry_joint*(ry_joint^-1);
304 Ty_endeffector(isnan(Ty_endeffector))=0;
305
306
307 rx3 = rx_joint-ka1*L2*z1/kt3;
308 Tz = rx3*kt3;
309 Tz_endeffector = Tz*rz_joint*(rz_joint^-1);
310 Tz_endeffector(isnan(Tz_endeffector))=0;
311
312
313 % print output
314 set(RFx,'String',['RFx = ', num2str(round(Fx_endeffector,2)), ' N'])
315 set(RFy,'String',['RFy = ', num2str(round(Fy_endeffector,2)), ' N'])
316 set(RFz,'String',['RFz = ', num2str(round(Fz_endeffector,2)), ' N'])
317 set(RMx,'String',['RMx = ', num2str(round(Tx_endeffector,2)), ' Nmm'])
318 set(RMy,'String',['RMy = ', num2str(round(Ty_endeffector,2)), ' Nmm'])
319 set(RMz,'String',['RMz = ', num2str(round(Tz_endeffector,2)), ' Nmm'])
320
321
322 end
323 end

```